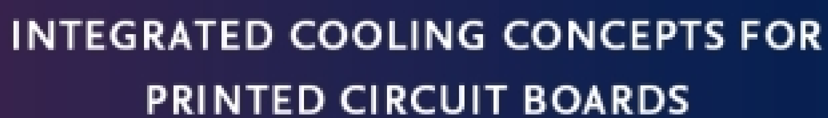

INTEGRATED COOLING CONCEPTS FOR PRINTED CIRCUIT BOARDS

Wessel W. Wits

INTEGRATED COOLING CONCEPTS FOR PRINTED CIRCUIT BOARDS

PROEFSCHRIFT

ter verkrijging van
de graad van doctor aan de Universiteit Twente,
op gezag van de rector magnificus,
prof. dr. W.H.M. Zijm,
volgens besluit van het College voor Promoties
in het openbaar te verdedigen
op donderdag 4 december 2008 om 15.00 uur

door

Wessel Willems Wits
geboren op 5 november 1977
te Amsterdam

Dit proefschrift is goedgekeurd door:

Prof. dr. ir. F.J.A.M. van Houten	promotor
Dr. ir. T.H.J. Vaneker	assistent promotor

INTEGRATED COOLING CONCEPTS FOR PRINTED CIRCUIT BOARDS

PhD Thesis

By Wessel Willems Wits at the Faculty of Engineering Technology (CTW) of the University of Twente, Enschede, the Netherlands.

Enschede, 4 december 2008

De promotiecommissie:

Prof. dr. F. Eising	Universiteit Twente, voorzitter, secretaris
Prof. dr. ir. F.J.A.M. van Houten	Universiteit Twente, promotor
Dr. ir. T.H.J. Vaneker	Universiteit Twente, assistent promotor
Prof. dr. ir. T.H. van der Meer	Universiteit Twente
Prof. dr. ir. H.J.M. ter Brake	Universiteit Twente
Prof. dr. A.G. Tijhuis	Technische Universiteit Eindhoven
Prof. dr. T. Tomiyama	Technische Universiteit Delft
Dr. R. Legtenberg	Thales Nederland B.V.

Keywords: Thermal Management, Electronics Cooling, PCB Cooling, Jet Impingement Cooling, Heat Pipe Cooling

---

ISBN 978-90-365-2731-6

Copyright © Wessel W. Wits, 2008
Cover design by Sylvia Bergsma-Lak
Printed by Gildeprint, Enschede
All rights reserved.

Aan mijn ouders,
aan Irma

Summary

Thermal management plays an increasingly dominant role in the design process of electronic products. Component sizes decrease while performance and functional demands increase, resulting in more power dissipation on smaller surfaces. In an effort to cope with these growing thermal challenges, industry continuously seeks cooling equipment with improved heat transfer performance. However, as thermal engineering is traditionally considered toward the end of the design process, the applied cooling solutions are often simply mounted onto the product. As such, cooling equipment for electronics is growing out of proportion compared to the electronic component it is supposed to cool.

This thesis describes the development of innovative cooling concepts for electronic products. Thermal criteria are considered during the conceptual design phase, in order to find more integrated solutions. This multidisciplinary approach strives to develop improved thermal management systems for electronic products, in terms of thermal performance, compactness and flexibility. To develop a cost efficient solution focus is also put on utilizing standardized electronic manufacturing processes, such as Printed Circuit Board (PCB) and Surface Mounted Device (SMD) production technologies. Cost considerations for high product volumes, enabling mass-market applications, are especially taken into account.

This research has led to the identification of two promising cooling concepts for electronic products.

The first concept – *directly injected cooling* – is based on (jet) air cooling. By manufacturing a coolant inlet port into the PCB underneath an electronic component, this component can be cooled directly from the bottom side. This concept excels in the area of high component density cooling, where many components on an electronic board must be cooled both independently and simultaneously.

The second concept – *integrated heat pipe cooling* – integrates a passive, two-phase heat transport device directly into the PCB. As the heat transfer mechanism

is based on phase change principles, it is capable of transporting large quantities of heat. The heat pipe is constructed inside the laminated structure that makes up the electronic board. This concept allows heat, dissipated by (multiple) components mounted onto the PCB, to be transported through the board structure with a very high efficiency.

For both concepts detailed analysis and experimental investigation have been conducted. Both concepts show promising results compared to state-of-the-art cooling systems, in terms of thermal performance and flexibility. The integrated design also leads to a lighter and more compact electronic product.

As thermal management systems are produced integrally, a significant cost reduction is reached. This is especially true for high volume production, where electronic manufacturing technologies, such as PCB production and SMD assembly, are appreciated for their low recurring cost. In the future, this allows engineers to design electronic products featuring full integration of thermal management systems and electronic circuitry.

This research pushes the boundary further toward more functionality in a smaller form factor for electronic products at a lower cost.

Samenvatting

Warmtebeheer speelt een steeds groter wordende rol binnen het ontwerpproces van elektronische producten. De afmetingen van de elektronische componenten worden kleiner, terwijl de prestaties en functionele eisen stijgen. Dit resulteert in meer warmte dissipatie op een steeds kleiner wordend oppervlak. Om deze groeiende warmteproblematiek te beheersen zoekt de industrie voortdurend naar koeltechnieken met verbeterde prestaties. Maar, omdat de thermische aspecten traditioneel pas aan het einde van het ontwerpproces aan bod komen, worden de toegepaste oplossingen om te koelen vaak simpelweg op het product gemonteerd. Hierdoor wordt de omvang van koelapparatuur van elektronica, vergeleken met de elektronische component die hij dient te koelen, steeds groter.

Dit proefschrift beschrijft het ontwikkelen van innovatieve concepten voor het koelen van elektronische producten. Thermische criteria worden reeds meegenomen tijdens de conceptuele ontwerpfase. Hierdoor worden meer geïntegreerde oplossingen gevonden. Deze multidisciplinaire aanpak is er op gericht verbeterde systemen voor warmtebeheer van elektronische producten te ontwikkelen, zowel in termen van thermische prestaties, als in termen van compactheid en flexibiliteit. Om tot een effectieve oplossing te komen, die bovendien kostentechnisch gunstig is, is gekozen voor het gebruik van gestandaardiseerde elektronische productieprocessen als *Printed Circuit Board* (PCB) en *Surface Mounted Device* (SMD) productietechnologieën. Met name bij grote productieaantallen is juist dit kostenaspect belangrijk. Hierdoor zijn namelijk toepassingen mogelijk voor een groot afzetgebied.

Dit onderzoek heeft geleid tot de identificatie van twee veelbelovende concepten voor het koelen van elektronische producten.

Het eerste concept – *directly injected cooling* – is gebaseerd op (jet) luchtkoeling. Door een instroomopening in de printplaat onder een elektronische component te maken, kan deze component direct vanaf de onderkant gekoeld worden.

Dit concept blinkt uit doordat het een grote componentdichtheid kan koelen. Bovendien is het mogelijk met dit concept de vele componenten op een elektronisch bord zowel onafhankelijk als gelijktijdig te koelen.

Het tweede concept – *integrated heat pipe cooling* – integreert een passief, tweefase mechanisme voor warmtetransport direct in een printplaat. De warmteoverdracht is gebaseerd op het principe van faseverandering. Daardoor is het mogelijk om grote hoeveelheden warmte te transporteren. De *heat pipe* is geconstrueerd in de gelamineerde structuur van de printplaat. Dit concept transporteert warmte, gedissipeerd door (meerdere) componenten op een printplaat, met zeer hoge efficiency door de structuur van de printplaat.

Voor beide concepten is een gedetailleerde analyse en experimenteel onderzoek uitgevoerd. Beide concepten laten, vergeleken met de huidige koelsystemen, een veelbelovend resultaat zien: goede thermische prestaties en grote flexibiliteit. Beide leiden ook tot een lichter and compacter elektronisch product.

Een significante kostenbesparing wordt gerealiseerd, omdat beide systemen voor warmtebeheer volledig geïntegreerd geproduceerd worden. Dit geldt met name voor grote productieaantallen omdat elektronische productietechnologieën zoals PCB-productie en SMD-assemblage erg aantrekkelijk zijn vanwege hun lage repeterende kosten. Ontwerpers kunnen hierdoor in de toekomst elektronische producten ontwerpen waarin warmtebeheer en elektronica volledig samengaan.

Dit onderzoek toont aan hoe, tegen lage kosten, in een elektronisch product, de beperkte ruimte optimaal benut wordt door meerdere functies geïntegreerd toe te passen.

Preface

“But I can assume you are taking on this Ph.D. project?”, those were the last words my professor asked me when I left his office after our first acquaintance four years ago. I guess I was playing hard to get by telling him I had to think about it. Nonetheless, I mumbled, “Yes”, confirming the beginning of this research.

As a Ph.D. student you know, it ain’t over till the book is done. Here we are, four years and exactly three months later. The book is finished! Contrary to what many others warned me about, it was not all that hard; it was actually very motivating and good fun. If at any time someone asks you, “Can I assume you are taking on this Ph.D. project?”, I would advice you to instantly say, “Yes!”

The reasons why it was such a positive experience probably lay in the people I had to work with. I guess this book, more than ever, is the appropriate place to thank them. Without their support, this book would not have existed.

The research described in this book was conducted not only at the Laboratory of Design, Production and Management of the University of Twente, but also at our industrial partner Thales Netherlands in Hengelo. Combining theoretical knowledge with practical expertise was a very pleasant approach. At first, you are thrown in at the deep end; there are however many experts nearby to help you out, exploring the unexplored.

I will start by thanking the people at Thales; especially the colleagues at the Surface Radar Department. In particular I must thank Jan Mannak. You were an inspiring figure to me. I am still amazed of your widespread, ready knowledge on components, materials, production techniques, you name it. Also, I have to thank Rob Legtenberg, for his spirited motivation to tackle any problem. Other people at Thales that I would like to thank are: Reinier, Gert Jan, Norbert, Simon, Ton, Maurits, Hans, Jan T., Bennie, Mark and Jan-Egbert, for the pleasant times and help throughout my research.

Also at our university there are many people I must thank. First of all, my professor and promoter for his trust and believe in my academic capabilities. In this light, I must also thank Tom Vaneker, my assistant promoter, for keeping me

on track during my research and for supporting me during the writing process. Wouter and Juan, the many interesting discussions we had made going to work a lot more pleasant. I am thankful you agreed to be my *paranimfen* and I am happy you will be standing next to me for the final stretch. Ashok, same project, same setbacks; I will be reading and commenting on your thesis next year. There are many other people I must mention here as well, too many to thank everyone by name. Colleagues from the *koffietafel* and roommates, thank you, for both the chats in between and the in-depth conversations from time to time. I am very joyful that I am staying on board as a university teacher with such great colleagues.

Several students also took a part in my research project. All of them have graduated by now. I must thank Mark, for his efforts to design and produce the heat pipe's integrated pressure gauge. Martijn for his work on the heat pipe's finite element analyses. Gerard, your work has contributed to the basis of Chapter 3. I can still remember the spontaneous enthusiasm when you showed us your initial (brainstorm) concepts. Pieter, for his work to optimize the heat pipe's wettability and wick structure properties, and for some of the very nice figures presented in this book. Bob, for developing (part of) the experimental set-up and doing many measurements to characterize our heat pipes. Thank you all.

I want to thank Sylvia for designing the cover of this book. She turned my vague ideas into this wonderful illustration, including photographs of some of the prototypes that were developed.

A special word of thanks also goes to the members of the promotion committee. I am thankful for your willingness to take a part in this committee. When you are reading through this book (again), you will probably find some of your feedback incorporated in the final version.

Last, but certainly not least, dank ik de onvoorwaardelijke steun van mijn ouders. Toos en Pim, wat boffen Egbert en ik toch met zulke ouders. Vanuit een veilig, warm huis konden we opgroeien tot waar we nu staan. Ik kijk uit naar onze gezamenlijke vakantie naar Indonesië om de bruiloft van Egbert en Nonie te vieren.

Oost (Enschede), West (Lelystad), maar thuis is het toch het best. Het is altijd fijn om thuis te komen, waar jij ook bent. Irma, je bent mijn steun en toeverlaat waar ik alles kwijt kan. Ik waardeer je nuchterheid, scherpte, aandacht en liefde, ook al kan ik dit niet altijd onder woorden brengen. Ik zie onze toekomst met plezier tegemoet, wie weet waar de liefde ons heen zal voeren.

– Wessel –

Table of Contents

Summary VII

Samenvatting IX

Preface XI

Table of Contents XIII

List of Abbreviations XVII

List of Symbols XIX

1 Introduction 1
- 1.1 Background 1
  - 1.1.1 Trends in Electronics 1
  - 1.1.2 Project Setting 4
- 1.2 Cooling Technologies 5
  - 1.2.1 State of the Art 6
- 1.3 Design Approach 9
  - 1.3.1 Traditional Design 10
  - 1.3.2 Thermal Aspects 11
  - 1.3.3 Multidisciplinary and Integrative Design 12
- 1.4 Goal 13
- 1.5 Outline 14

2 Development of Cooling Concepts 17
- 2.1 Introduction 17
  - 2.1.1 Thermal Constraints 18
- 2.2 Compact Thermal Model 20

2.3 Integrated Thermal Design Approach . . . 23
2.4 Concept Generation . . . 25
2.4.1 Cooling on the Opposite Side . . . 25
2.4.2 In-board Cooling . . . 26
2.4.3 Directly Injected Cooling . . . 27
2.4.4 Integrated Heat Pipe Cooling . . . 28
2.5 Conclusions . . . 29

3 Directly Injected Cooling **31**
3.1 Introduction . . . 31
3.2 Concept Embodiment . . . 33
3.2.1 Jet Optimization . . . 34
3.2.2 Thermal Jet Power . . . 36
3.2.3 Jet Pressure . . . 36
3.2.4 Design for High Component Density Cooling . . . 39
3.3 Prototype & Test Set-up . . . 40
3.4 Measurement Results . . . 42
3.4.1 Flow Measurements . . . 43
3.4.2 Thermal Measurements . . . 44
3.5 Concept Evaluation . . . 49

4 Integrated Heat Pipe Cooling **51**
4.1 Introduction . . . 51
4.1.1 Integrated Heat Pipe Construction . . . 54
4.2 Concept Embodiment . . . 56
4.2.1 Steady State Analysis . . . 59
4.2.2 Steady State Numerical Simulation . . . 62
4.2.3 Transient Analysis . . . 65
4.2.4 Transient Numerical Simulation . . . 69
4.2.5 Design for High Power Density Cooling . . . 73
4.3 Prototype & Test Set-up . . . 74
4.4 Measurement Results . . . 77
4.5 Concept Evaluation . . . 80

5 Evaluation of Presented Concepts **83**
5.1 Introduction . . . 83
5.2 Directly Injected Cooling Concept . . . 84
5.2.1 Synthetic Jet Cooling . . . 84
5.2.2 Modular System . . . 86
5.3 Integrated Heat Pipe Concept . . . 88
5.3.1 Rack Cooling System . . . 88
5.3.2 Other Embedded Heat Pipes . . . 90
5.4 Conclusions . . . 91

6 Conclusions & Recommendations 93
6.1 Conclusions . . . 93
6.1.1 Directly Injected Cooling . . . 94
6.1.2 Integrated Heat Pipe Cooling . . . 95
6.2 Recommendations . . . 96

List of References 99

Appendices

A Electronic Manufacturing Processes 107
A.1 Introduction . . . 107
A.2 Printed Circuit Board Production . . . 107
A.2.1 Via Production . . . 108
A.3 Surface Mounted Device Assembly . . . 110

B Test Set-up Directly Injected Cooling 113
B.1 Measurement Set-up . . . 113
B.1.1 Diode Calibration . . . 115
B.1.2 Jet Layouts . . . 115
B.2 Jet Measurement Datasets . . . 117

C Test Set-up Integrated Heat Pipe Cooling 121
C.1 Measurement Set-up . . . 121
C.2 Heat Pipe Measurements . . . 123

D Thermal Resistance Values 125
D.1 Electronic Package . . . 125
D.2 Ball Grid Array . . . 127
D.3 Printed Circuit Board . . . 127
D.4 Rack Cooling . . . 128

E Transient Energy Balance 129
E.1 Expanded Energy Balances . . . 129
E.2 Additional Elements . . . 130

F Fluid Flow Assumptions 131
F.1 Hydraulic Diameter . . . 131
F.2 Proof Laminar Flow . . . 132
F.3 Proof Incompressible Vapor Flow . . . 132
F.4 Vapor Friction Factor . . . 133
F.5 Liquid Friction Factor . . . 133

G Thermodynamic Properties **135**
G.1 Properties of Dry Air 135
G.2 Properties of Water 136

About the Author **137**
List of Publications 138

List of Abbreviations

APAR	Active Phased Array Radar
BGA	Ball Grid Array
CCA	Circuit Card Assembly
COTS	Commercial Off-The-Shelf
CPU	Central Processing Unit
FC	FluoroCarbon
FR-4	Flame Retardant 4
IC	Integrated Circuit
JEDEC	Joint Electronic Device Engineering Council
LCP	Liquid Crystal Polymer
NCG	Non-Condensible Gas
PACMAN	Phased Array Communication antenna for Mass-market Application Needs
PCB	Printed Circuit Board
RF	Radio Frequency
SMD	Surface Mounted Device
TEC	Thermal Electric Cooler

List of Symbols

A	area	$[\mathrm{m}^2]$
c_p	specific heat	$[\mathrm{J/kgK}]$
d	diameter	$[\mathrm{m}]$
e	specific internal energy	$[\mathrm{J/kg}]$
F	force	$[\mathrm{N}]$
F	heat pipe friction factor	$[\mathrm{s/m^4}]$
f	Fanning friction factor	[-]
fRe	friction factor	[-]
g	gravitational constant	$[\mathrm{m/s^2}]$
H	jet-to-target spacing	$[\mathrm{m}]$
H	vapor height	$[\mathrm{m}]$
H_{fg}	specific latent heat of vaporization	$[\mathrm{J/kg}]$
h	groove height	$[\mathrm{m}]$
h	heat transfer coefficient	$[\mathrm{W/m^2K}]$
h	liquid height	$[\mathrm{m}]$
k	thermal conductivity	$[\mathrm{W/mK}]$
L	length	$[\mathrm{m}]$
Ma	Mach number	[-]
m	mass	$[\mathrm{kg}]$
$\dot{m}$	mass flow	$[\mathrm{kg/s}]$
N	number of grooves	[-]
Nu	Nusselt number	[-]
n	number of jets	[-]
P	pressure	$[\mathrm{Pa}]$
Q	energy, heat	$[\mathrm{J}]$
$\dot{Q}$	power, heat transfer rate	$[\mathrm{W}]$
R	thermal resistance	$[\mathrm{K/W}]$
Re	Reynolds number	[-]

r	radius	[m]
s	ridge width	[m]
T	temperature	[K] or [°C]
t	thickness	[m]
t	time	[s]
U	velocity	[m/s]
V	volume	[m^3]
W	vapor width	[m]
w	groove width	[m]

Subscripts

a	adiabatic
avg	average
c	condenser
cap	capillary
cond	conductive
conv	convective
diss	dissipated
e	evaporator
eff	effective
eq	equivalent
ex	exchange
fc	forced convection
fg	phase change
g	gravity
h	hydraulic
i	liquid-vapor interface
l	liquid
max	maximum
nc	natural convection
p	package
r	reference
s	source
ss	steady state
v	vapor

Greek symbols

α	aspect ratio	[-]
Δ	difference	[-]
ϵ	area ratio	[-]
γ	inclination angle	[rad]
μ	dynamic viscosity	[Ns/m^2]
ν	kinematic viscosity	[m^2/s]
φ_v	volumetric flow rate	[m^3/s]
ρ	density	[kg/m^3]
Σ	sum	[-]
σ	surface tension	[N/m]
θ	contact angle	[rad]

Chapter 1

Introduction

In this thesis, conceptual cooling solutions for electronic products are researched. This chapter discusses the background of this research. It introduces the project setting and current state of the art in electronics cooling. Also, the design approach that has been applied is discussed. At the end, the research goal of this study and outline of this thesis are presented.

1.1 Background

The last two decades, thermal management is becoming *the* challenge area in electronic product design. Worldwide, both consumer and industry continuously demand more functionality, better performance and increased product miniaturization. As a result, power dissipations increase on even smaller surfaces, thus intensifying local heat fluxes. To cope with these growing thermal issues, the thermal design process of electronic products plays an increasingly dominant role in the total design process.

In this thesis, novel cooling strategies that can be applied in the electronic product design are explored. However, as modern electronic products are often compact and complex systems, this is easier said than done.

1.1.1 Trends in Electronics

Electronic products are controlled by their Integrated Circuits (ICs), formed by a collection of transistors. Looking at the history of electronic products, we see that the transistor density increased at an incredible pace. In the 1950s the first semiconductor IC integrated a large number of tiny transistors into a chip. This replaced the manual assembly of discrete components used until that time, thus cutting down tremendously on production time and cost, as well as product sizes. In 1965, Moore [42] believed the number of transistors in a chip (a measure for

Figure 1.1: *Moore's law; data from Intel [25, 35].*

the computational performance) would double every year. By now, Moore's law has been corrected to double the number of transistors every 2 years. The solid line in Figure 1.1 shows this trend for CPU processors produced by Intel.

According to Moore's law, the number of transistors integrated into one IC is expected to pass one billion around 2008-2009. To sustain this rate and continuously achieve the increased computational performance demanded, feature sizes decrease and the IC runs at higher frequencies. As a consequence the IC's required power input increases as well. This trend, shown in Figure 1.1 by the dashed line, approximately doubles every 3 years [35]. According to the Uptime Institute [4], the latter trend will cause "the economic meltdown of Moore's law", as "by 2009, the 3-year cost of electricity per server will exceed the purchase cost of the server".

In operation, all transistors crammed together generate heat which must be extracted from the IC. As the power leakage of ICs is an appreciable percentage of the overall power input [37], the amount of dissipated power also increases according to the aforementioned power trend. Until two decades ago, this was not seen as a problem as Moore stated in his publication [42]: "Since integrated electronic structures are two-dimensional, they have a surface available for cooling close to each center of heat generation." The transistor or junction temperature of ICs remained low enough to guarantee a reliable product, throughout its life expectancy.

However, by now this assumption no longer holds. The continuous increase in

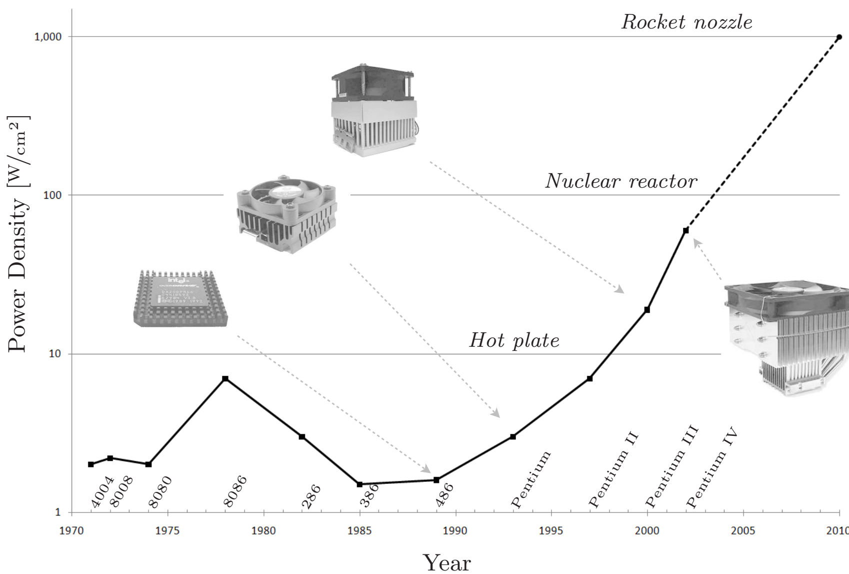

Figure 1.2: *Power density; data from Vassighi [60].*

transistor density and power, also resulted in an increase in power density. Thus as computational performance advances, internal heat fluxes also increase. The dramatic effect of this trend is shown in Figure 1.2, where the power density of the same CPU processors of Figure 1.1 is shown. According to Vassighi [60], around 2010 the power density of a microprocessor will reach the level of a rocket nozzle (1,000 $^{\mathrm{W}}/_{\mathrm{cm}^2}$).

To effectively manage the heat dissipation of ICs, a wide variety of cooling concepts and equipment has been developed, of which some examples are shown in Figure 1.2. By now, these cooling devices are becoming quite large in size, especially compared to the chip's dimensions they are supposed to cool. Furthermore, recent surveys show increasing amounts of power are consumed by cooling issues, instead of a primary task as computing [23, 67], thus strengthening the notion of an economic meltdown.

Although the trends presented in Figures 1.1 and 1.2 apply to high-performance microprocessors (such as CPUs), electronic components in general also suffer from this development. For instance, where in the past only CPU cooling was required for personal computers, now graphics card, memory and other chips need to be cooled as well. This indicates serious challenges for the design of future cooling systems and electronic products, especially since the demand for ultra thin, compact products is growing. Thermal management of local hot spots on high-performance chips (i.e. non-uniform cooling), as well as uniform cooling of entire electronic products needs to be considered.

1.1.2 Project Setting

Electronic products are developed in all sorts and sizes. Companies in the business of developing these products obviously require electronic components, for which they rely on the semiconductor industry. In fact, the ICs produced by the semiconductor industry can be considered Commercial, Off-The-Shelf (COTS) components nowadays. However, the thermal effects, illustrated in the previous section, greatly influence the packaging of these components within their respective products. Moreover, as stipulated, these effects will eventually affect the entire design of electronic products; something companies developing electronic products must anticipate.

The research presented in this thesis is part of a larger project* aiming to develop a Phased Array Communication antenna for Mass-market Application Needs (PACMAN). The project focuses on the design considerations and manufacturing methods, when shifting from one-off to mass-market production of phased array antennae, a very complex electronic product.

Phased Array Antenna

The combined elements of a phased array antenna have the ability to electronically direct (e.g. steer, focus) its beam(s), as illustrated in Figure 1.3. Because the antenna surface does not have to physically move (i.e. rotate), this results in a highly flexible and fast responding antenna system. Until now, these antenna systems have been used mainly for "high-end" applications, such as radar systems (defense industry) and radio telescopes (astronomical science), particularly due to their high manufacturing cost. The goal of the PACMAN project is to produce these antenna systems much more affordable by implementing the latest advances of the semiconductor industry and by designing for efficient mass-production technologies. This innovation would enable the application of phased array antennae in other domains as well, such as telecom, wireless internet and automotive, among others.

The design of a phased array antenna system is highly complex, as it involves the collective knowledge of many engineering disciplines. Especially in the case of modern radar systems, for instance the Active Phased Array Radar (APAR), where both transmit and receive functionality of the electromagnetic signal is integrated into a single antenna system. To produce the next-generation APAR economically competitive, more power, to increase range, accuracy and speed, is required at low cost. This implies – among many things that fall outside the scope of this study – the use of more powerful, and thus more heat dissipating, COTS electronic components. However, as the currently developed thermal management systems for these components require more and more space, they are in conflict

* The project consortium consists of one industrial partner: Thales Netherlands, and three scientific institutes: the Netherlands Institute for Radio Astronomy (Astron), the University of Eindhoven (TU/e) and the University of Twente (UT).

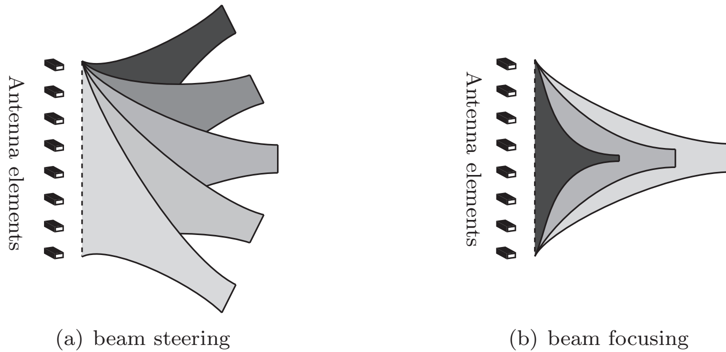

(a) beam steering (b) beam focusing

Figure 1.3: *Electronic beam directing of a phased array antenna.*

with the antenna features, predominantly constrained by electromagnetic requirements. For instance the use of add-on cooling devices, as shown in Figure 1.2, in an APAR is not viable, due to geometrical, practical, weight and cost issues; especially since an affordable, mass-market antenna system is considered.

Hence, the research presented in this thesis was initiated to explore and to develop novel cooling strategies for complex electronic products, entangled by many restricting and often contradicting criteria. However, as the global demand for more compact and powerful electronic products continuously increases, the explored cooling strategies will also be applicable to electronic products in general. As electronic components are considered COTS, emphasis is put on both their packaging and the design of the entire electronic product, including its cooling system. In order to keep cost down, the developed cooling concepts should have minimum impact on the current electronic production technologies. As each additional production technology requires (financial) investment, well-established and mainstream fabrication processes, which will be defined in Chapter 2, are adhered.

1.2 Cooling Technologies

Until now, cooling via (forced) convection of air is used for many applications, as it is relatively straight-forward, cost effective and safe to implement. However, using this principle the required cooling performance cannot always be achieved, due to physical limitations in heat transfer capabilities. As heat dissipations will continue to increase, switching to alternate cooling principles, with increased heat transfer capabilities, seems unavoidable. Some potential principles in the temperature region of interest for electronics cooling (i.e. 0-100°C are shown in Figure 1.4. Here, the theoretical attainable heat transfer coefficients, as presented by Bejan [3], are shown for air and water, the most common coolants.

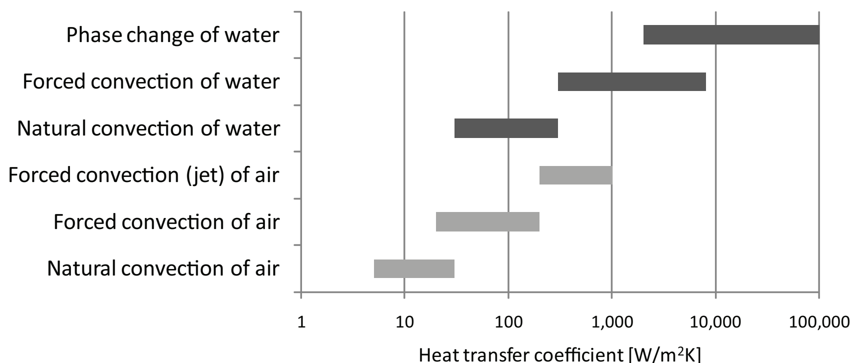

Figure 1.4: *Heat transfer coefficients per cooling principle; data from Bejan [3].*

As mentioned, the use of air is quite common for electronics cooling; however, its performance is limited. In an effort to stretch this limit, heat sinks are developed to have larger heat exchange areas and enhanced coolant flow. This trend can also be observed from the cooling devices that are shown in Figure 1.2. As Figure 1.4 suggests, improved heat transfer coefficients can be obtained by means of water cooling. As the medium is denser, it can absorb and transport more power (heat). Depending on thermodynamic properties, other fluids (e.g. alcohol or glycol) follow similar trends; however, the applicable temperature region may shift accordingly. The best performance, known at this point in time, can be achieved by phase change behavior, as during vaporization and condensation large quantities of heat are either absorbed or released, respectively.

1.2.1 State of the Art

While Figure 1.4 gives a general impression of attainable heat transfer coefficients based on the applied cooling principle, in practice its functionality is limited. As long as parameters such as area (or volume) and temperature gradient are unconstrained, virtually any device can be cooled via natural convection of air. Cooling capacity of a design in terms of power density, in combination with volumetric and thermal characteristics, is more useful. Furthermore, the complete electronic product will dictate an appropriate volume and cost for the cooling system in terms of material and production. Also, the cooling system must comply with overall product standards, such as reliability, acoustic emissions, etc.

Henceforth, a summary of available cooling systems is given – some albeit in a lab environment – for each of the cooling principles of Figure 1.4. They are considered state of the art at this point in time. Also, some of the most important design challenges are mentioned.

Natural Convection of Air

As no additional driving mechanism is required, *natural convection of air* is the preferred way of cooling. Many electronic devices, such as stereo-sets, TVs, LCD-screens and others, rely on this mechanism. However, even with a heat sink, total heat fluxes are limited to approximately 0.05 W/cm², which makes this principle rather unsuitable for high power components.

Forced Convection of Air

In this category, the *heat sink & fan* is the most common form of electronics cooling. With a standard fan, a cooling capacity of about 1 W/cm² can be achieved. For a specially designed heat sink, similar to the ones in Figure 1.2, around 50 W/cm² can be reached [32]. As a rule-of-thumb, the larger the required capacity, the bigger the device. Its design is relatively straight-forward, cost effective and safe to implement; hence, its widespread use nowadays. Non-thermal limits are mainly in the area of maintenance and redundancy. As every fan is bound to stall at a (un)certain point in time, periodic maintenance and perhaps some downtime must be acceptable. In some industries, for instance the defense industry, this is unacceptable.

A more reliable mechanism is the *piezo fan* [51]. A blade is vibrated by the piezo effect and induces an airflow. It has a small form factor and gives a 100% enhancement (0.1 W/cm²) compared to heat transfer based on natural convection [32]. The piezo fan requires only a low voltage (12-15 VDC) and uses little power. Moreover, it is very reliable.

Another method to induce airflow is through *nanolighting*. Here, two electric fields generate a micro-scale ion driven airflow. Such a device is small enough to implement on a chip, with possible heat fluxes around 40 W/cm² [32]. Even though it is quiet, a substantial voltage is required for ionisation. Thorrn Micro Technologies [58] expects to have a cooling device based on this technology available on the market around 2009.

Finally, *gas expansion* may be used to cool components [48]: when non-ideal gases expand, they absorb energy. This is also known as the Joule-Thomson effect. However, best efficiencies are achieved at relatively low temperatures, generally too low for electronics cooling. Also, relatively high pressures are required.

Jet Air Cooling

By locally breaking through the thermal boundary layer, higher heat transfer coefficients can be attained. *Jet impingement* is possible by jetting air (10-100 m/s) against a hot surface. The jet is induced by forcing conditioned air through a nozzle. With an external compressor, used to induce the airflow, heat fluxes up to 60 W/cm² can be cooled. This is approximately the limit for air cooling in general [62].

Through a pulsating diaphragm a *synthetic jet* can be realized, small enough to implemented in a heat sink. This way, cooling of heat fluxes up to 17 $^{W}/_{cm^2}$ can be realized [36]. Non-thermal limits for jet air cooling are practical implementations and undesired noise levels (acoustic emissions).

Liquid Cooling

Through liquid cooling, heat can be transported away from hot components either indirectly, the coolant is pumped through a heat exchanger, or directly, where the coolant is in direct contact with the electronics. For *indirect liquid cooling* heat transfer values improve as smaller feature sizes in the heat exchanger are used. However, this also requires higher pumping pressures. Heat fluxes up to 100 $^{W}/_{cm^2}$ can be realized [32]. Common fluids are water, alcohols, glycol and liquid metals. Non-thermal design issues are reliability and practicality. Unlike air, liquid needs to be returned; also leakage of a conductive liquid, such as water, leads to short circuits. To prevent short circuits for *direct liquid cooling*, either a dielectric liquid, such as FluoroCarbons (FCs), must be used or all electronics needs to be sealed.

Analogous to air, *liquid jet impingement* also improves heat transfer significantly. Power density values up to 120 and 460 $^{W}/_{cm^2}$ have been reported for FCs and water, respectively [15]. *Spray cooling*, where a special nozzle nebulizes the liquid into tiny droplets, results in a more uniform temperature distribution compared to jetting. Here, values up to 60 $^{W}/_{cm^2}$ are feasible [15].

In research labs, the use of microchannels produced directly on ICs has further improved heat flux values up to 1300 $^{W}/_{cm^2}$ locally on the chip. Other forms of liquid cooling are *vibration induced droplet atomization* (up to 420 $^{W}/_{cm^2}$) and *electrohydrodynamic cooling* (up to 90 $^{W}/_{cm^2}$) [32]. These latter forms are mostly demonstrated in laboratories and by research projects. Although these values are relatively high and seem promising, they are local power densities; therefore, the practical challenge is to bridge the micro-scale cooling system to a macro-scale heat exchanger. Some devices are becoming commercially available; however, most are specially designed and therefore certainly not low cost.

One other form worth mentioning is the *compression cycle*, known from refrigerators. This can also be applied for electronics cooling. A fluid absorbs heat at a low pressure and releases it at a higher pressure. Also phase change of the fluid is possible. However, similar to indirect liquid cooling, reliability and practicality are important design issues in this case as well.

Phase Change Principles

The highest (macro-scale) heat transfer values, known at present, can be achieved by phase change principles. As a liquid evaporates, it absorbs large quantities of heat. The vapor caused by the evaporation is transported to other locations, where the latent heat is recovered as the vapor condenses. This is the general mechanism by which *heat pipes*, *loop heat pipes*, *vapor chambers* and *ther-*

mosyphons operate. All of them are capable of reaching values of 300 $^{W}/_{cm^2}$ and beyond [32].

The design of such a heat transport system, in general, requires more work. A delicate structure to return the condensate to the evaporator region is required, often complicated by gravitational and frictional effects. Its form factor is relatively small, and, as it is a passive device that requires no external pump or fan, when properly designed, it is very reliable and maintenance free. Although production and charging requires precision work, especially for miniature sizes [59], this type of cooling system is already implemented in many modern high power electronic devices, such as notebooks, game consoles and others. It is also used for products requiring a high reliability without frequent maintenance intervals, such as satellite systems.

Other Coolers

One type of cooling device not mentioned so far are solid state coolers. The *Peltier element* or *Thermal Electric Cooler* (TEC) is probably the best known. Though very useful for (fine)tuning of cooling power, their efficiency is low due to the fact that the power it consumes and dissipates to operate must also be transported away. As such, they are not practical for continuous cooling.

Other types of coolers worth mentioning are, among others: *magnetic refrigeration*, *cryogenic microcooling* [6], *thermotunneling* (hot electrons over a vacuum), *thermoacoustic refrigeration* (oscillation of an inert gas) and *phase change material* (emergency cooling through melting) [32]. However, for the cooling of (COTS) electronic components, these types lack either the appropriate temperature range, practical dimensions or continuous cooling capability.

1.3 Design Approach

The state of the art, presented in the previous section, has led to the development of many advanced cooling systems. However, most developed systems focus primarily on thermal criteria and the maximization of the cooling heat flux. In other words, they try to develop improved cooling solutions to be utilized on existing electronic products (i.e. add-on cooling devices). As no real integrative action is applied, electronic component and electronic product design from a thermal point-of-view does not evolve fast enough. Consequently, as thermal properties are getting more stringent, electronic engineers focus on designing energy saving and less dissipating components. This monodisciplinary action will result in small (temporary) relief; however, a giant leap in electronic product design will not be realized.

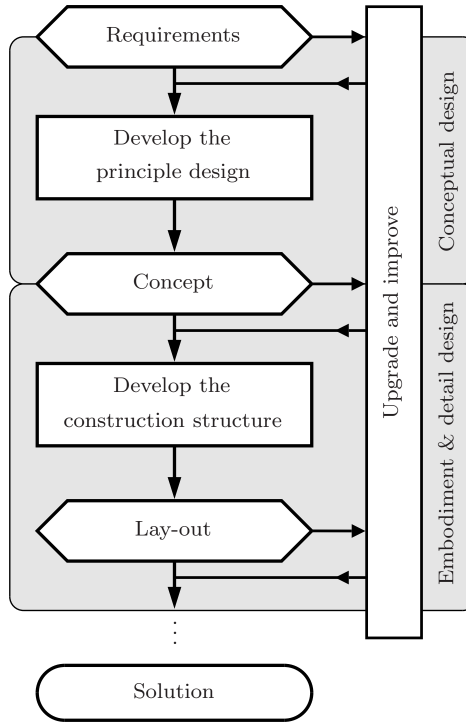

Figure 1.5: *Design process according to Pahl & Beitz.*

1.3.1 Traditional Design

When designing, traditionally one tries to progress from requirements to an acceptable solution that is as optimal as possible. According to Pahl & Beitz [46] – "presumably the most familiar model for the design phase, widely used in industry" [34] – during the design process several phases are completed. Figure 1.5 illustrates a condensed version of this design process. First, during the conceptual design phase a principle design is developed based on the requirements. The resulting concept is then further developed during the embodiment and detail design phase. Continuous upgrading and improving is possible during all design phases, until a solution is finally reached.

During the conceptual design phase, a concept is developed that fulfills the primary functions of the product. Whereas during the embodiment and detail design phase this concept is given its detailed description. The latter phase is illustrated more elaborately in Figure 1.6. Through a synthesis process the concept is developed into a distinct embodiment, which incorporates specific product form and dimensions. This detailed description is required for the analysis process, which predicts product performance. Finally, in an evaluation process these

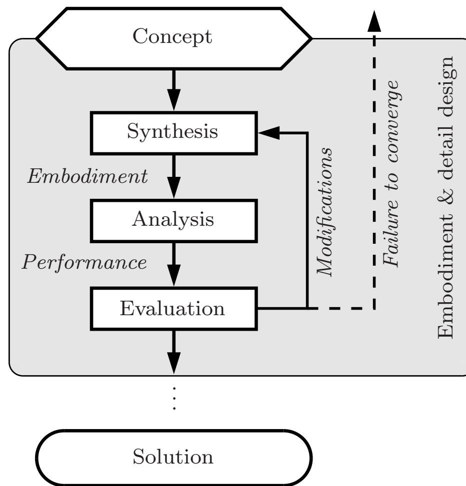

Figure 1.6: *Embodiment and detail design phase.*

performances are compared to the initial specifications. To optimize product performance, the embodiment may be modified by returning to the synthesis process, after which the altered version is analyzed and evaluated again. Depending on the number of iterations, an optimal embodiment (the solution) of a (one) certain concept is reached.

Industry generally prefers to stick to tried and tested concepts, as this gives a short time-to-market at minimal development cost. Pugh [50] refers to this as "cut and run", as engineering is started before the conceptual design phase is thoroughly examined. This applies also to the electronics industry, where today's product is dispensable in 2 to 3 years time. Hence, they concentrate on the embodiment and detail design phase for their product development. The iterative loop shown in Figure 1.6 is sometimes also referred to as a trial-and-error approach.

When requirements are updated, proven concepts might not be able to fulfill these specifications and the design process will fail to converge to an acceptable solution. Subsequently, to reach an acceptable solution, one has to return to the conceptual design phase to develop new concepts. This is indicated by the dashed line in Figure 1.6. Needless to say, this is more time consuming and costly; hence, the industry tries to avoid this.

1.3.2 Thermal Aspects

As thermal management aspects, until recently, scarcely impeded an acceptable product design, thermal analyses were addressed toward the end of the design process or not at all. Cooling was considered a support function, as it supports the

primary functions. Consequently, cooling should not impede primary functions, as this leads to an unrealizable concept design. When thermal limits became increasingly critical, issues were initially addressed only in the embodiment and detail design phase. As the concepts themselves did not evolve, product changes were relatively small; hence, the ever-growing heat sinks.

Until now, the electronics industry has primarily relied on improved (growing) heat sink designs and as long as there is ample space to accommodate such cooling devices, this tendency will probably continue. Some have integrated (phase change) heat spreaders to enhance heat distribution. Also heat pipes, which transport heat very efficiently, are commonly used to physically separate heat source and heat sink from their respective locations. Other technologies, for instance liquid or jet cooling, have been used only in small numbers, as at present it still has many practical issues, regarding reliability, flexibility, high-volume production and cost. However, as at present the basic concept of many electronic products is still not influenced by the thermal aspects, they all have one commonality: a cooling device is considered an add-on device.

Many reviews indicate that thermal control has already become a critical factor in the design of electronic equipment. For instance for mobile phones, thermal management is a critical issue since the 1990s. Especially in the case of lengthy call durations and with respect to battery usage, the loss of reliability due to increased internal temperatures was significant. According to Yeh [65] in 1995 more than fifty percent of all electronics failures are caused by undesirable temperature control. As air cooling of electronics is reaching its limits, researchers are exploring ways to extend this limit. Bar-Cohen [1] believed in 1997 that enhanced, air-cooled heat sinks and passive immersion modules were two distinct thermal packaging technologies that may play a pivotal role in future electronic systems.

1.3.3 Multidisciplinary and Integrative Design

Continuing to focus on thermal issues as a support function eventually will lead to conflicting requirements. The persistent growth of thermal management systems, such as heat sinks, contradicts the development of – in particular small and compact – electronic products. Especially for high power electronic products this means product dimensions and positioning of components are no longer determined by primary functions; instead the embodiment will be strongly affected by thermal criteria, a support function. Moreover, as mentioned, product design may even fail to converge, due to thermal constraints.

To solve these issues, a more substantial thermal engineering effort, earlier in the design phase, thus further integrating primary and support functions, is required. The design of electronic products in a monodisciplinary manner, for instance by focusing on electrical aspects only, should be avoided. Instead, a multidisciplinary and integrative approach must be utilized in order to achieve an optimal system configuration.

A first step toward such a multidisciplinary and fully integrated design pro-

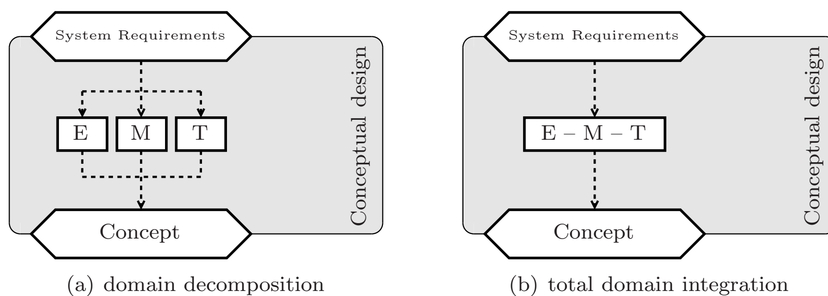

(a) domain decomposition

(b) total domain integration

Figure 1.7: *Conceptual design phase for a phased array antenna.*

cess is to decompose the system requirements according to the domains involved. Figure 1.7(a) illustrates this for electronic products, where electrical (E), mechanical (M) and thermal (T) engineering aspects are considered. In the case of a phased array antenna system, this is augmented by electromagnetic aspects. The combined knowledge of these domains has an influence on the conceptual design phase. However, as they are still considered separate and do not share a mutual engineering "language", even small changes in one domain can have profound effects in other domains. This is not the case for total domain integration, as is illustrated in Figure 1.7(b), where system requirements are no longer decomposed into separate blocks. The knowledge of the engineering disciplines involved is directly related to each other and a mutual language has been developed. Evidently, both cases require in-depth and coherent knowledge of the engineering fields involved. At present, the latter conceptual design phase is still an abstract, hypothetical case.

In this thesis, special consideration is given to the thermal engineering contribution in combination with the existing electrical and mechanical knowledge present within the project consortium. Cooling concepts for electronic products are explored, considering thermal aspects at the very beginning of the design phase. As thermal aspects are more integrated, cooling systems will not necessarily be considered an add-on device. Although, the development of a mutual engineering language is not the direct aim of the current study, it certainly is a future prospect.

1.4 Goal

In this thesis, we will *not* try to develop yet another improved heat sink. Instead, the multidisciplinary and integrative design approach discussed in the previous section is adopted. Through this approach, a level of product integration previously unseen in cooling solutions is aimed for. However, this integration should not be at the cost of flexibility. Still an overall flexible design in terms of scalability,

electronic component layout and electronic product embodiment is demanded.

Not discussed in detail so far, but of equal importance to the electronic product evolution is the industries' ability to continuously reduce cost. Standardized electronic production technology is based on batch processes with low recurring (variable) costs. Especially for high product volumes, these manufacturing techniques are very cost effective. Therefore, on average, new electronic products do not only perform better, they also cost relatively less. This trend should not be impeded by the required cooling devices. Therefore, our goal is not only an integrated cooling system with improved performance capabilities, but also a cost effective one.

The aim of this research is to apply a multidisciplinary and integrated design approach to the future development of thermal management systems for electronic products. The focus will be on adopting thermal aspects into the conceptual design phase, where electrical and mechanical aspects have prevailed from day one. New concepts should result in a more compact product design with advantages in terms of performance, weight and production efficiency. Also, a substantial (factor 3-10) cost reduction for the complete electronic product is sought-after.

1.5 Outline

The development of several conceptual cooling solutions will be described in the next chapter. A general overview of the electronic products and manufacturing techniques considered is presented. Two thermal constraints are identified that are representative for most thermal design issues. An insight is given into the present thermal behavior and bottlenecks of an electronic product. Finally, some innovative concepts are developed and evaluated.

In Chapter 3 the first of two promising cooling techniques is described. This concept is based on the principle of jet air cooling. A conceptual embodiment is presented for this concept. Some design rules to determine an optimal heat transfer coefficient are given. The prototype developed for the experimental investigation is presented together with the measurement results. Finally, the results are discussed and the concept is evaluated.

In Chapter 4 the second of the two promising cooling techniques that have been identified is described. This concept is based on the principle of phase change behavior of fluids. For this concept, an embodiment and design rules to optimize heat transfer are also presented. A prototype will be shown together with the measurement results. Finally, the results will be discussed and the concept will be evaluated.

Both concepts developed are compared to current state-of-the-art electronic cooling systems in Chapter 5. The evaluation is based on cost, thermal performance and compactness. Also, some redesign approaches are illustrated to incorporate the novel cooling concepts into a real electronic product.

Finally, Chapter 6 will present the conclusions of the design strategy adopted

in this research. Also, a wrap-up is given for both the developed cooling concepts. At the end, some recommendations for the further development of the presented integrated cooling concepts into future industrial applications are given.

Chapter 2

Development of Cooling Concepts

This chapter describes the development of two novel cooling concepts. From a thermal perspective, two extreme cases will be considered: high component density cooling and high power density cooling. The former case results in a concept based on jet air cooling, whereas the latter case can be managed through a concept based on phase change principles. The compact thermal model, which will be used in this thesis, is also discussed.

2.1 Introduction

Although electronic products exist in all sorts and sizes, inside a (multilayer) Printed Circuit Board (PCB) connecting all components generally forms the backbone. It serves as a carrier, holding all components in place and through its integrated circuitry it also connects these components electronically. In the electronics industry, multilayer PCB technology is considered an established mass-market production method, appreciated for its high degree of integration of mechanical and electronic functions. A typical multilayer PCB consists of polymeric layers pressed together with bonding layers in between. On each polymeric layer, a conductive pattern can be produced, through which all components can be connected electronically. The top and bottom sides of the PCB is used for the assembly of these components, such as ICs, resistors, connectors and others. Together this forms a Circuit Card Assembly (CCA).

Figure 2.1 shows a general view of a such a CCA. Here, two Surface Mounted Devices (SMDs), a resistor and an IC, are assembled on top of a multilayer PCB. The components are positioned and soldered onto the surface. The solder connection realizes a mechanical fixation, as well as an electrical contact. Routing of the

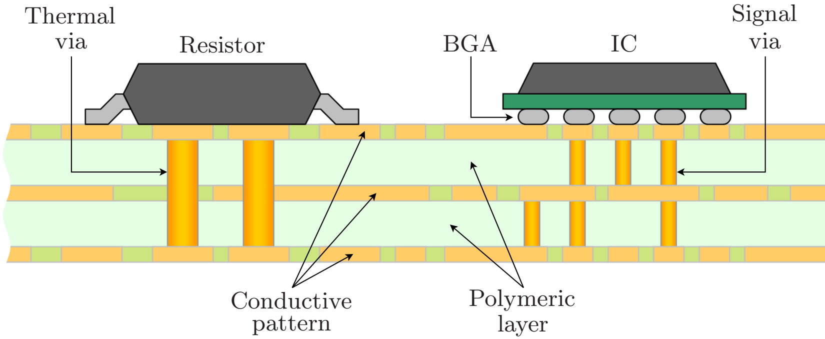

Figure 2.1: *Schematic cross section of a Circuit Card Assembly (CCA).*

electronic signals through the PCB is realized by the conductive pattern on each layer and plated holes (signal vias) connecting both sides of a layer. The number of layers is determined by the complexity and number of (inter-connecting) components that need to be placed on the board. As the polymeric layers are generally poor thermal conductors, this hampers the transport of heat dissipated by the mounted components. This is one of the reasons why the top surface of electronic components is often used for the extraction of heat.

To transport heat more efficiently through the board structure, thermal vias can be positioned directly below high-dissipating components. In fact, adding additional amounts of metal and using thicker metallic layers is generally seen as a genuine method to enhance cooling capabilities through board structures. Needless to say, this is not very weight efficient.

SMD components interface with the board through various standardized packaging types. For instance, the IC in Figure 2.1 is connected by a Ball Grid Array (BGA). At present, the BGA is one of the common packaging types used by the industry. Solder balls are placed between the board and the IC to facilitate the mechanical and electronic connection.

A more elaborate description of the electronic manufacturing processes considered well-established and mainstream throughout this thesis is presented in Appendix A.

2.1.1 Thermal Constraints

As electronic products often contain multiple components, the design of two extreme cases, from a thermal perspective, can be considered:

- High component density cooling
- High power density cooling

For example, in the first case many components are packed together on a board. As illustrated in Figure 2.2(a), the increased component density limits the avail-

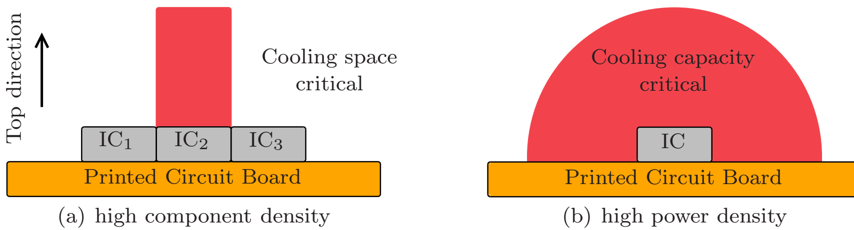

Figure 2.2: *Two extreme cooling cases considered.*

able cooling area to about the size of the component, which in turn limits the size of the heat sink. Hence, the miniaturization of electronic products and the increasing density of components causes a challenge in the thermal design, as cooling space gets critical. In the second case, a high power component is placed on a board, such that cooling of this single component already causes a challenge. This is illustrated in Figure 2.2(b), where sufficient space is available, however no conventional heat sink has the required capacity to cool this component. Evidently, in practice, these two cases do not portray a black-and-white scenario. Both merge in a transition area, where design engineers face the challenge to cool a relatively dense board with relatively high power components.

Traditional (low cost) cooling concepts primarily make use of the top direction, as implicitly considered in Figure 2.2. The continuous increase in component and power densities leads to exorbitant requirements of proven cooling concepts, in terms of size and weight. Moreover, these concepts start to dictate overall product dimensions. Therefore, to develop a more compact cooling solution a multidisciplinary design approach, where concessions in other domains are considered, is utilized here. For the new cooling concepts explored accordingly, other directions are logically also considered. For instance, to produce more compact products the bottom direction, in particular, seems interesting. However, this will require careful integration, as then all requirements (electrical, mechanical and thermal) make use of this direction simultaneously.

Before new cooling concepts are explored based on the design approach discussed, a more detailed view of a mounted component is considered. Figure 2.3 illustrates a more elaborate view of the BGA package type shown before. The heart of the package is formed by the IC, also referred to as the (bare) die. Here, all active electronic processes take place, and thus all heat is also generated here. As packaging requirements make it often impossible to attach an IC directly to the PCB, a rigid laminate is used in between. Electronic signals to and from the IC run through bondwires to the intermediate rigid laminate. The vias in the laminate and the BGA further connect the IC to the PCB. Finally, to protect both the IC and the bondwires from the environment, the package is encapsulated by a mold compound.

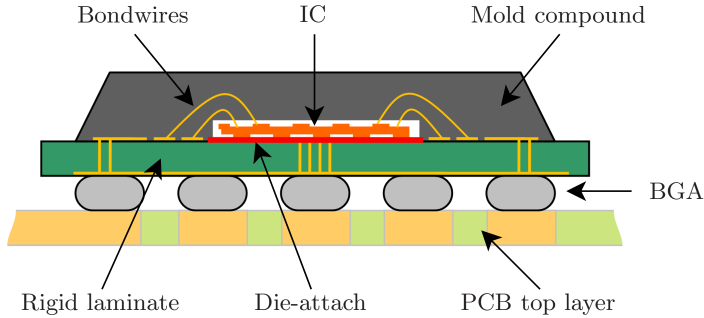

Figure 2.3: *Schematic of a Ball Grid Array (BGA) package.*

2.2 Compact Thermal Model

To illustrate the thermal behavior of a very basic electronic product, a board with (just) one component is considered. The component, a BGA package, is mounted in the center of a board retained on two opposite sides. Heat from the component can be dissipated either (or both) through the top of the package via a heat sink to the ambient air, or through the package and the board to the rack structure. Here, liquid water cooling, instead of air cooling, can be assumed. Figure 2.4 shows a cross section of such an electronic product, including both general heat flow trajectories. Note that this is just an initial experimental thought to identify possible cooling concepts.

To model the basic thermal characteristics of the complete assembly, a nodal representation is used. A generalized model, where distinct component parts or interfaces are represented by a node, is constructed to identify thermal bottlenecks early in the design phase. However, in a later stage a nodal representation can also be used to construct a very detailed model, similar to a finite element

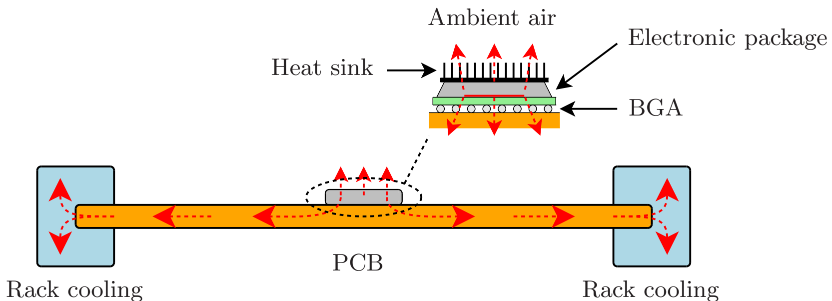

Figure 2.4: *General cooling trajectories for electronic packages.*

analysis. Each node contains properties about its temperature. The temperature gradient across nodes drives the thermal transport capability between nodes. This representation resembles the resistance network found in electronic connections, where voltage across nodes drives a current between nodes. Fourier's law of conduction and Newton's law of cooling are used to determine the thermal resistance between nodes, similar to Ohm's law being used to determine electrical resistance. In a unidirectional, integrated form both laws transform to relatively simple linear relations. The rate of heat transfer for Fourier's and Newton's laws are shown in the following equations, respectively:

$$\dot{Q} = \frac{k \cdot A}{L} \cdot \Delta T \tag{2.1}$$

$$\dot{Q} = h \cdot A \cdot \Delta T \tag{2.2}$$

where k and h denote the thermal conductivity and heat transfer coefficient, respectively. The former is used to calculate heat transfer through a material (conduction), whereas the latter is used to calculate heat transfer across an interface or when heat is transfered to another medium (convection). ΔT equals the temperature gradient between the nodes in question. Also, geometric features such as the heat exchange area (A) and the conductive length (L) have an influence.

The thermal resistance (R) between nodes is defined as the temperature drop per unit of dissipated power. For a conducting path through a material with known dimensions and thermal conductivity, Equation (2.1) can be rewritten, to determine the path's thermal resistance, as:

$$R_{cond} = \frac{\Delta T}{\dot{Q}_{diss}} = \frac{L}{k \cdot A} \tag{2.3}$$

where $\dot{Q}_{diss}$ denotes the total amount of thermal power transported (i.e. dissipated) between both nodes. Similarly, for a known heat transfer coefficient and heat exchange area, the path's thermal resistance can be determined as:

$$R_{conv} = \frac{\Delta T}{\dot{Q}_{diss}} = \frac{1}{h \cdot A} \tag{2.4}$$

The advantage of this representation is that the resistance values between nodes can be obtained from either theoretical values or practical thermal measurements.

In the case of the mounted BGA package, most heat generated by the IC will be disposed either through the top or bottom interface. Cooling sideways (on a package level) is negligible, as the exposed area is small compared to the area in the top and bottom directions. This assumption is adopted by the compact nodal representation, illustrated in Figure 2.5. Here, both the thermal paths are shown: cooling through the top of the package (top branch) and cooling through the bottom of the package (bottom branch). The top branch includes

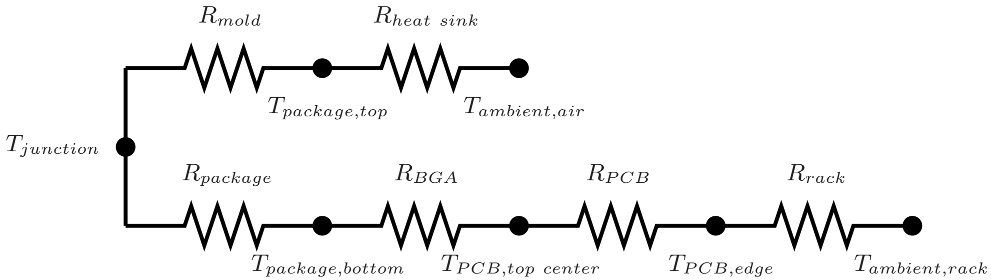

Figure 2.5: *Compact thermal model of Figure 2.4.*

heat dissipation through the mold and the heat sink. Here, the value of $R_{heat\ sink}$ includes both conduction through the heat sink and convection to the air. The bottom branch includes heat dissipation through the package itself, the BGA, the PCB and the rack structure.

The allowed peak temperature of the IC is often specified by the manufacturer as the maximum temperature at the junction ($T_{junction}$). For the IC to work reliable during its life expectancy, the junction temperature should remain below this limit. This is due to the fact that the mean time to failure of electronics increases rapidly for increasing junction temperatures. In the BGA package model of Figure 2.3 the junction is located on the top of the IC, where also the bondwires are attached. Therefore, heat must first travel through the package itself to reach the bottom. This set-up is especially useful for bottom cooling, as the thermal resistance in this direction is much lower than that of the mold compound protecting the IC and bondwires. It is also the least complex set-up, which allows visual inspection and repair work on the bondwires prior to molding. Also, instead of molding, sometimes a hollow package with a lid is used to protect the IC and its bondwires inside. In this case, there is no substantial thermal path to the top of the package at all.

In situations where top cooling is preferred, the junction and connections can also be designed on the bottom of the IC. This is regarded as the flip-chip design. Here, a solder connection, similar to a BGA connection, on the bottom of the IC serves to hold and connect the chip, instead of the die-attach to hold, and bondwires to connect the chip. Now, the mold compound protecting the top is no longer required and a heat spreader can be attached directly to the IC, resulting in a much lower thermal resistance to the top of the package. This set-up is more complex, due to the delicate solder process on the bottom of the IC. Also, special tools (for instance X-ray) are required to verify this connection, as visual inspection is no longer possible.

As many design engineers struggle with package thermal performances, by now the nodal representation of Figure 2.5 is widely accepted for thermal modeling of electronic packages. In fact, it has been standardized and well documented by the

Joint Electronic Device Engineering Council (JEDEC) [14]. For instance, JEDEC standard JESD51-12 discusses guidelines for reporting and using electronic package thermal information.

2.3 Integrated Thermal Design Approach

From a functional perspective, the top branch of the presented thermal model of Figure 2.5 is primarily used for cooling purposes. It can be considered an individual cooling solution, as it has very little influence on adjacent components, albeit the effect of increasing air temperature. As a result, the sensitivity to nearby components is quite low. This uncoupled nature of air cooling is very advantageous during the design phase, as components can be placed unconstrained by their thermal properties.

To produce more compact products, as is the goal of this study, cooling support can no longer be disconnected from other product functions. Both high component density and high power density cooling, as illustrated in Figure 2.2, already have an influence on the product lay-out. By focusing on the bottom side of the package, and thus the bottom branch of Figure 2.5, cooling capacity can be optimized for the most compact and highest level of integration. Moreover, for integrated sensors (camera), integrated visual indicators (high power LED, TV, laser) or in the case of this study to develop a next-generation APAR, the space above the electronic component cannot be obstructed by a top cooling device.

The bottom branch of the presented thermal model of Figure 2.5 already incorporates several functions, for instance the mechanical fixation and the electronic connections. Hence, cooling through the bottom would be just one integration step further. However, the fact that the board structure affects thermal behavior is undesirable, as an individual cooling solution is more preferable. Adjacent components may influence each other and, as such, thermal criteria must also be considered during the placement of these components. The fact that design complexity increases with each added function is a logical effect of integration.

To illustrate the concept of such an integrated approach, it is evaluated for a 10 W dissipating component* mounted on the center of a PCB. The assumptions made for each component in the assembly are listed in Table 2.1. Based on the bottom branch of the compact thermal model of Figure 2.5, the characteristic thermal values for this assembly are listed in Table 2.2. In this rough estimate, the thermal contribution of the PCB is only considered in parallel, the best conducting, direction. The resulting ambient rack temperature of -42°C – be it air or water cooling – is clearly not feasible. As 10 W thermal dissipation, compared to the values of the microprocessors in Section 1.1, is relatively low and electronics in general comprise many more components, this example emphasizes the fact that additional effort for thermal issues is required, when striving toward more compact electronic products.

---

* This is approximately the specification for the electronic components in the next-generation APAR.

Table 2.1: *Assembly component assumptions**.

Package	The electronic package comprises an IC attached to a rigid laminate, as was shown in Figure 2.3. The package, positioned in the center of the PCB, has a footprint area of 15x15 mm. The thermal resistance from junction to bottom is assumed to be 1.5 K/w. This value includes thermal conductance through the IC, die attach and laminate, and also heat spreading resistance through the laminate. The maximum allowed junction temperature specified by the manufacturer is 150°C.
BGA	The electronic package is attached to the PCB via a BGA by reflow soldering. The solder connections have a thermal resistance of 3.6 K/w. This value depends on the type of solder used and the size and amount of solder balls present in the BGA.
PCB	The PCB, assumed to be 200x200 mm with a thickness of 1.6 mm, consists of polymeric layers pressed together. The polymeric layers themselves are poor conductors, however the metallic patterns on the layers conduct very well. Therefore, the overall thermal conductivity depends on the amount of layers and percentage of metalization that remains on each layer after producing the electronic circuits. As conduction through the laminated layers depends on the direction, thermal resistance is specified in parallel (in-plane) and normal direction. Typical values are 11.4 and 17.3 K/w for parallel and normal directions, respectively.
Rack	The rack structure is designed to retain and cool the PCB. Boards are slid and clamped into a U-profile, similar to Figure 2.4. A typical value for the thermal resistance is 2.7 K/w. This value includes clamp interface resistance, conduction and heat transfer to the coolant.

** A detailed calculation of the values above is described in Appendix D.*

Table 2.2: *Nodal temperatures for a 10 W dissipating component.*

		R [K/w]	ΔT [K]	T [°C]
$T_{junction}$				150
	$R_{package}$	1.5	15	
$T_{package,bottom}$				135
	R_{BGA}	3.6	36	
$T_{PCB,top\ center}$				99
	R_{PCB}	11.4	114	
$T_{PCB,edge}$				-15
	R_{rack}	2.7	27	
$T_{ambient,rack}$				-42

Even in its lowest thermal resistance direction, the main bottleneck according to Table 2.2 is the PCB itself. As the board structure affects thermal behavior dramatically, nearby components will have a strong influence on each other. Ideally a low sensitivity is obtained, as this allows components to be placed unconstrained of their thermal properties. Suppose the layout can be altered in such a way that conduction through the board is eliminated; then with the temperature at the top center of the PCB kept at 99°C, the minimum heat transfer coefficient from this location to the ambient can be determined by rewriting Equation (2.4):

$$h = \frac{\dot{Q}_{diss}}{A \cdot \Delta T} = \frac{10}{(15e^{-3})^2 \cdot (99 - 20)} \approx 563\ W/m^2 K \tag{2.5}$$

Here, an ambient temperature of 20°C and a heat exchange area equal to the footprint area of the electronic package are assumed. To identify candidate cooling technologies, the result of Equation (2.5) is compared to the heat transfer coefficients per cooling principle of Figure 1.4. According to this figure, air cooling in a jet configuration and water cooling are possible solutions. As air cooling is relatively straight-forward and harmless to electronics, it is the preferred method. In the case of water cooling, both forced convection and phase change principles suffice. However, water cannot be brought in direct contact with the package without protecting the electronic parts.

2.4 Concept Generation

To develop viable cooling solutions, the electronics industry has already considered several (not so novel) options, for instance the use of thicker copper layers inside the PCB to conduct heat more efficiently. Also, thermal vias, as shown in Figure 2.1, to reduce the thermal resistance in normal direction through the board are used quite often. These solutions are mainly design variations at the embodiment and detail design level and, as such, break-through results are not to be expected. However, as a starting point they are considered in the next section.

2.4.1 Cooling on the Opposite Side

Suppose no space is available for a cooling device on top of the package, as in the case of an integrated sensor or indicator, or a packed board with many components, then perhaps the most simple concept is to provide a cooling solution on the opposite side of the board, as illustrated in Figure 2.6. To transport the heat efficiently through the board, thermal vias must be placed between the package and the cooling device. This type of cooling can be applied by mounting a single cooler, such as a heat sink, to the board (Figure 2.6(a)) or by mounting the entire board on a coldplate (Figure 2.6(b)).

There are many drawbacks to this approach. For instance, by mounting a cooling device on the opposite side, the ability to use this side for mounting

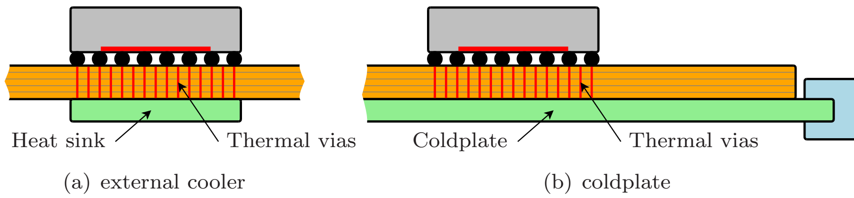

(a) external cooler

(b) coldplate

Figure 2.6: *Concept illustration with a cooling device on the opposite side.*

electronics is lost. Especially in the case of a coldplate, half the available area is lost. This could be solved by splitting the board and attaching a coldplate in between. However, now electronic connections between both boards must run outside around the coldplate via some connector. Also, depending on the number of components that need to be cooled simultaneously, a fairly thick, and thus heavy, coldplate will be required. In light of this study, this approach does not result in a more compact electronic product, as in fact only the location of the cooler shifts from the top to the bottom. As such, it is also questionable whether the cost reduction aimed for is achievable.

To come up with a novel, improved solution during the conceptual design phase, it was tried not to be biased by established electronic products and focus more on a system design level. As shown in the previous section, from a thermal point-of-view the PCB's influence is a dominant factor. Suppose the PCB could be thermally bypassed and components could be cooled appropriately, then they would be less sensitive to their location and nearby components on the board. Hence, denser boards can be designed, which leads to more compact boards as well. In an effort to diminish the thermal effects of the PCB, the heat exchange location is brought closer to its corresponding heat source. In other words, the electrical and mechanical domains literally have to make room for the thermal domain. This approach leads to the next concept of in-board cooling.

2.4.2 In-board Cooling

With *in-board cooling* the heat exchanger is placed inside the board directly below the electronic package, as shown in Figure 2.7. The heat exchange area is fabricated by machining a cavity into one of the intermediate layers prior to laminating the PCB. From the opposite side two holes must be drilled to connect inlet and outlet ports to the cavity inside. For efficient heat transfer, thermal vias can be placed in the board layers separating the top and the cavity inside.

A coolant, gas or liquid, can be pumped through the cavity to transport the heat away from the component. As no external heat sink or coldplate is required, this saves assembly steps and weight for the final product. However, additional assembly steps are necessary to supply each cavity with a coolant. For air one cooling line suffices, as the hot air from the outlet can be bled directly into the

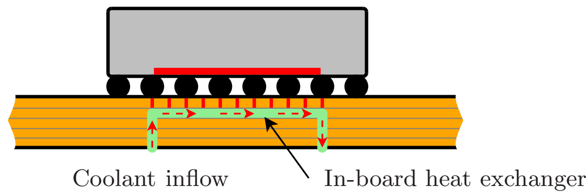

Figure 2.7: *Concept illustration of in-board cooling.*

environment; for other coolants two lines are required to return the heated fluid as well. For liquid coolants the connection between the connecting lines and the board must be made reliable, as any leakage may directly cause short circuits.

A similar approach has been reported by Schütze et al. in 2001 [54]. They developed a PCB-compatible, integrated cooling system, where cooling channels were directly etched into a thick (400 μm) copper layer*. Instead of using standard layer material and drilling to the cavity, they use an in-plane copper layer and sacrifice this entire layer for their cooling system. They claim to obtain a heat dissipation capability of 20 W per channel and heat source, using water as a coolant. However, they also report that this requires a very high via density around the cooling channels.

As both the inlet and outlet ports of the presented in-board approach are on the same side, this implies the use of cooling lines to supply coolant to the heat sources. These cooling lines are the main drawback of this concept, as, especially for a PCB with multiple heat sources, many are required. This issue is resolved in the next concept, where the heat exchange area is moved further up toward the heat source.

2.4.3 Directly Injected Cooling

Upon closer inspection, the BGA interface bears quite some resemblance to a traditional heat sink heat exchanger. Both have a flat base and extensions to enlarge surface area. In a BGA interface the extensions are formed by the solder balls. The concept of *directly injected cooling* is illustrated in Figure 2.8. Coolant flows through the BGA, extracting heat from the electronic package through the bottom side. Hence, the BGA not only has an electrical and mechanical function, but also acts as a heat exchanger; possibly reaching total functional integration in light of this research.

The only dedicated feature of this concept is a through hole in the PCB, which can be produced using standard PCB production techniques. As the coolant approaches the hot surface from a perpendicular direction a jet impingement effect will occur at the interface, improving heat transfer rates. In its simplest form conditioned, cool air is pumped from the backside to the front through the hole in

* Generally copper layers for electronic signals are around 35 μm thick.

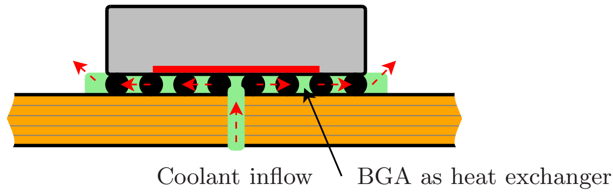

Figure 2.8: *Concept illustration of directly injected cooling.*

the PCB. Instead of connecting a cooling line to each individual heat exchanger, the entire PCB can also be placed on a pressure chamber to supply coolant to all heat exchangers simultaneously. This concept is especially promising for high component density cooling where many components need to cooled simultaneously.

In the case of high power density cooling, air will probably not have sufficient capacity to dissipate all the generated heat. Although water, or any another liquid, can also be used as a coolant in this concept, either all electronic connections need to be sealed or a sealed compartment needs to be realized within the BGA to prevent short circuits*. Also, the liquid must be collected and returned, whereas the hot air can be bled directly into the environment. As indicated in the previous section, returning the fluid to the backside via a second through hole, requires all heat exchangers to have individual cooling lines and makes the use of a pressure chamber impossible. Hence, in practice, this concept is most viable for (high component density) air cooling purposes.

2.4.4 Integrated Heat Pipe Cooling

In order to achieve more cooling capacity close to heat dissipating components, another concept is developed. Instead of air, this concept focuses on the use of water as a heat transfer medium to attain higher cooling capacities. To have a reliable concept with water, special care is required concerning leakage. Therefore, a phase change heat transfer mechanism is selected. This allows the cavity to be hermetically sealed. Moreover, for the device to work properly, it is required to be hermetically sealed.

The concept of *integrated heat pipe cooling* is illustrated in Figure 2.9. Here, a heat transport area is positioned inside the board, by machining a cavity in an individual PCB layer prior to the laminating process, similar to the previous concept of in-board cooling. The cavity is extended directly below the heat dissipating component. Instead of disposing the heat directly into the environment, as in the case of the previous concept, it is transported away from the component first. At another location, the heat is extracted again and dissipated further.

* With the exception of a dielectric liquid.

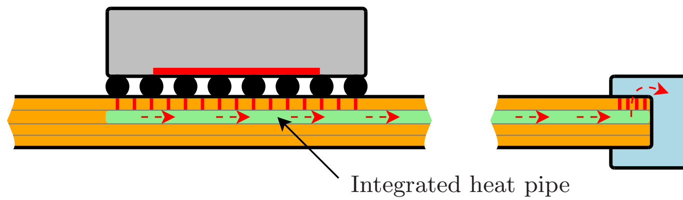

Figure 2.9: *Concept illustration of integrated heat pipe cooling.*

Inside the cavity, a two-phase flow must coincide. In this case, vapor flowing away from the hot component, thereby transporting large quantities of heat, and a liquid flow returning the condensate. The pressure to return the condensate is obtained by a capillary structure attached to the inner walls of the cavity, which renders this concept a heat pipe; a heat pipe integrated into the laminated structure of a PCB. Also in this concept, thermal vias are used to transport heat effectively through the top layer(s).

As a heat pipe is capable of reaching extremely high heat transfer rates, the thermal resistance between the hot (evaporator) and cold (condenser) ends of the heat pipe is minute. Hence, analogous to the concept of directly injected cooling, placement of the electronic components is thermally unconstrained. The cold end of the heat pipe can be designed anywhere in the board, although in practice along the edge, as indicated in the figure, the heat can simply be extracted through the rack structure. Depending on the density of the electronic circuitry, the thickness of a PCB with an integrated heat pipe will probably increase. However, compared to a board with a heat sink or a coldplate attached to it, a considerable decrease of overall thickness is realized. Also, as a heat pipe is a passive device, no external pump or (electrical) power is required for its operation.

This concept was identified to be especially promising for high power density cooling. However, a heat pipe can also transport heat away from various sources as it meanders through the board, which makes it useful for high component density cooling as well.

2.5 Conclusions

This chapter focused on developing novel cooling strategies for electronic products. The goal was to find an integrated, flexible and cost effective cooling concept to realize more compact electronic products. The concepts described resulted from a multidisciplinary and integrative approach, where rigorous interventions in other domains were not avoided.

From a thermal perspective, the design of two extreme cases was considered: high component density cooling and high power density cooling. Through the concept of *directly injected cooling* conditioned, cool air is injected directly under-

neath an electronic package, which cools the package with virtually no interaction to adjacent components. Hence, a high component density cooling strategy is realized at a high level of integration. Through the concept of *integrated heat pipe cooling* a phase change heat transfer mechanism is integrated into the PCB. The heat pipe is able to transport heat very efficiently in a compact set-up.

Both cooling strategies have been identified as innovative cooling concepts for future electronic products. In addition, as both require little adjustment of the manufacturing processes involved, their cost effectiveness is promising. A comprehensive description, detailed analysis and experimental verification of the directly injected cooling concept is described in Chapter 3. For the integrated heat pipe, this is described in Chapter 4.

Chapter 3

Directly Injected Cooling

This chapter presents the directly injected cooling concept as an effective solution for high component density cooling cases. The principles of jet air cooling are discussed in order to find suitable design criteria for the prototype. The technology demonstrator that has been developed is presented together with the measurement results. At the end of this chapter, the concept will be evaluated.

3.1 Introduction

The concept of directly injected cooling is a combination of confined channel flow and jet impingement effects. The influence of both effects on thermal properties has been studied for numerous decades. However, the combination with PCB production techniques and the integration into an electronic product has been identified as an innovative approach*.

The boundary layer present between the wall and bulk fluid in flow profiles has a large influence on the thermal profile of heat transported from the wall to the bulk fluid. Obstructions in the channel (e.g. solder balls) and perpendicular flow (jet impingement) cause turbulent flow patterns, which minimize boundary layer effects and consequently promote the transfer of heat.

Jet impingement cooling has been applied in many industrial applications, such as cooling of metals and glass or in grinding and rolling processes. Jet impingement of air for electronics cooling is currently studied by researchers in an effort to extend the limits of air cooling. As the jet is issued into a region of the same fluid (air in air), it is classified as a submerged jet. Typical jet cooling devices are split up into two distinct categories: unconfined and confined jets. Both configurations are shown in Figure 3.1.

* A patent “Directly injected forced convection cooling for semiconductor components” was granted in 2007 [5].

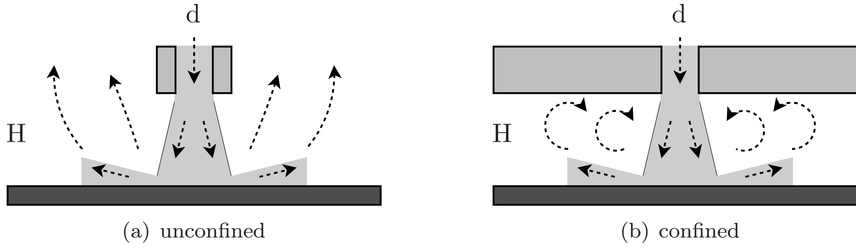

(a) unconfined (b) confined

Figure 3.1: *Jet configurations.*

In the case of an unconfined jet, the radial spread of the fluid after impinging is not confined by a top surface. Conversely, confined jets are restricted to a narrow channel after impingement. As the fluid is trapped between both surfaces, parts of it will recirculate into the main jet, which generally results in a decrease of the overall heat transfer. The geometric feature $\frac{H}{d}$, i.e. the ratio of jet-to-target spacing and jet diameter is a key parameter in determining the jet's thermal performance. Obot et al. [45] reported in 1982 that the reduction of the heat transfer rate due to jet confinement was minimal at:

$$\frac{H}{d} = 6 \tag{3.1}$$

Other studies [2, 21] have indicated that at lower ratios, around unity, heat transfer increases again, due to radial fluid accelerations after impingement. Another important parameter for jet cooling is the Reynolds number of the flow, defined as:

$$Re = \frac{\rho \cdot d \cdot U}{\mu} \tag{3.2}$$

where d denotes the characteristic length of the flow passage's cross section (in this case the jet diameter), ρ and μ represent the density and viscosity of the fluid, respectively, and U denotes the mean velocity of the (jet) flow. Also, the nozzle's outlet contour and in the case of multiple jets the total number and spacing of the jets influence heat transfer performance [27].

Most publications found in the field of electronics cooling focus on cooling via the top surface, i.e. the jet is positioned to impinge on the top surface of the electronic component. Higher heat transfer coefficients are achievable compared to traditional heat sink & fan set-ups. However, a cost reduction – especially for mass-market applications and cooling of multiple components – will probably not be realized, due to the additional assembly cost of connecting a high pressure pipe system locally to all heat dissipating components. Hence, at present such a product is not seen on the market very often.

In the concept of directly injected cooling the jet is positioned to impinge on the bottom surface of the electronic component, as illustrated in Figure 3.2. After

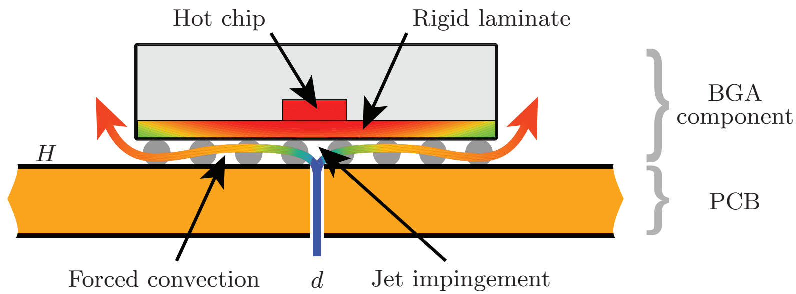

Figure 3.2: *Concept of directly injected cooling.*

impinging on the bottom surface, the air spreads radially underneath the component. Here, the solder balls of the BGA are not only used for the transmission of electronic signals and mechanical fixation, but also act as an integrated heat exchanger. As the heated air reaches the edge of the component it is bled into the environment. The jet nozzle is formed by drilling a through hole in the PCB. The number of through holes – and thus number of jets – should be determined by the thermal criteria of the mounted component. However, it is obviously limited to the footprint area of the package.

3.2 Concept Embodiment

The standoff distance of a BGA component is usually determined by the size of the solder balls and the amount of solder required to make a reliable electrical and mechanical connection. However, in this concept, adequate height must also be realized for the coolant medium to pass through, absorbing as much power as required; for instance, by selecting smaller or larger solder balls.

By injecting air directly into the BGA, the air is brought very close to the hot underside of the rigid laminate, thus bypassing several thermal resistances (e.g. conduction through the PCB and rack structure). In addition, as the cooling air approaches the hot surface from a perpendicular direction, the jet impingement effect will also occur. This increases the heat transfer rate compared to tangent flow by locally breaking through the thermal boundary layer, as discussed in Section 3.1. Finally, as a BGA typically has a large number of solder connections, the heat exchange area is relatively large. As the air spreads underneath the package, the solder balls act as a static mixer, which improves forced convection heat transfer even further. In an advanced set-up, the balls could even be placed in such a way that cooling potential is maximized.

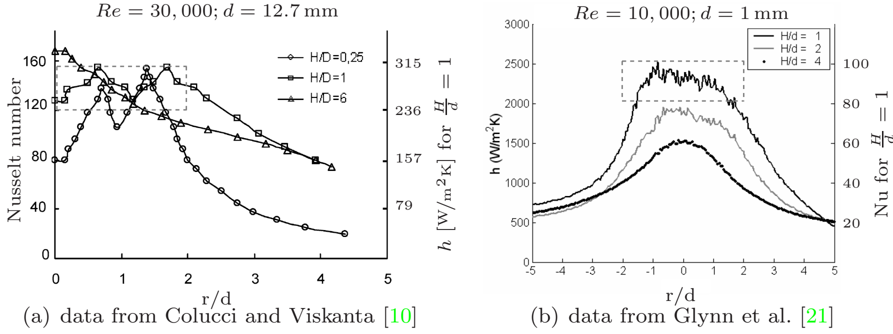

(a) data from Colucci and Viskanta [10] (b) data from Glynn et al. [21]

Figure 3.3: *Heat transfer values for a confined impinging air jet.*

3.2.1 Jet Optimization

To quantify and optimize the effect of heat transfer caused by the impinging jet, some rough assumptions on the component geometry must be made. The dimensions of the component (15x15 mm) and board structure (200x200x1.6 mm) of the previous chapter are assumed; other assumptions will be clearly stated in this section.

To compare heat transfer by convection and by conduction in the boundary layer of a fluid, the nondimensional Nusselt number is used. It is defined as:

$$Nu = \frac{h \cdot L}{k} \tag{3.3}$$

where L denotes the characteristic length normal to the boundary layer. In this case, this is the jet-to-target spacing or standoff distance of the electronic component. As Equation (3.3) suggests, a high Nusselt number corresponds to a situation with high convective heat transfer compared to conduction and vice versa.

As mentioned, important parameters for confined jet impingement are the Reynolds number of the air flow, and the ratio of jet-to-target spacing and jet diameter. According to some sources, this ratio should be low ($\frac{H}{d} \leq 6$) for optimal heat transfer. For a confined impinging air jet with a Reynolds number of 30,000, Colucci and Viskanta [10] report Nusselt numbers from 80 up to 160 for $\frac{H}{d}$ values of 0.25, 1 and 6 in the direct region of the jet. Glynn et al. [21] also report increased heat transfer values for a confined air jet with $\frac{H}{d}$ values of 1, 2 and 4, and a Reynolds number of 10,000. The reported results for both measurements are shown in Figure 3.3.

In both experiments performed by Colucci and Viskanta, and Glynn et al., an air jet was impinged onto a heated plate in a confined space. The heat transfer coefficients were measured locally by an imaging technique. The horizontal location relative to the jet center is given as the ratio of $\frac{r}{d}$, where r represents the

radial coordinate and d denotes the jet diameter. The values reported by Colucci and Viskanta are presented by the local Nusselt number, whereas Glynn et al. reported the value of the local heat transfer coefficient. To compare both results, on the axis on the right hand side the converted values are shown, according to Equation 3.3, for the $\frac{H}{d} = 1$ measurement. A characteristic length equal to the jet-to-target spacing and a thermal conductivity of air of $0.025\,\mathrm{W/mK}$ at 20°C [3] are used.

The heat transfer coefficients of both measurements differ significantly due to their respective geometries. However, the Nusselt numbers are in relative accordance, confirming that the ratio of $\frac{H}{d}$ is representative for the jet's performance. Also, the benefit of using a nondimensional comparison is illustrated.

Both figures show increased heat transfer rates in the region of the jet center. The rates reduce significantly as the air spreads outward. Figure 3.3(a) indicates that less heat transfer occurs in the direct jet center (the stagnation point) for $\frac{H}{d} \leq 1$. For this geometry, due to global continuity, the air continues to accelerate as it spreads radially, thereby increasing heat transfer [10]. This causes a (first) peak in heat transfer around $\frac{r}{d} \approx 0.5$. A second peak is formed around $\frac{r}{d} \approx 1.6$, due to a local recirculation zone of the confined flow. According to Colucci and Viskanta [10], "This secondary recirculation zone becomes stronger with increasing Reynolds number and decreasing nozzle-to-plate spacing." In Figure 3.3(b), these peaks are less pronounced, probably due to the small geometry. Here, the effects manifest themselves as flattening of the heat transfer values. For larger $\frac{H}{d}$ ratios these effects do not occur. In both figures the shape of the graph smoothens, indicating a gradual decline of heat transfer values as the air spreads radially.

In the case of this directly injected cooling concept, the largest overall heat transfer coefficient is sought-after. According to the data presented in Figure 3.3 best results can be obtained for a diameter approximately equal to the standoff distance (i.e. $\frac{H}{d} = 1$) and in the region of $\frac{r}{d} \leq 2$. Here, on average the heat transfer coefficients are the highest, as indicated by the dashed gray boxes. An average Nusselt number of at least 80 should be feasible.

Outside the main jet area the local heat transfer coefficient drops considerably. Multiple jets can be applied to cool a larger surface, as opposed to cooling via forced convection underneath the component, which will be less effective. To maximize heat transfer, the thermally affected areas should be connected directly to each other. Hence, according to the presented data, the spacing between the jets should equal four times the jet diameter.

In practice however, the jets will influence each other, as air exiting one jet will spread outward into the next jet and vice versa. This might influence overall jet performance negatively as velocities decrease and stagnation points may occur. Conversely, recirculation zones may also be enhanced, which would increase the jet's performance. According to Huber and Viskanta [24], for $\frac{H}{d} \leq 1$ the highest average Nusselt number is obtained for a jet spacing of four diameters, as in this case the secondary peaks are maximized. However, in their study spent air exit holes are present between the air inlet holes, which cannot be constructed in our

cooling concept. The effect on the average heat transfer coefficient when using multiple jets in our case will be determined experimentally.

Also, to optimize heat transfer a high Reynolds number, and thus high air flow velocity should be used. In practice, this is limited by both the maximum pressure the system can endure and pumping capacity.

3.2.2 Thermal Jet Power

To determine the number of jets required for a specific cooling performance in the case of the directly injected cooling concept, the performance of a single jet is considered first. Suppose the standoff distance of the BGA is 1 mm and a hole with a diameter of also 1 mm is manufactured directly below the BGA. Here, locally an average heat transfer coefficient of 2,000 W/m²K should be feasible, based on a Nusselt number of 80. Neglecting heat transfer outside the thermally affected area, this would result in an estimated thermal resistance value for one jet of approximately:

$$R_{jet} = \frac{1}{h \cdot A} = \frac{1}{2000 \cdot \frac{1}{4}\pi(4e^{-3})^2} \approx 40\ \frac{K}{W} \tag{3.4}$$

Here, the area A is assumed to be the area thermally affected by the jet, i.e. four times the jet diameter. Assuming the jet performance to be independent, neglecting the effect of multiple jets, each additional jet will deliver an equal performance. Hence, the total resistance is:

$$R_{jet,total} = \frac{R_{jet}}{n} \tag{3.5}$$

where n denotes the number of jets. These relations can be used to design the directly injected cooling system.

Suppose an integrated jet cooling system is designed according to Figure 3.4 with four jets (⌀1 mm) to cool an electronic component (15x15 mm) dissipating 10 W. The through holes (nozzles) of the jet layout are offset to maximize the density of the thermally affected area. The overall thermal performance of this cooling concept is listed in Table 3.1. Instead of the -42°C previously determined in Section 2.3, the required ambient jet air temperature is now estimated to be 35°C. Hence, theoretically this concept is viable for the cooling of a 10 W dissipating electronic component, assuming there still is sufficient space between and outside the jet nozzles for the solder balls to mount the package onto the PCB.

Note that this is a very rough estimation, as effects inside the jet area are averaged and interaction between the jets is neglected.

3.2.3 Jet Pressure

The estimated thermal resistance value applies only for a Reynolds number of at least 10,000. Via the definition of the Reynolds number, the mean velocity of the

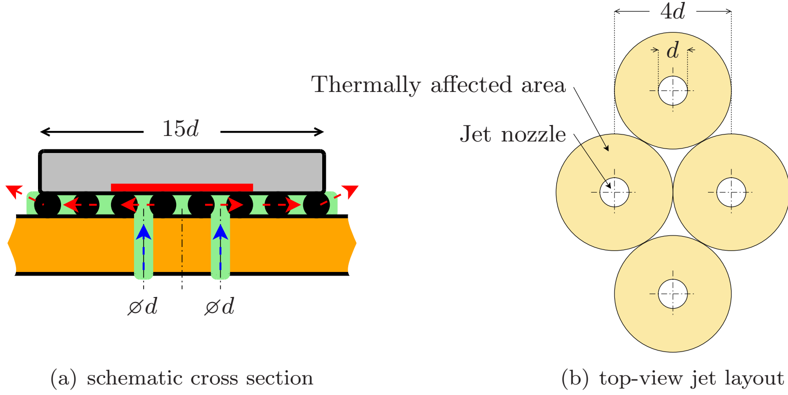

(a) schematic cross section

(b) top-view jet layout

Figure 3.4: *Directly injected cooling concept with 4 jets.*

Table 3.1: *Nodal temperatures for 10 W dissipation with directly injected cooling.*

		R [K/W]	ΔT [K]	T [°C]
$T_{junction}$				150
	$R_{package}$	1.5	15	
$T_{package,bottom}$				135
	$R_{jet,total}$	10	100	
$T_{ambient,jet\ air}$				35

air inside the ⌀1 mm jet equals approximately:

$$U_{jet} = \frac{\mu \cdot Re_{jet}}{\rho \cdot d} = \frac{1.81e^{-5} \cdot 10,000}{1.205 \cdot 1e^{-3}} \approx 150 \ \frac{m}{s} \tag{3.6}$$

Here, thermodynamic air properties are evaluated at 20°C and at atmospheric pressure. Compared to the values presented in Section 1.2.1, this is a relatively high velocity for an impinging air jet. The pressure required to propel air through a pipe with a certain mean velocity is correlated as [3, 41]:

$$\Delta P = f \cdot \frac{4L}{d} \cdot \frac{1}{2}\rho U^2 + \frac{1}{2}\rho U^2 \tag{3.7}$$

where L denotes the length of the pipe and f is known as the Fanning friction factor. The first term on the right hand side represents the pressure loss for a fully developed flow, whereas the second term accounts for the entrance effects. As PCBs are thin, the length of the through hole will also be small. Hence, the entrance effects must be taken into account.

In this case, two flow patterns should be superimposed: the flow through the hole in the board (the jet) and the flow underneath the component. For a fully developed turbulent flow through a circular pipe, the value of f can be determined via Moody's chart [3]. In this chart, the value of $4f$ is shown as a function of the Reynolds number and the relative surface roughness of the pipe. For a Reynolds number of 10,000 the values for a smooth pipe to a rough pipe vary from:

$$0.03 < 4f < 0.075 \tag{3.8}$$

To determine the maximum pressure, the drilled through hole is assumed to be very rough. Hence, the required pressure to facilitate sufficient flow through a jet nozzle may go up to:

$$\Delta P_{jet} = \frac{0.075}{4} \cdot \frac{4 \cdot 1.6e^{-3}}{1e^{-3}} \cdot \frac{1}{2}1.205 \cdot 150^2 + \frac{1}{2}1.205 \cdot 150^2 \approx 15,200 \ Pa \tag{3.9}$$

Here, the board thickness (pipe length) is assumed to be 1.6 mm. This calculation also illustrates that the entrance effects contribute up to almost 90% of the total pressure drop.

As the airflow leaves the direct jet region ($\frac{r}{d} = \frac{1}{2}$) radially, its velocity for this set-up ($\frac{H}{d} = 1$) will diminish to one quarter of the initial value, as:

$$U_{out} = \frac{A_{in}}{A_{out}} \cdot U_{in} = \frac{\frac{1}{4}\pi d^2}{H\pi d} \cdot U_{jet} = \frac{1}{4} \cdot U_{jet} \tag{3.10}$$

As the velocity contribution is related quadratically with its pressure, the additional pressure required to propel the air radially underneath the component can be neglected. As the air spreads outside the thermally affected region, the

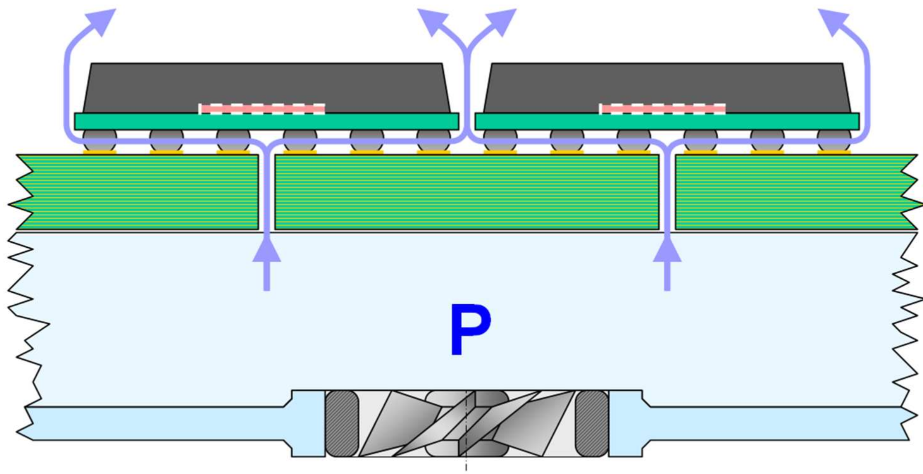

Figure 3.5: *Cross sectional view of a concept design for simultaneous cooling of multiple packages; illustration by Mannak [38].*

velocity is reduced to $\frac{1}{16}$ of the initial value. This illustrates also that the forced convection heat transfer outside the thermally affected jet area will be relatively low compared to the jet convection itself, as assumed before and also visible in Figure 3.3.

The total pressure requirement of approximately 15 kPa is relatively strenuous on the board structure and its electronic components. Especially the strain on the solder balls of the BGA must be regarded. To reduce the strain, either the Reynolds number can be lowered or the jet nozzle can be enlarged. Both effects will decrease the velocity proportionally; the pressure however decreases quadratically. The assumed jet velocity was relatively high; therefore, now levels according to Section 1.2.1 will be reached. Experimental investigation should determine the influence of these adaptations on the thermal performance.

3.2.4 Design for High Component Density Cooling

In this concept, the only dedicated feature on the electronic product is a (non-plated) through hole in the PCB, which can be produced using standard PCB production techniques. This is especially advantageous when multiple components on a board must be cooled. As each heat source has an individual cooling support, the heat from multiple sources can be transported simultaneously without introducing unacceptable temperature gradients across the PCB. A concept design for high component density cooling is illustrated in Figure 3.5.

One jet per component is shown, but as demonstrated previously, the exact number of jets is determined by the thermal criteria of the component. Also, the

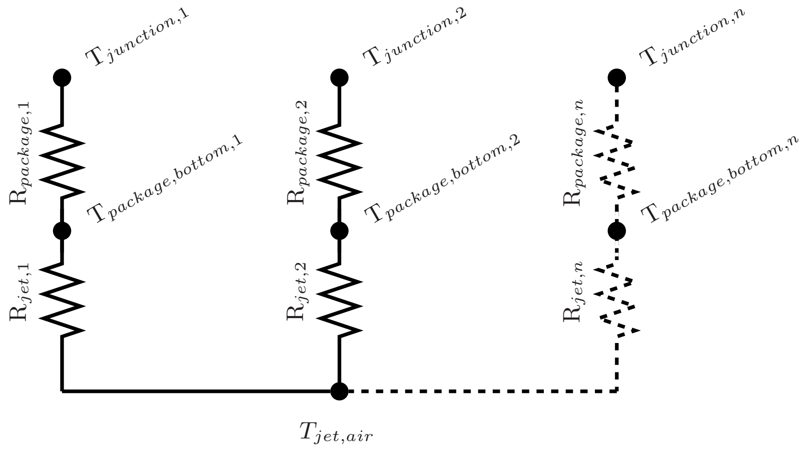

Figure 3.6: *Compact thermal model for the directly injected cooling concept.*

board is mounted on a pressure chamber, which is pressurized via an external pump. The pump can be dimensioned to fit any pressure requirements, however the board and components must be able to sustain this pressure, as discussed before.

From a thermal perspective, there is no coupling between the individual components. The thermal properties of the PCB, which normally affect overall thermal behavior dramatically, is now circumvented by the directly injected cooling. This is illustrated in the compact thermal model of Figure 3.6. Here, the thermal properties of each branch are affected only by conduction through the component itself and by convection to the local jet(s). This is valid for any number of components, as long as they fit on the PCB and sufficient jet power can be maintained. Hence, this concept excels in the case of high component density cooling, defined as one of the extreme cases in the previous chapter.

3.3 Prototype & Test Set-up

In order to validate the concept of this new cooling strategy, a technology demonstrator was developed. To discriminate between the jet effect and heat transfer from the bottom surface through the solder balls, two test boards were manufactured. The first with electronic components occupying an area of just 2.25 cm^2 (15x15 mm); the second with larger components occupying an area of 20.25 cm^2 (45x45 mm). Each component consisted of a copper laminate, 1.1 mm thick, with a diode, acting as a power source, mounted onto its surface. They were connected through a BGA interface to the board structure. Solder balls were attached in the area of the diode and around the circumference of the laminate. As such,

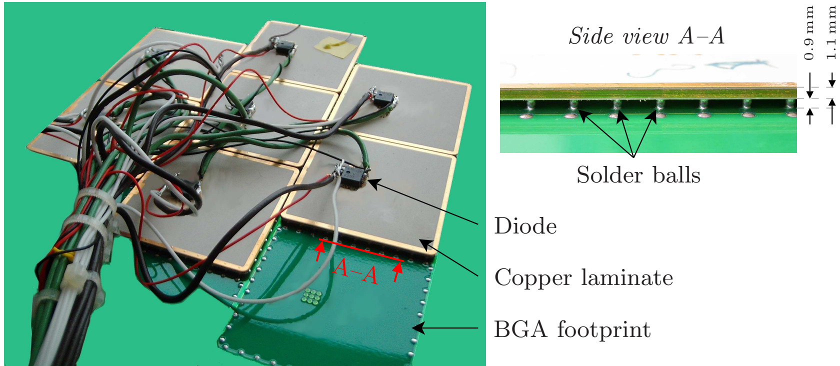

Figure 3.7: *Test board with seven large (20.25 cm^2) components.*

the solder ball density for the small components was much larger. The standoff distance of the laminate was 0.9 mm. Each board had a thickness of 1.6 mm and comprised seven components, as shown in Figure 3.7.

Each component was equipped with an individual cooling support, by drilling through holes directly underneath the diode. As such, the number, spacing and layout of the holes could be tested for seven different arrangements and two package sizes. The seven arrangements are listed in Table 3.2. In the case of multiple jets, they are positioned offset. The exact jet arrangements are shown in Appendix B.1.2. As Table 3.2 indicates, three small packages could not be tested as either the solder connection between the diode and the laminate failed, or the package was not soldered onto the board properly.

During the measurements, the entire board was placed on a pressure chamber. Power – and thus heat – was dissipated through the diode, while air was fed to the pressure chamber. Both air pressure and velocity, as well as temperature were measured continuously. The electrical resistance of the diodes varies proportion-

Table 3.2: *Operational jet layouts for BGA packages.*

Layout*	Large BGA package	Small BGA package
10x1	✓	-
1x2	✓	✓
2x2	✓	-
3x2	✓	✓
5x2	✓	✓
1x3	✓	✓
1x4	✓	-

* *Layouts are defined as number of holes x hole diameter in mm.*

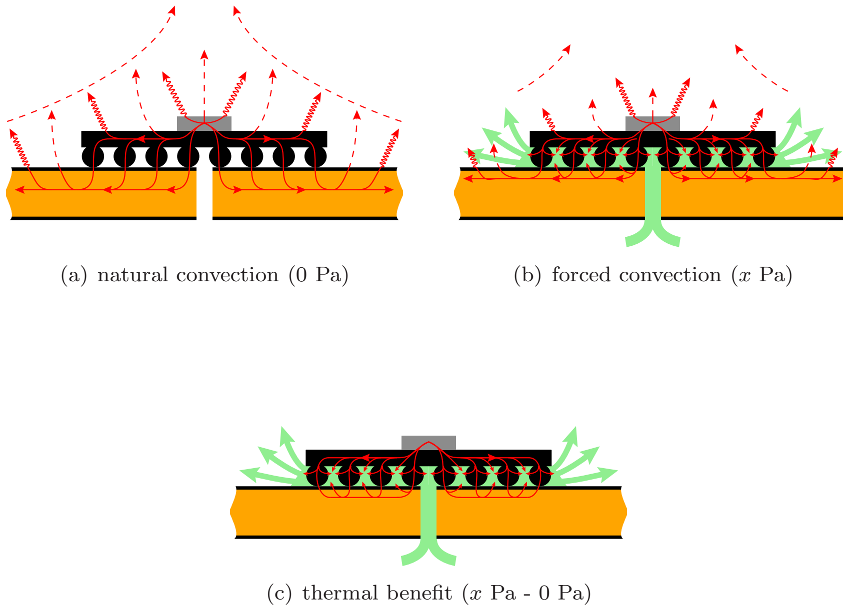

(a) natural convection (0 Pa)

(b) forced convection (x Pa)

(c) thermal benefit (x Pa - 0 Pa)

Figure 3.8: *Illustration of the thermal benefit.*

ally with its temperature. Therefore, by alternating a power current (to heat-up the diode) and a measuring current, the diodes were also used to measure the junction temperature. The switching frequency was in the order of 1 Hz; therefore, junction temperatures are not considered precise. The diode's thermal dynamics respond faster, hence the temperatures recorded will be slightly lower. However, to differentiate between the thermal performances of the jet arrangements this is sufficient. By opening and closing the air inlet holes for each component separately, the performance of each arrangement was determined individually. The measurement set-up and calibration of the diodes are discussed in more detail in Appendix B.

3.4 Measurement Results

To determine the thermal benefit of the developed prototypes, they were measured both unpressurized and pressurized. The former is equivalent to the case of natural convection, whereas the latter introduces both forced convection through the confined channel and the theoretically dominant impinging jet effect. By subtracting both measurements from each other, as illustrated in Figure 3.8, the thermal benefit can be determined.

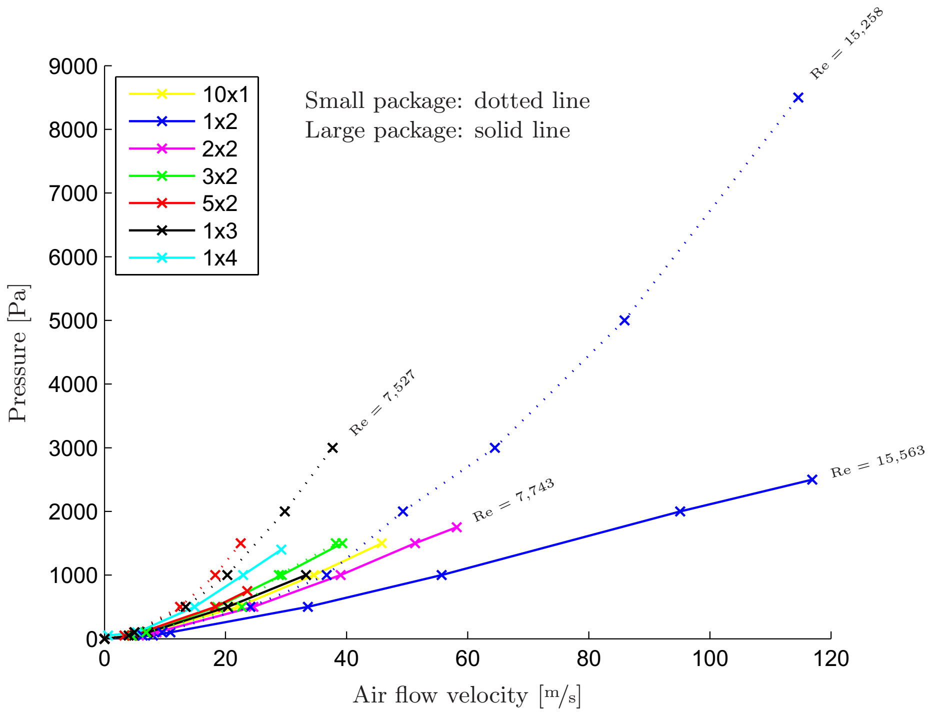

Figure 3.9: *Air flow velocity versus the pressure profile.*

3.4.1 Flow Measurements

In all cases, the air velocity increased as the pressure was increased. Figure 3.9 shows the measurement results for the jet layouts listed in Table 3.2. The dotted lines correspond to the small packages, whereas the solid lines correspond to the large packages. The measurement set-up was limited to a continuous volumetric air input flow of about 1350 l/h. The highest pressure and flow were recorded for the small package with the smallest overall jet area: the 1x2 jet. For the large package with the 1x2 jet an equal flow could be reached, but at a much lower pressure. As the overall jet area increases both the flow and the pressure decrease. Also, the Reynolds number for some of the final measurement points are shown in the figure.

For an equal flow and jet configuration, more pressure is required for a small package. This is due to the fact that for smaller packages the air encounters more solder balls obstructing the flow per unit area. Hence, more pressure is required. As in this experiment only one jet layout was activated each time, air could also spread underneath adjacent packages. Therefore, the radial spread through the confined channel around the solder balls of the adjacent packages influences the air

Table 3.3: *Dataset for small package with one ⌀2 mm hole.*

Measurement			Theory	
ΔP_{jet} [Pa]	U_{jet} [m/s]	Re	ΔP_{jet} [Pa]	error [%]
0	0	0	0	
50	6.3	839	25	49.3
100	9.5	1,266	58	42.2
500	24.1	3,204	370	26.0
1,000	36.7	4,882	859	14.1
2,000	49.3	6,561	1,551	22.5
3,000	64.5	8,590	2,658	11.4
5,000	85.9	11,443	4,717	5.7
8,500	114.6	15,258	8,386	1.3

flow as well. If all packages were pressurized simultaneously, the escape channels between the packages could also potentially influence the air flow.

According to Equation (3.7), there is a quadratic relation between the pressure and the velocity of the impinging jet(s). This quadratic relation is consistent with the measurement results, especially for the small packages. The measured dataset for the small package with one ⌀2 mm hole is presented on the left side of Table 3.3. On the right side of the table, the theoretical values are shown calculated according to Equation (3.7). For higher pressures the error decreases, as the entrance effects become more dominant and because the frictional values were estimated for a Reynolds number of 10,000.

In the theoretical values of Section 3.2.3, the entrance effect of the jet had the largest influence on the pressure. This corresponds well with the measurement results of the small packages. For the large packages, in theory, an equal pressure drop should be present. The measurements however indicate a significant lower pressure drop at approximately equal air velocities. Hence, the influence of the airflow underneath the packages, which was not accounted for, is in practice influential. Its influence seems well described by Equation (3.7) for small packages, however not for large packages. Finding a better definition for the pressure equation was not investigated further, as this is not of great importance for this conceptual design. The complete dataset of some of the flow measurements is also presented in Appendix B.

3.4.2 Thermal Measurements

In all cases, heat transfer improved as the air pressure – and thus air velocity – was increased. Hence, more power could be dissipated at a lower junction temperature. Figure 3.10 shows the temperature profile of the small 1x2 package for increasing amounts of dissipated power. After increasing the power input, sufficient time

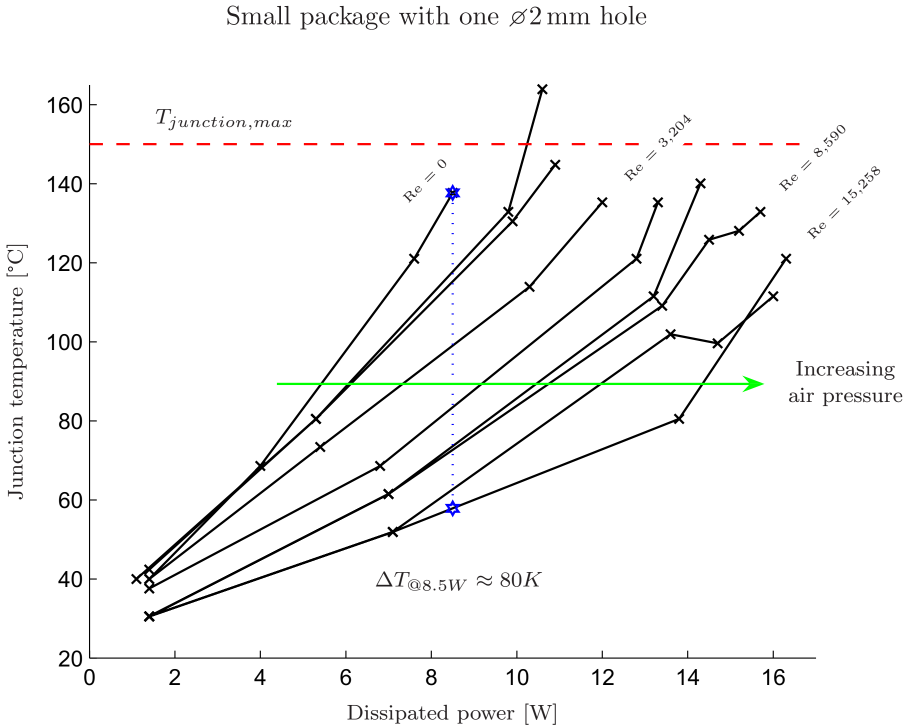

Figure 3.10: *Junction temperature for increasing power dissipations.*

was taken to record a steady junction temperature. As the maximum allowable temperature was reached, the measurement was stopped and the apparatus was allowed to cool down. Subsequently, the air pressure was increased and a similar measurement was started. The ambient jet air temperature was 21°C.

The top black measurement line in Figure 3.10 indicates no air flow, hence the Reynolds number equals zero. As the air pressure was increased, according to the green arrow, more power could be dissipated. At the final measurement, indicated by the bottom black line, the pressure was increased to 8,500 Pa ($U \approx 115\,{}^{m}/_{s}$). This measurement corresponds to the top right measurement point in Figure 3.9, where a Reynolds number of approximately 15,258 was observed. Also, the maximum allowed junction temperature of 150°C specified for many electronic components, as mentioned in Section 2.3, is indicated in the figure by the dashed red line.

The thermal benefit – determined by the difference between the natural convection measurement and a pressurized measurement – is indicated by the dotted blue line in Figure 3.10. It shows that a temperature decrease of about 80 K can be realized at 8.5 W of power dissipation. At higher dissipated values, directly

injected cooling also clearly demonstrates its merit, as the apparatus can operate safely, without reaching crucial thermal criteria.

Heat Transfer Coefficient

At the top of the blue line, 8.5 W is dissipated via natural convection only. Here, the average heat transfer coefficient h_{nc}, as determined by Equation (2.5), equals approximately:

$$h_{nc} = \frac{\dot{Q}_{diss}}{A \cdot \Delta T} = \frac{8.5}{2.25e^{-4} \cdot (138 - 21)} \approx 323 \; \frac{W}{m^2 K} \tag{3.11}$$

For natural convection this value is exceedingly high. At this temperature the amount of heat dissipated through radiation can still be neglected* for such a relatively small area. Hence, during the measurement, the apparent heat exchange surface must be enlarged by heat conduction through the BGA and board structure to the adjacent modules. Experts [16, 41] suggest that a natural convection heat transfer coefficient of approximately 5 $\mathrm{W/m^2K}$ is realistic for a horizontal, flat set-up. Hence, the real heat exchange area is at least 60 times larger. At the bottom of the blue line, where the pressure was at its highest value, the heat transfer coefficient $h_{fc,max}$ equals approximately:

$$h_{fc,max} = \frac{8.5}{2.25e^{-4} \cdot (58 - 21)} \approx 1,021 \; \frac{W}{m^2 K} \tag{3.12}$$

As such, air injected through a ⌀2 mm inlet hole underneath a small BGA package, resulted in a threefold improvement of the heat transfer coefficient. The latter value is also comparable with the data presented before by Glynn et al. [21]. It must be noted however, that in this approximation the area of the entire is package is used. When the effective jet area of four times the diameter – as was derived from Figure 3.3 – is used, the heat transfer coefficient becomes:

$$h_{jet,eff} = \frac{8.5}{\frac{1}{4}\pi(8e^{-3})^2 \cdot (58 - 21)} \approx 4,570 \; \frac{W}{m^2 K} \tag{3.13}$$

This value is no longer in agreement with data from Glynn et al., nor is it in agreement with jet impingement data from other sources, even when this value is reduced with the value in the case of natural convection. This means that also in this case the real heat exchange area is much larger than assumed. This was also evident on infrared images, taken during some of the measurements.

An image of a large BGA package exposed to 13.6 W is shown in Figure 3.11. The diode, shown in red, dissipates its heat evenly across the copper laminate (green). On the bottom side the heat is disposed by cool air injected at 500 Pa, however the light blue color indicates that the board and adjacent modules also heat-up. This might be caused by the passing hot air, however the previously calculated values also indicate heat transfer by conduction. In addition, some power is lost through the electric wiring.

* $\dot{Q}_{radiation@411K} \approx 0.36$ W.

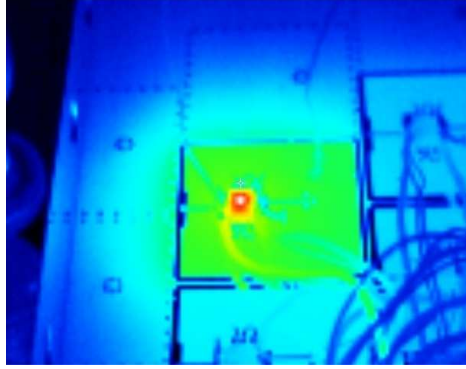

Figure 3.11: *Infrared image taken at $\dot{Q}_{dissipated}$ = 13.6 W and P = 500 Pa.*

As the amount of heat conducted away is not known, the real jet heat transfer coefficient cannot be quantified from the measurement data. Qualitatively however, the measurements make it clear that directly injected cooling has a positive effect on the cooling potential of the mounted packages.

Thermal Resistance

For each distinct jet configuration (i.e. fixed pressure and jet layout) temperature measurements were recorded for increasing power inputs. For each measurement the thermal resistance value from junction to ambient jet air can be determined as:

$$R_{junction \to jet\ air} = \frac{T_{junction} - T_{jet\ air}}{\dot{Q}_{dissipated}} \tag{3.14}$$

This value should be constant for each of the configurations as jet conditions (i.e. $\frac{H}{d}$, Re, number of jets) do not change. The thermal resistance for each configuration can be computed as the average of the measured values. These resistances are shown in Figure 3.12 as a function of the Reynolds number.

Heat transport through the top of the package to the ambient air (i.e. natural convection) is neglected. Theoretically, in the last presented case (1x2 small package) this value equals:

$$\dot{Q}_{nc} = h_{nc} \cdot A \cdot \Delta T = 5 \cdot 2.25e^{-4} \cdot (58 - 21) = 0.04\ W \tag{3.15}$$

This value is even overestimated, as the temperature of the copper laminate is lower than the junction temperature. Compared to the total dissipated power (8.5 W), the calculated value is low. Hence, heat transport through the top of the package can be neglected.

According to Figure 3.12, for higher Reynolds numbers (i.e. increased air flow) the resistance values drop, as expected. In the case of natural convection

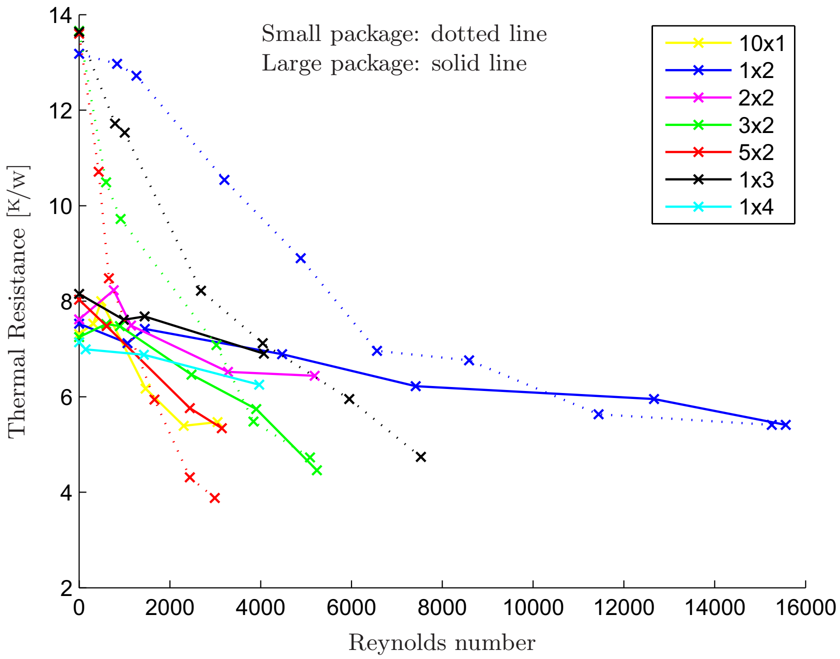

Figure 3.12: *Thermal resistance value versus Reynolds number.*

($Re = 0$) the resistance value for small packages converges to about 13-14 $^{\mathrm{K}}/_{\mathrm{W}}$; for large packages this is about 7-8 $^{\mathrm{K}}/_{\mathrm{W}}$. The lowest thermal resistance values are reached for relatively open jet configurations (5x2 and 3x2), as their thermally affected area is larger. The fact that the 1x2 jet reaches higher Reynolds numbers, does not result in the lowest resistance value. For the 5x2 jet a lower resistance value is reached at a much lower pressure. This is an advantage with respect to the structural integrity of the board structure and electronic components, and also for the pump requirements.

For small packages, increasing the Reynolds number has a significant thermal effect; for the large packages however, the increasing Reynolds number has a relatively low effect. This is due to the fact that the thermally affected jet area for large packages is low compared to the package itself and, as determined before, the heat spreads significantly through the laminate and board structure. Hence, constructing more jets underneath a large package would be beneficial. In terms of jet configuration, increasing the number of jets seems to give better results, than increasing the jet diameter. Probably as this gives a better flow profile underneath the packages. This also confirms the positive effect the recirculation zones of the impinging jets have on the heat transfer value, as discussed in Section 3.2.1.

Best results were recorded for a small package with 5 jets, ⌀2 mm. The overall resistance value of these 5 jets ($\approx 4\,^{\mathrm{K}}/_{\mathrm{W}}$) equals half the value of its theoretically calculated value ($\frac{40}{5} = 8\ ^{\mathrm{K}}/_{\mathrm{W}}$). Although this was for a $\frac{H}{d}$ ratio of one. For the 10x1 jet configuration the measured and theoretical values amount to 5.5 and 4 $^{\mathrm{K}}/_{\mathrm{W}}$, respectively. For thermal predictions these values are rather accurate. However, it must be noted that due to the unknown amount of heat conducted away, quantitatively these values should be used with caution. Qualitatively, the results can be applied for any jet configuration to be designed.

The complete dataset of some of the thermal measurements are presented in Appendix B.

3.5 Concept Evaluation

The concept of directly injected cooling through a BGA package has been presented. By incorporating thermal aspects at an early stage in the design process, a more integrated solution was realized. By adding just one (non-plated) through hole in the PCB, an electronic package can be cooled efficiently. Especially in the case of high component density cooling, this feature is beneficial from a production perspective. Instead of assembling a heat sink & fan on each component, in this case only the PCB has to be mounted on a pressure chamber. The overall clearance of heat sink, fan and overhead air volume for a fan to work properly, is replaced by the less height consuming pressure chamber. Moreover, reliability issues of individual fans no longer exist. It is replaced by a pump system, which can be installed more redundantly.

As a proof-of-principle, experimental investigation has shown that increased

heat transfer values can be realized. For instance, a temperature drop of 80 K compared to the case of natural convection was obtained at a power dissipation of 8.5 W. The measured values indicated that better results are feasible for small packages, as then the thermally affected jet area is relatively large compared to the package size. Adding more holes, and thus increasing the affected jet area, decreases the thermal resistance from junction to ambient jet air. A jet diameter of 2 mm proved to be optimal, for a standoff distance of 0.9 mm. Hence, an $\frac{H}{d}$ ratio of approximately one half.

As heat transport could not be isolated and dissipated only by the designed jet(s), the heat transfer values from other sources do not compare very well with the measured results. As the heat also spreads through the laminate and board structure, heat transfer values computed are relatively high. Therefore, care must be taken when utilizing the values reported. To get more accurate data on solely the jet performance, other temperatures, such as board and adjacent package temperatures must be recorded as well, to quantify the amount of heat conducted away.

Cooling of multiple packages simultaneously, with air flow fully interacting with adjacent, activated packages, is an underexposed area in the present study. This must be further investigated, before an industrial application can be considered. Also, in these measurements, the jet performance of one configuration can be isolated. This is due to the fact that in this case the heat cannot spread to the adjacent packages, as they are also heated.

At present, the concept of directly injected cooling is still promising and viable. The presented concept is very scalable, as electronic products on which multiple components need to be placed can be cooled both uniformly and simultaneously. For PCB technology in general, the concept of directly injected cooling may lead to new manufacturing strategies, where thermal management, electronics and mechanics are fully integrated. As the components have an individual cooling support, they are considered thermally decoupled, which is less constrained on the integrated design process. As such, the increased design freedom facilitates a less restrictive multifunctional product design. Altogether, this would result in a more compact electronic system, produced at a lower cost.

Chapter 5 will describe a detailed comparison of production techniques and cost between a state-of-the-art electronic product with a conventional cooling system and a similar product with an integrated directly injected cooling system.

Chapter 4

Integrated Heat Pipe Cooling

This chapter presents the integrated heat pipe cooling concept as an effective solution for high power density cooling cases. The working principle of a heat pipe and its limitations are presented. The concept embodiment and the effects of its design parameters are discussed. A detailed simulation model is given to perform both steady state and transient evaluations. The technology demonstrator that has been developed is presented together with the measurement results. At the end of this chapter, the concept will be evaluated.

4.1 Introduction

The concept of integrating a heat pipe directly into the PCB aims to deliver an electronic product equipped with a passive heat transport device embedded directly into its structure. Transporting heat by means of a heat pipe has already been used in many applications, for instance in space operations and nuclear research centers. The heat pipe was invented by Gaugler [20] in 1942; later Grover [22] reinvented, developed and first demonstrated its benefits in 1963. He also gave it its name "the heat pipe". The use of heat pipes as a reliable thermal management device for electronics was introduced by Cotter [12] in 1965. As the heat pipe offers very high thermal coefficients for heat transport, it is increasingly used to manage heat dissipations in electronic products, such as laptops, desktop computers and game consoles, primarily as add-on device. Integration of the heat pipe directly into the board structure – instead of mounting it as an add-on device – using standardized PCB production techniques, as will be shown in this chapter, has been identified as an innovative approach*.

* A patent "Planar heat pipe for cooling" was granted in 2007 [64].

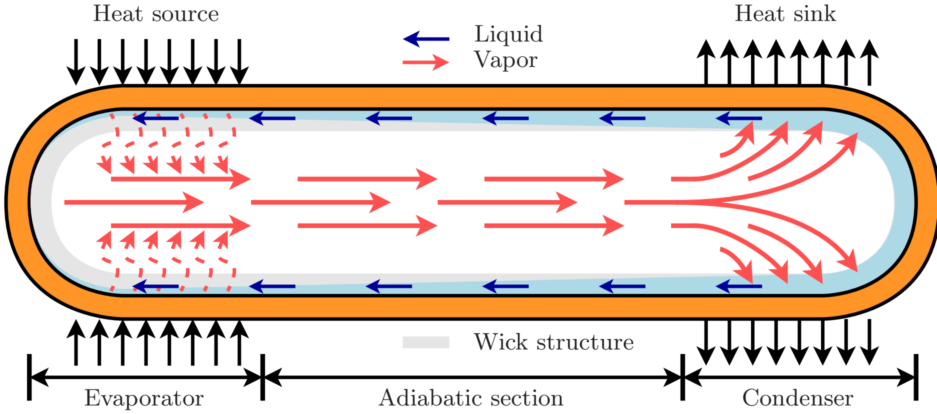

Figure 4.1: *Heat pipe principle.*

Other advantages, besides the increased thermal performance, are: the heat pipe requires no external power, moving parts or pump, and the temperature gradient across its length is extremely low. In fact, its equivalent thermal conductivity greatly exceeds that of any known metal. Moreover, the cross sectional area of the heat pipe is also very low, compared to, for instance, conducting heat sinks or coldplates. Finally, it also responds more quickly to a change of state, compared to conducting metals [19].

Traditionally a heat pipe, as shown in Figure 4.1, is manufactured as a tubular metal structure closed at both ends. It encompasses three essential parts: an evaporator, an adiabatic transport section and a condenser. Inside the heat pipe a working fluid is present both in the liquid and the vapor phases. A heat flux entering the evaporator, for instance from a hot component, vaporizes any available coolant liquid, thereby absorbing large quantities of heat. The vapor, indicated by the red arrows, travels through the adiabatic transport section to the condenser, propelled by the difference in pressure. In the condenser the vapor condenses as the temperature is lower, releasing its latent heat. This heat can be extracted from the heat pipe by a heat sink. To complete the cycle, the condensed liquid must be pumped back to the evaporator, as indicated by the blue arrows.

The fluid return is facilitated by a capillary or wick structure, indicated in gray. The wick structure, saturated with the liquid phase of the working fluid, is able to transport the fluid, due to the capillary pressure caused by the difference in curvature of the liquid menisci. This is illustrated schematic in Figure 4.2(a) by the liquid-vapor interface across the length of the heat pipe [19]. Here, L_e, L_a and L_c denote the evaporator, adiabatic and condenser sections, respectively. As the liquid vaporizes in the evaporator, the liquid level drops and the curvature of the meniscus increases locally (r_{small}). At the condenser end, where the vapor condenses the curvature flattens (r_{large}).

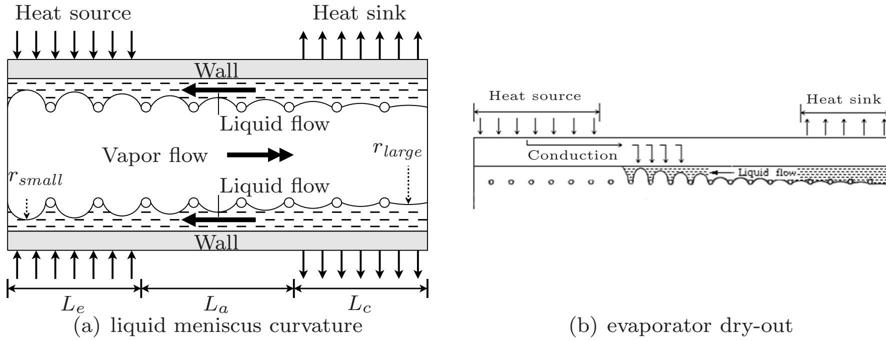

Figure 4.2: *Liquid-vapor interface across the heat pipe length [19].*

In a basic heat pipe analysis, the two counterflowing fluids (liquid and vapor phases) are analyzed, as they facilitate the continuous circulation of the working fluid. When the wick structure cannot pump sufficient working fluid to the heat source, evaporator dry-out occurs as illustrated in Figure 4.2(b). Locally no liquid can be evaporated; therefore, the heat will be transported through conduction. As such, the heat pipe temperature at the evaporator side will rise unacceptably and heat pipe failure occurs. An analysis method to predict the amount of power a heat pipe is able to transport will be presented in Section 4.2.

As mentioned before, no external power, moving parts or pump is required for the liquid transport mechanism. Common wick structures for heat pipes are screens, sintered metals and axial grooves. The smaller the pore size of the wick, the larger the capillary pressure. However, as frictional effects also increase for smaller pore sizes, a trade-off must be made. Complex composite wick structures, optimizing this trade-off, are researched constantly [29, 31, 63]. Since the goal of this study is a cost efficient integration of the heat pipe into the PCB, a wick structure will be selected that is compatible with standardized PCB production techniques.

For the heat pipe to function properly, it must be charged with the working fluid at its saturated pressure, i.e. the liquid and the vapor phases should be in equilibrium. As such, any extra heat is instantly absorbed by a shifting liquid-vapor balance. Filling of the heat pipe is a delicate procedure, as only the working fluid should be inside. A method often used in practice is to clean the heat pipe thoroughly and evacuate it, draining it of any residual gases, after which the working fluid is inserted and the heat pipe is pinched off, sealing it permanently.

Any presence of fluids other then the working fluid inside the heat pipe must be avoided; therefore, a high quality vacuum must be realized prior to the filling procedure. Fluids that do not condense at the working fluid's saturated pressure will occupy a certain volume inside the heat pipe. In operation, these Non-Condensible Gases (NCGs) migrate, together with the working fluid, toward the

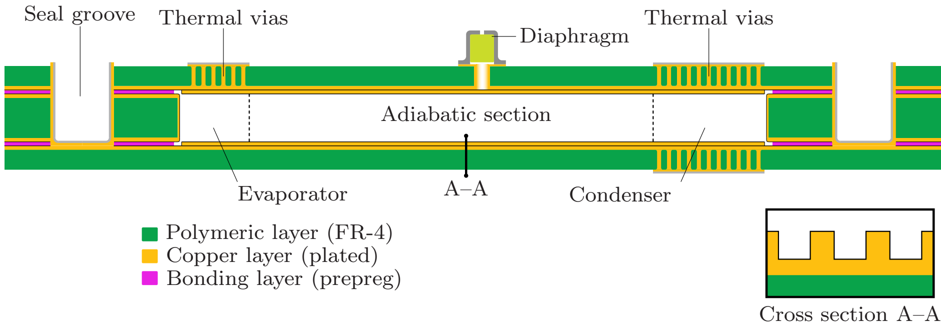

Figure 4.3: *Schematic layout of a heat pipe embedded into a PCB.*

condenser region. As they do not condense, they will block the condensation sites, causing a decrease in heat pipe performance or worse heat pipe failure. In practice, the most common NCG is residual air left inside prior to the filling procedure. Also, electrochemical reactions or galvanic corrosion may lead to the creation of undesirable gases.

4.1.1 Integrated Heat Pipe Construction

The concept of an integrated heat pipe design aims to construct the heat pipe directly into the board structure, using only standardized PCB production techniques already on site, as discussed in Appendix A. This equips the board with an integrated heat transport device at virtually no additional cost.

A typical multilayer PCB consists of polymeric layers pressed together with bonding layers (prepreg) in between. On each polymeric layer (FR-4), a metallic pattern can be produced (plated). This feature is utilized to construct a cavity – fully metalized – inside the PCB, which resembles the metal structure of a conventional heat pipe. The cavity is realized by machining a rectangular slot in an intermediate layer. Figure 4.3 illustrates an embedded heat pipe using one (thicker) intermediate layer. However, the height of the cavity, and thus the height of the heat pipe, can also be varied by stacking multiple layers in between the top and bottom layers. As the polymeric laminates and bonding layers are permeable to both water and gases, a groove is machined and plated around the cavity, ensuring a hermetically sealed enclosure.

The wick structure of the heat pipe, shown in cross section A–A, is composed of axially oriented capillary microgrooves. The ridges forming the microgrooves are realized by a selective plating process, also used for metallic patterning. Groove dimensions can be optimized for the applicable production process. For conventional dry film lithography, commonly used in PCB manufacturing, a minimum groove width of 50 μm and aspect ratios (height vs. width) around unity are feasible. However, wider grooves are more convenient to manufacture, as removal

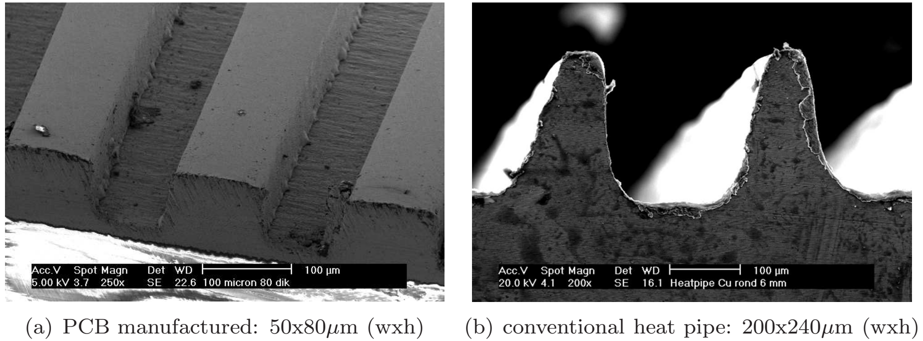

(a) PCB manufactured: 50x80μm (wxh) (b) conventional heat pipe: 200x240μm (wxh)

Figure 4.4: *Capillary microgroove structure of a heat pipe.*

of the dry film after the plating process is less strenuous. Figure 4.4(a) shows a magnified image of two microgrooves produced using this technique. As the height of the microgrooves increases, they tend to be less squared, due to the manufacturing process. However, as long as the capillary effect in not negatively influenced, this is not a problem. Compared to the groove structure of a conventional heat pipe [11], as shown in Figure 4.4(b), the producible groove widths are already four times smaller.

In the evaporator and condenser regions, the heat must travel through the laminated layers. These polymeric layers are poor thermal conductors. Therefore, to transfer the heat into and out of the embedded heat pipe efficiently, an array of thermal vias, as discussed in Section 2.1 and Appendix A.2.1, is placed at both the evaporator and the condenser locations.

Conventional heat pipes are usually charged through one side of the tube, after which the tube is pinched off. In this concept, this is not possible. Therefore, to charge the heat pipe, a low-profile diaphragm is developed. The diaphragm, designed for automated assembly as any other SMD component, consists of a metal cap filled with an airtight elastomeric barrier. By inserting a hollow needle connected to a vacuum system, the integrated heat pipe can be evacuated. After depressurization, the heat pipe cavity can be filled with its working fluid by inserting a second (scaled) needle through the diaphragm. Finally, to guarantee a permanent hermetically sealed heat pipe, the inlet hole of the diaphragm can be sealed with a small drop of solder.

To allow rework and repair on the electronic board, the heat pipe can be deactivated by removing the solder seal, opening the diaphragm with a needle and draining the working fluid. After maintenance, the heat pipe can be reactivated in the same manner as described before. The option to rework and repair is an important advantage of this heat pipe design, which has already shown its merit, as during research, prototypes had to be frequently reworked and refilled.

Due to the dimensions and cross sectional geometry of the heat pipe inside

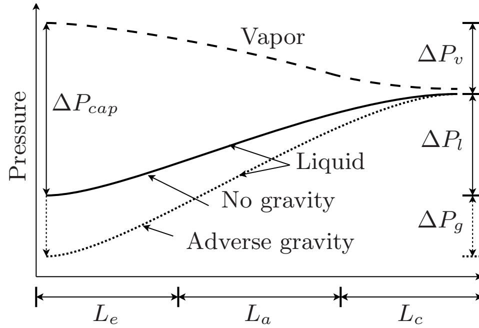

Figure 4.5: *Pressure distribution across the heat pipe length.*

the board structure, it is classified as a flat miniature heat pipe [7]. This general construction concept is expected to work well for all types of multilayer (PCB) designs.

4.2 Concept Embodiment

During operation, a heat pipe can encounter various limitations. In 1993, Cao [7] presented a comprehensive review of miniature heat pipes and their operating limitations. In the application of electronics cooling, the most critical limitation for miniature heat pipes is the capillary limit. This is the limit reached when the wick structure cannot pump sufficient working fluid to the evaporator region. The evaporator dries out and subsequently heat transport fails, as discussed in Section 4.1.

For the fluid to cycle continuously through the heat pipe, the capillary pressure must be larger than or equal to the sum of all pressure losses [19]. This is illustrated in Figure 4.5, where horizontally the heat pipe length is considered from the evaporator (left) to the condenser (right).

As the vapor travels from the evaporator to the condenser, pressure is lost due to frictional effects. Also, as the liquid flows back to the evaporator, pressure is lost due to friction. Depending on the heat pipe's orientation, gravity may either hinder or assist the fluid circulation. If the liquid has to ascend against gravity – the evaporator is located above the condenser – additional gravitational losses occur as shown in Figure 4.5. For a heat pipe in the opposite orientation – the evaporator is located below the condenser – the effect reverses. For the heat pipe to operate continuously, the combined pressure losses must be smaller than or equal to the capillary pressure. Hence:

$$\Delta P_{cap} \geq \Delta P_v + \Delta P_l + \Delta P_g \tag{4.1}$$

In this expression, the pressure losses due to phase changes are neglected; other body forces are also not considered.

Capillary Pressure

The capillary pressure is caused by the difference in curvature of the liquid menisci. The pressure difference across the fluid's liquid-vapor interface is described by the Young-Laplace equation and is determined by the surface tension of the liquid and the shape of the surface. For a circular capillary structure the Young-Laplace equation can be written as [19]:

$$\Delta P_{cap} = \frac{2\sigma cos\theta}{r_{eff}} \tag{4.2}$$

where σ and θ denote the surface tension and the contact angle, respectively, and r_{eff} represents the effective pore radius of the capillary structure. In the case of a wick structure based on capillary microgrooves, the effective pore radius across the groove is limited by the width of the groove. In axial direction of the groove the radius is infinite. Hence, the maximum capillary pressure constrained by the wick's geometry is:

$$\Delta P_{cap} = \frac{2\sigma cos\theta}{w} \tag{4.3}$$

where w denotes the width of the microgroove. In this case, the width of the microgrooves is considered constant across the entire groove length. According to Equation 4.3 for a high capillary pressure the surface tension, determined by the selected working fluid, should be large. Also, for the liquid to penetrate the wick structure efficiently, a low contact angle is required. This depends on both the working fluid and the material of the wick structure selected, as well as the roughness and structuring of the wick's surface. Finally, a small groove results in more capillary pressure; however, as mentioned before, the value of the liquid pressure losses (ΔP_l) will also increase. The resulting trade-off will be discussed in Section 4.2.1.

Working Fluid Selection

The working fluid determines to a great extent the capillary pressure and thus heat pipe performance. Its selection and the heat pipe operating temperature are closely linked to each other, as thermodynamic properties of the fluid vary with temperature. To select the best working fluid, a figure of merit is used. This figure is defined by Chi [9] as the *liquid transport factor*:

$$\frac{\sigma \cdot \rho_l \cdot H_{fg}}{\mu_l} \tag{4.4}$$

It distinguishes between four thermodynamic fluid properties that have an influence on the heat pipe performance. As Equation (4.4) suggests, surface tension (σ), liquid density (ρ_l) and the specific latent heat of vaporization (H_{fg})* all

* Against convention, the specific latent heat is denoted by H_{fg}, as otherwise it can mistakenly be interpreted as the local heat transfer coefficient at the liquid-vapor interface.

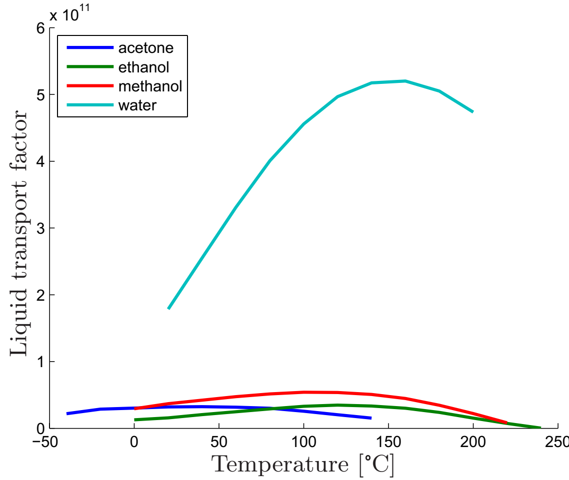

Figure 4.6: *Liquid transport factor for increasing temperature.*

have a positive influence on the heat pipe performance as their value increases. Conversely, the liquid viscosity (μ_l) has a negative influence for increasing values. The influences of these thermodynamic properties will also be demonstrated analytically during the steady state analysis in Section 4.2.1.

The liquid transport factor of Equation (4.4) is evaluated as a function of temperature for four commonly used fluids in the temperature range of electronics cooling: acetone, ethanol, methanol and water. The results are shown in Figure 4.6.

In the range of electronics cooling – above zero degrees Celsius and below the maximum allowed junction temperature of 150°C – water delivers by far the best performance. This is due to the fact that water has strong intermolecular forces caused by hydrogen bonding. Also, its molecular structure is small compared to the other fluids. Water acts in an electrochemically stable manner with copper, commonly used in PCB manufacturing. This makes it an excellent candidate as the working fluid for heat pipes. In addition, the non-hazardous nature and common availability of water are convenient. In fact, many COTS heat pipes in this temperature range use copper as metal structure and water as working fluid. Copper is also a very good conductor of heat.

Some studies also incorporate the thermal conductivity of the working fluid into their figure of merit. Chi [9] defines this as the *liquid conductance factor*. For a wick structure based on microgrooves, where most heat is conducted through the ridges, the conductivity of the working fluid is less important. However, even for a figure of merit including liquid conductivity, water remains the best candidate.

(a) contact angle definition (b) untreated copper (c) copper with surface finish

Figure 4.7: *Influence of a surface finish on the contact angle.*

Contact Angle

For the liquid to penetrate the wick structure efficiently, the contact angle must be low. The contact angle is defined as the angle θ between a liquid droplet and the solid surface, as shown in Figure 4.7(a). In principle, the contact angle is a physical property of three media in contact (solid, liquid and vapor); neither the geometry, nor gravity has an influence on the (static) contact angle [53].

A low contact angle wets the surface well; therefore, for wick structures to operate effectively, a low angle is compulsory. As PCB multilayer technology permits each board layer to be individually treated with a surface finish, the wettability of the wick structure can be significantly improved. By structuring the surface such that it has a high surface energy, the contact angle can be lowered.

As part of this research project, Nieboer [43] in 2008 demonstrated the positive effects of an oxidizing surface finish that enhances the surface energy by increasing the surface roughness. This is also demonstrated in Figure 4.7. Here, Figure 4.7(b) shows a single droplet of water on an untreated copper surface. The droplet has a contact angle of about 90 degrees. As such, the fluid will not spread and, as Equation (4.3) indicates, no capillary pressure will be achieved. Figure 4.7(c) shows a similar copper surface, however now it is treated with a surface finish. The surface finish consists of a chemical oxidation process, which increases the surface roughness. Traditionally, this finish is applied during the PCB manufacturing process to enhance the bonding strength between the laminated layers. As depicted, the contact angle drops dramatically, to almost zero. In practice, a contact angle below 10 degrees suffices as then, according to Equation (4.3), the influence of the constant angle on the maximum capillary pressure is minimal. Hence, the equation can be rewritten as:

$$\Delta P_{cap,max} = \frac{2\sigma}{w} \tag{4.5}$$

4.2.1 Steady State Analysis

As the heat pipe is a closed system, in a steady state the mass flow rate of the liquid must be equal to – but in opposite direction of – the vapor mass flow rate [8, 47]. According to the geometry of the integrated heat pipe concept and assuming that the microgrooves are completely filled with liquid, the following

relations can be deduced:

$$\dot{m}_l = \dot{m}_v \tag{4.6}$$

$$h \cdot w \cdot N \cdot U_l \cdot \rho_l = H \cdot W \cdot U_v \cdot \rho_v \tag{4.7}$$

where h, w and N denote the height, width and number of the microgrooves, respectively, H and W denote the height and width of the heat pipe vapor space, respectively, and U represents the velocity of the liquid or vapor flow.

Also in a steady state, the created mass flow rate can be computed as:

$$\dot{m}_v = \frac{\dot{Q}_{in}}{H_{fg}} \tag{4.8}$$

where $\dot{Q}_{in}$ equals the amount of dissipated power. According to Equations (4.7) and (4.8), the vapor and liquid velocities can be expressed as a function of geometric features, thermodynamic properties and the amount of dissipated power.

These vapor and liquid velocities are required to determine their respective pressure losses. These losses are evaluated using the general pipe flow equation, also shown in the previous chapter:

$$\Delta P = f \cdot \frac{4L}{d_h} \cdot \frac{1}{2}\rho U^2 \tag{4.9}$$

As both the vapor and liquid flow cross sections are rectangular, the hydraulic diameter is adopted here. Its definition is given in Appendix F.1. As the vapor and liquid velocities are relatively low and the heat pipe length is large compared to its hydraulic diameter, the entrance effects can be neglected. Equation 4.9 is valid for laminar and incompressible fluid flows, which is the case for both flows inside the heat pipe, as is proven in Appendices F.2 and F.3.

Using the definition of the Reynolds number, as presented in Equation 3.2, the pressure difference can also be written as:

$$\Delta P = \frac{2(fRe_h)\mu L}{{d_h}^2} \cdot U \tag{4.10}$$

The frictional effects of the vapor flow depend on the vapor space cross section. For a flat, rectangular cross section the flow encounters more friction, whereas a square cross section results in less friction. In 1987, Shah and Bhatti [55] presented a vapor friction factor ($fRe_{h,v}$), which depends only on the aspect ratio of the vapor flow cross section. In their approximation the perimeter of the cross section is considered stationary. In a heat pipe this can be assumed as the counterflowing liquid velocity is far less than the vapor velocity, due to the large difference between the vapor and liquid densities (Equation 4.7).

In contradiction to the vapor flow, the frictional effects of the liquid flow are not only dependent on the cross sectional geometry, but also on the counterflowing

vapor. For wide capillary microgrooves and thin vapor cross sections, the liquid encounters more friction. In 1980, Schneider and DeVos [52] considered the effect of a planar free liquid surface in their liquid friction factor ($fRe_{h,l}$) for various liquid cross sections. Both frictional effects are discussed and mathematically expressed in Appendices F.4 and F.5.

Gravitational Effect

The gravitational effect on the heat pipe's working fluid can be written as:

$$\Delta P_g = \rho_l g L sin\gamma \tag{4.11}$$

where L denotes the length of the heat pipe and γ represents the inclination angle of the heat pipe. Body forces on the vapor phase are neglected. As the PCB is considered stationary and body forces due to velocity changes or rotating systems are disregarded, g is the gravitational constant. However, other values can be adopted for instance for space applications.

Maximum Capillary Limit

Using Equations (4.5) to (4.11), the maximum transferable power according to the capillary limit of Equation (4.1) can be expressed as:

$$\dot{Q}_{cap,max} \leq \frac{\frac{2\sigma}{w} - \rho_l g L sin\gamma}{L_{eff}(F_l + F_v)} \tag{4.12}$$

where:

$$F_l = \frac{2\mu_l(fRe_{h,l})}{{d_{h,l}}^2 hwN\rho_l H_{fg}} \tag{4.13}$$

$$F_v = \frac{2\mu_v(fRe_{h,v})}{{d_{h,v}}^2 HW\rho_v H_{fg}} \tag{4.14}$$

$$L_{eff} = \frac{1}{2}L_e + L_a + \frac{1}{2}L_c \tag{4.15}$$

The effective heat pipe length (L_{eff}) is introduced as, on average, liquid will evaporate halfway the evaporator; similarly, vapor, on average, will condense halfway the condenser. The impact of gravity is directly related to the wick's capillary pressure. For positive inclination angles, where gravity hinders the liquid flow – the evaporator is located above the condenser – the sum of the capillary and gravitational contributions reduces, lowering the maximum transferable power. Conversely, for negative angles the maximum transferable power increases.

Also, as the friction factors F_l and F_v increase, for instance due to a smaller cross section, the maximum transferable power decreases. Here also the trade-off mentioned before is distinguishable, as a low pore radius, and thus a small groove

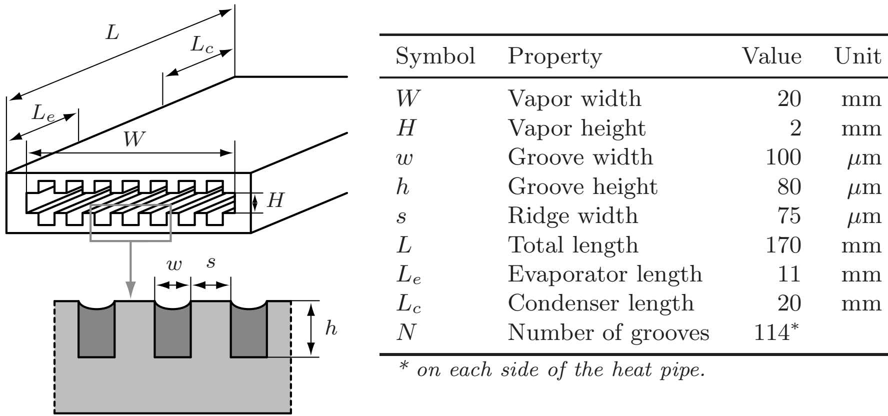

Symbol	Property	Value	Unit
W	Vapor width	20	mm
H	Vapor height	2	mm
w	Groove width	100	μm
h	Groove height	80	μm
s	Ridge width	75	μm
L	Total length	170	mm
L_e	Evaporator length	11	mm
L_c	Condenser length	20	mm
N	Number of grooves	114*	

** on each side of the heat pipe.*

Figure 4.8: *Assumed heat pipe geometry.*

width, introduces more friction; but, at the same time, increases the capillary pressure contribution. In the numerical simulation of the next section the trade-off will be further evaluated. Finally, a shorter heat pipe is able to transport more power. The effective length is a relatively dominant term. For instance in a horizontal set-up, the maximum transferable power is inversely proportional to the effective length.

4.2.2 Steady State Numerical Simulation

The capillary limit for a flat miniature heat pipe can be evaluated for various geometries using Equation (4.12) of the steady state analysis. This is especially useful for the initial prototype design, as it gives a quick insight into the effect of parameter changes. During these preliminary analyses the initial heat pipe geometry is based on average PCB, electronic component and heat sink dimensions.

The heat pipe length is chosen as the maximum distance from the center to the edge of an average board, 170 mm. The heat pipe is oriented horizontally and has an operating temperature of 55°C. Water is selected as the working fluid, due to its outstanding properties shown in Figure 4.6. The dimensions assumed are listed in Figure 4.8, unless they are part of the parameter investigation in question. Thermodynamic properties of the working fluid are listed in Appendix G.

Figure 4.9 illustrates the heat pipe performance for various parameter changes. In these analyses the number of microgrooves is determined by:

$$N = \left\lfloor \frac{W}{w+s} \right\rfloor \tag{4.16}$$

where $\lfloor\ \rfloor$ represents truncation.

Firstly, the effect of increasing vapor cavity dimensions is considered. Figure 4.9(a) shows the capillary limit for an increasing vapor height at five different

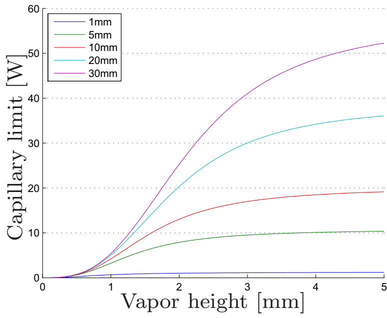

(a) vapor height for 5 heat pipe widths

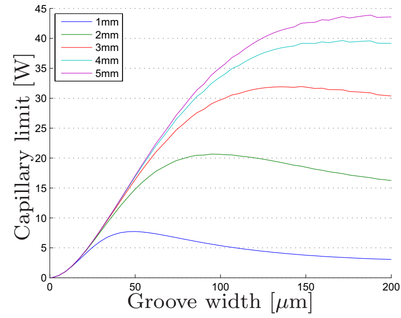

(b) groove width for 5 vapor heights

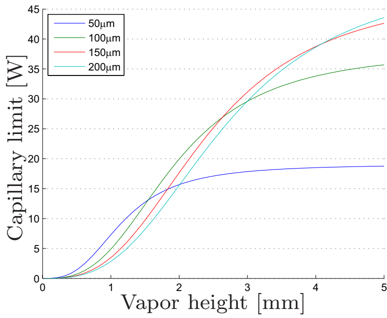

(c) vapor height for 4 groove widths

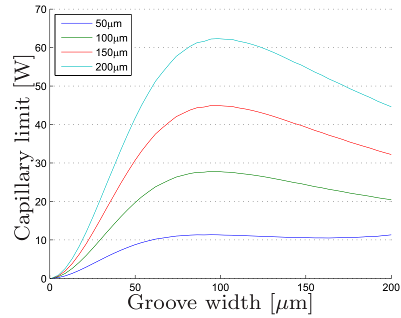

(d) groove width for 4 groove heights

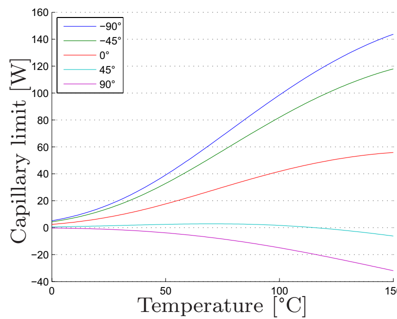

(e) heat pipe temperature for 5 orientations

Figure 4.9: *Performances for various dimensions, orientations and temperatures.*

vapor widths. As the vapor width increases, so does the number of grooves (w and s are constant). The figure shows that depending on the vapor width, increasing the vapor height after a certain threshold value no longer gives increased performance. This is due to the fact that in that case the vapor friction factor no longer is a limiting factor. Hence, for each vapor width a minimum vapor height can be selected, after which further enlargement is not beneficial.

Secondly, the effect of increasing microgroove width is considered. Figure 4.9(b) shows the capillary limit for an increasing groove width at five different vapor heights. Here, the total width (W) remains constant; hence as grooves widen, the number of grooves decreases. The figure shows that increasing the groove width is only beneficial for relatively large vapor heights. For thin heat pipes (1-2 mm), optimal performance is achieved for groove widths around 50-100 μm. This is due to increasing frictional effects on the liquid surface, caused by a wider groove in combination with a small vapor cross section. Also, this figure demonstrates the trade-off between the capillary pressure and friction effects mentioned before.

Thirdly, the effect of an increasing vapor height independent of the vapor width is considered. Figure 4.9(c) shows the capillary limit for an increasing vapor height at four different groove widths. The figure shows that by increasing the vapor height the performance improves. However, for small groove widths the performance increase levels off after a certain threshold value.

Fourthly, the effect of the groove height is considered. Figure 4.9(d) shows the capillary limit for an increasing groove width at four different groove heights. For any groove height maximum performance is reached around a similar groove width, 100 μm. Hence, from a design point-of-view groove height is not correlated, it should be chosen as high as possible. However, from a production perspective, groove height and width are very much related, as aspect ratios around unity were best feasible (Section 4.1.1).

Finally, the influence of the heat pipe orientation and operating temperature is shown in Figure 4.9(e). Negative values on the Y-axis are physically not possible, however mathematically a negative power can be computed. Heat pipes oriented against gravity (45° and 90°) barely operate, as the microgrooves do not deliver sufficient capillary pressure to pull the liquid up. For both the horizontal and gravity assisted orientations the maximum amount of power increases considerably with increasing temperature. This is due to the improving thermodynamic properties of water, as discussed in Section 4.2 and also visible in Figure 4.6. As a heat pipe almost dries out, the evaporator temperature will rise. Hence, in such a situation this feature automatically boosts heat pipe performance and can in some cases delay or prevent failure.

As part of this research project, Pijpers [49] in 2007 developed a design strategy to get maximum performance of such an integrated heat pipe for a constraint geometry. Firstly, the heat pipe width should be chosen as wide as the constraints allow. Typically this is the width of the electronic component to be cooled. Secondly, according to Figure 4.9(a) and the power requirement, a minimal vapor height can be deduced. Thirdly, according to Figure 4.9(b) an optimal groove

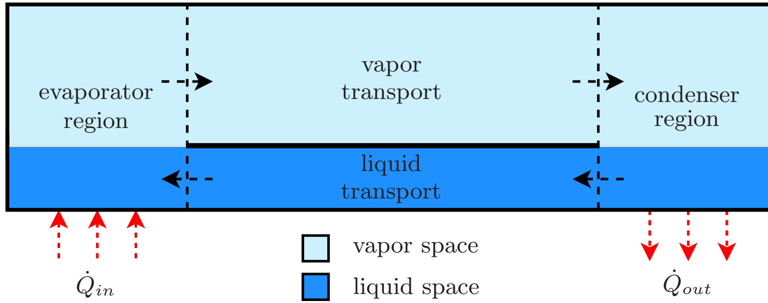

Figure 4.10: *Control volume elements for a single evaporator heat pipe.*

width can be selected. Finally, the microgroove height should be maximized according to the production process, assuming groove and vapor heights remain in a different order (μm vs. mm range).

4.2.3 Transient Analysis

The steady state analysis is very insightful as the effect of various heat pipe parameters on the heat pipe performance can be computed quickly and related to each other directly. From a design point-of-view the generated performance graphs are very useful to deduce an optimal heat pipe geometry. The disadvantage of this approach however is that transient effects are ignored.

This section discusses a transient heat pipe model. The model is capable of determining the heat pipe performance, based on a chosen geometry. Start-up effects and a change of state can be analyzed with such a model. Also, more complex heat pipe structures can be considered, for instance, a heat pipe with multiple evaporators. This allows the heat pipe to transport the heat of multiple components through the board structure toward the edge.

The transient analysis is also based on assessing the capillary limit of the fluid circulation. In the steady state analysis, simplified mass, energy and momentum equations of the two fluid flows were considered. The transient model also considers these balances; however, in this case, time-dependent influences are also accounted for. The heat pipe is divided into four control volumes [61]: an evaporator (1) and a condenser (2) region, and a liquid (3) and a vapor (4) transport section. For a basic heat pipe with one evaporator, the configuration of these control volume elements is shown schematically in Figure 4.10.

The advantage of using control volume elements, compared to finite element models, is that the model can be expanded with additional evaporator and condenser components very easily. Actual PCBs with multiple dissipating components, cooled by a flat miniature heat pipe, and the parameters effects can be analyzed quickly, without the necessity of complex and time-consuming finite element analysis.

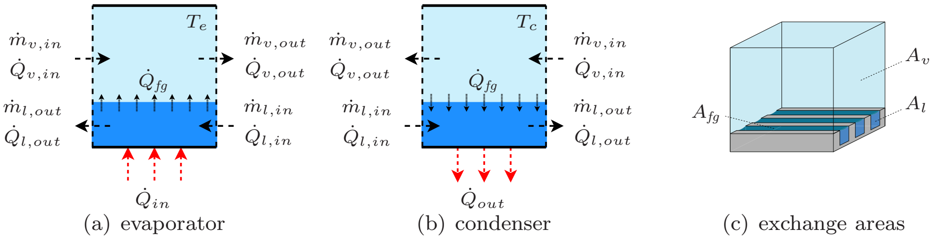

(a) evaporator (b) condenser (c) exchange areas

Figure 4.11: *Control volume elements for phase change regions.*

Mass Conservation Balance

For each of the control volumes the mass conservation balance equals [3]:

$$\frac{\partial m}{\partial t} = \sum_{in} \dot{m} - \sum_{out} \dot{m} \tag{4.17}$$

On the left hand side the local mass change is evaluated, whereas on the right hand side the inflowing and outflowing masses are accounted for. As the heat pipe is hermetically sealed, there can be no depletion or addition of mass. Hence, the total mass inside the system must remain constant at all times. Due to the one dimensional characteristic of the axially grooved wick structure, the local continuity equation for a phase change region can be written as a time-dependent change of the liquid height in the grooves:

$$A_{fg} \frac{d}{dt}\Big[h\rho_l\Big] = A_l\Big(\rho_{l,in}U_{l,in} - \rho_l U_{l,out}\Big) + A_v\Big(\rho_{v,in}U_{v,in} - \rho_v U_{v,out}\Big) \tag{4.18}$$

where A_{fg} and h denote the phase change area and local liquid height for the phase change region in question, respectively. The cross sectional area of the liquid and vapor flows are denoted by A_l and A_v, respectively. The fluid velocity of the flows into and out of the control volume in question are expressed as U_{in} and U_{out}, respectively. The subscripts l and v represent liquid or vapor flow, respectively.

Similar to the steady state analysis, the local change in vapor mass is neglected due to the large difference between the vapor and liquid densities. As the density (ρ) is determined by the local temperature, the density for an inflowing mass flux depends on the temperature of the adjacent control volume. For an outflowing mass flux the local temperature determines the density. The balance of mass fluxes is also illustrated in Figure 4.11 for both an evaporator and a condenser region. Also, the various fluid flow areas are shown.

Energy Conservation Balance

As the heat pipe is embedded into the PCB, it is surrounded with polymeric layers of low thermal conductivity. As such, the heat pipe can be assumed insulated

across the adiabatic vapor and liquid transport sections. For the phase change areas, where thermal vias are inserted into the polymeric layers, the heat exchange with the environment must be accounted for. In fact, the heat exchange with the environment should equal the heat absorbed c.q. released by the phase change effects. Therefore, the energy conservation equation for a phase change region equals [3]:

$$\frac{\partial(me + Q_{fg})}{\partial t} = \dot{Q}_{ex} + \sum_{in} \dot{m}e - \sum_{out} \dot{m}e \tag{4.19}$$

where e denotes the specific internal energy. As in the case of mass conservation, on the left hand side the change of local energy is considered and on the right hand side inflowing and outflowing energies are accounted for. Q_{fg} represents the (latent) heat associated with a change of state; evaporation is considered positive, condensation negative. $\dot{Q}_{ex}$ denotes the rate of heat exchange with the environment; its value is considered positive for heat input (evaporator) and negative for heat output (condenser). Equation 4.19 is in fact a rewritten form of the first law of thermodynamics.

The thickness of the copper layers required for the hermetically sealed enclosure is relatively thin. Therefore, the heat capacity of the enclosure and axial conduction of heat are negligible. Also, other heat losses are considered negligible. Therefore, the following energy conservation equations for the evaporator and condenser regions are deduced, respectively, as:

$$\frac{d}{dt}\Big[m_e c_{p,e} T_e\Big] + \dot{m}_{i,e} H_{fg} = \dot{Q}_{in} + \sum_{in} \dot{m} c_p \Delta T - \sum_{out} \dot{m} c_p \Delta T \tag{4.20}$$

$$\frac{d}{dt}\Big[m_c c_{p,c} T_c\Big] - \dot{m}_{i,c} H_{fg} = -\dot{Q}_{out} + \sum_{in} \dot{m} c_p \Delta T - \sum_{out} \dot{m} c_p \Delta T \tag{4.21}$$

where c_p denotes the specific heat at a constant pressure. The subscripts e and c refer to the evaporator and condenser regions, respectively. The mass flux changing state, crossing the liquid-vapor interface, inside the control volume element is represented by $\dot{m}_i$. The last two terms in both equations, accounting for the inflowing and outflowing energies, can be further expanded in a similar manner as Equation (4.17). The fully expanded equations are shown in Appendix E. The energy balances are also illustrated in Figure 4.11.

The heat leaving the system ($\dot{Q}_{out}$) is conducted through the thermal vias in the top and bottom layers of the heat pipe in the condenser region. The PCB is assumed to be clamped in a rack structure, which further disposes the heat into the ambient environment. Similar to Equation (2.3), this is modeled as a thermal resistance; therefore:

$$\dot{Q}_{out} = \frac{T_c - T_{ambient}}{R_{c \rightarrow ambient}} \tag{4.22}$$

where $R_{c \rightarrow ambient}$ represents the thermal resistance from the condenser region to the ambient coolant of the external cooler.

Momentum Conservation Balance

Fluid flow in the transport sections, connecting the phase change regions, is governed by the momentum balance. For a one dimensional flow inside a transport section the momentum balance equals [3]:

$$\frac{\partial(mU)}{\partial t} = \sum F + \sum_{in} \dot{m}U - \sum_{out} \dot{m}U \tag{4.23}$$

The change in local momentum on the left hand side is caused by the sum of external forces ($\sum F$) and by the inflowing and outflowing masses. This equation is a rewritten form of Newton's second law of motion. The external forces on the fluid flow inside the heat pipe, as frictional losses and gravitational effects, are considered.

The fluid cross section is considered constant across the axial length of the transport section. Therefore Equation (4.23) can be rewritten in a more convenient form, which considers the frictional and gravitational losses equivalent to the losses discussed in Section 4.2.1:

$$L_{\mathit{eff}} \frac{d}{dt}\Big[\rho U\Big] = \Delta P - \frac{2(fRe_h)\mu L_{\mathit{eff}}}{{d_h}^2} \cdot U - \rho_l g L sin\gamma \tag{4.24}$$

In fact, with the left hand side equal to zero, this equation is equivalent to the steady state analysis. The last term of Equation (4.24) accounts for the gravitational effect of the liquid flow. Depending on the heat pipe's orientation, this either has a positive of negative influence on the momentum balance. The effective transport length L_{eff} denotes the distance between the halfway points of the interconnected phase change regions.

As the vapor is in a saturated state, the pressure difference across the vapor channel can be calculated from the temperature difference. The liquid pressure difference also depends on the capillary pressure produced by the wick structure. In theory, the wick's geometry leads to a maximum capillary pressure, as shown in Section 4.2. This maximum is often used to determine the optimal heat transport capacity of a heat pipe, as was the case in the steady state analysis.

Since the liquid height in the microgrooves is defined by continuity Equation (4.18) in the transient analysis and the flow resistance per unit length in the grooves is considered constant, a first order linearization of the maximum capillary pressure between two phase change regions can be utilized. For instance, the pressure difference between an evaporator and a condenser can be written as:

$$\Delta P_l = \frac{2\sigma}{w}\left(\frac{h_c - h_e}{h_c}\right) - \Delta P_v \tag{4.25}$$

As the pressure difference is dependent on the liquid height in the microgrooves, more realistic transient simulation results, than for steady state analyses, can be

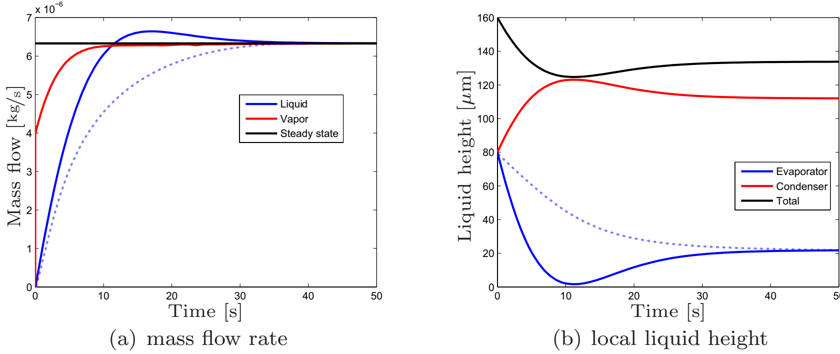

(a) mass flow rate

(b) local liquid height

Figure 4.12: *Heat pipe analysis for 15 W continuous dissipation horizontally.*

obtained. According to Equation (4.25), when the liquid level in both evaporator and condenser regions is equal, no capillary pressure is computed. Conversely, for a dried-out evaporator the maximum capillary pressure is computed.

In Appendix E the energy conservation Equations (4.20) and (4.21) are further expanded for the implemented transient analysis.

4.2.4 Transient Numerical Simulation

To verify the steady state values and consider transient effects, a transient analysis using the control volume approach discussed is applied. Since the temperature changes during the analysis, thermodynamic properties, such as specific heat (c_p), density (ρ) and dynamic viscosity (μ), as well as the vapor pressure difference (ΔP_v) are varied with temperature. In all numerical analyses presented, the temperature controlled properties lack an integration step. The geometry as was shown in Figure 4.8 is used throughout this analysis. The ambient rack temperature is assumed to be 25°C, and the thermal resistance from condenser to ambient ($R_{c \to ambient}$) is assumed to be 2 K/w.

By incrementing the value of the input power and rerunning the simulation, a maximum value for any given geometry can be determined. For the assumed geometry in a horizontal set-up, this turned out to be 15 W. The numerical prediction of the mass flow rate at this input value is illustrated in Figure 4.12(a). The steady state mass flow rate, depicted by the black line, can be calculated as:

$$\dot{m}_{ss} = \frac{\dot{Q}_{in}}{H_{fg}} \tag{4.26}$$

where H_{fg} denotes the specific latent heat of vaporization of water evaluated at the final simulation temperature of 55°C. The blue and red lines illustrate the time evolution of the liquid and vapor phase mass flows, respectively.

Due to inertia effects, the mass flow rate of the liquid phase overshoots the steady state value by about 5%. This overshoot is a consequence of a diminishing local liquid height in the evaporator. The height of the liquid in the microgrooves is shown in Figure 4.12(b).

The blue and red lines indicate the local liquid heights in the evaporator and condenser regions, respectively. The black line indicates the sum of both. Before reaching a steady state, the liquid level in the evaporator first reaches a minimum. At this point in time, a maximum in liquid pressure difference occurs, according to Equation (4.25). This accelerates the liquid through the microgrooves, causing the 5% overshoot. For higher input values the local liquid height in the evaporator drops below zero, indicating local dry-out and heat pipe failure. Hence, the maximum input power can be found iteratively.

According to Figure 4.12, the maximum performance is determined by the liquid flow dynamics. When, instead of a step input, a more gradual power input is applied, the overshoot and local minimum shift to the right until a critically damped situation is reached. This is illustrated by the dotted blue lines. Damping can be achieved by adding (thermal) mass.

At the start of the simulation, the liquid height in the microgrooves is level: both the evaporator and the condenser heights are $80\,\mu$m; the height of the grooves. As the heat pipe is transporting heat and the system temperature increases, the total liquid height decreases. Energy is stored in the vapor phase, as thermodynamic properties are temperature-dependent.

Table 4.1 lists the maximum transportable power as predicted by the analysis methods. In the steady state, where any time derivative vanishes, transient effects are neglected, resulting in a higher predicted value.

Table 4.1: *Predicted maximum transport capacity.*

Analysis method	Power [W]
Steady state (55°C)	20
Transient	15

Multiple Evaporators

Transient analyses that are based on control volume elements have an advantage over finite element models. Different parameter effects of the embedded heat pipe can be analyzed quickly, without the necessity of complex and time-consuming finite element analyses. Another advantage of this approach is the opportunity to expand the model, for instance with multiple distributed evaporators, with relative ease. This allows designers to rapidly analyze a fully populated PCB, with multiple dissipating components cooled by a single flat miniature heat pipe. Figure 4.13 illustrates a schematic heat pipe model with one additional evaporator. The second evaporator is placed halfway into the previously simulated heat pipe.

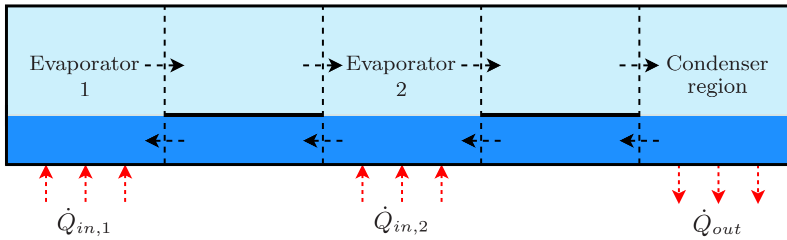

Figure 4.13: *Heat pipe model with an additional evaporator.*

As such, in practice two hot components can be cooled with just one integrated heat pipe.

For the evaporator and condenser regions at both ends of the heat pipe a similar mathematical formulation is used as in the single evaporator model. For the evaporator halfway however, all in- and outflows of Figure 4.11(a) must be accounted for. Also, in the expanded model four adiabatic transport sections are present: two for the liquid phase and two for the vapor phase. Hence for the liquid phase, two first order linearizations are adopted in sequence. As such, iterating with many more elements would, in the end, result in a finite element model. However, as mentioned before, this is not the aim of this model.

Figure 4.14(a) shows the operating area of the multiple evaporator model in a horizontal set-up. As illustrated in Figure 4.13, evaporator 1 (X-axis) is located at the end of the heat pipe and evaporator 2 (Y-axis) is located halfway. The red lines in Figure 4.14(a) show the maximum performance of the steady state model at various operating temperatures. As discussed before, at higher temperatures increased heat pipe performance is possible. For the transient analysis, the maximum performance is represented by the black line. In the transient analysis the temperature is not constant, it is dependent on the amount of power dissipated. For instance, at the two extreme cases, X and Y, the temperature equals 87°C and 141°C, respectively.

As illustrated in the steady state analysis, the value of the effective length (L_{eff}) in the momentum balance of Equation (4.24) is a relatively dominant term. Therefore, in the steady state model, evaporator 2 can approximately dissipate double the amount of heat compared to evaporator 1, as its location is halfway the heat pipe. Also in this case, steady state analyses result in higher predicted values than those that can actually be achieved when taking system dynamics into account. For instance at case X the temperature equals 87°C, whereas a steady state analysis at this temperature would result in performances even greater than the presented steady state performance line at 85°C.

For the two extreme cases, X and Y, in Figure 4.14(a), the liquid height in the microgrooves is shown in Figure 4.14(b). The solid lines in Figure 4.14(b) represent case X, where most power is dissipated at the end of the heat pipe. The simulation results are similar to the single evaporator heat pipe model. Evapora-

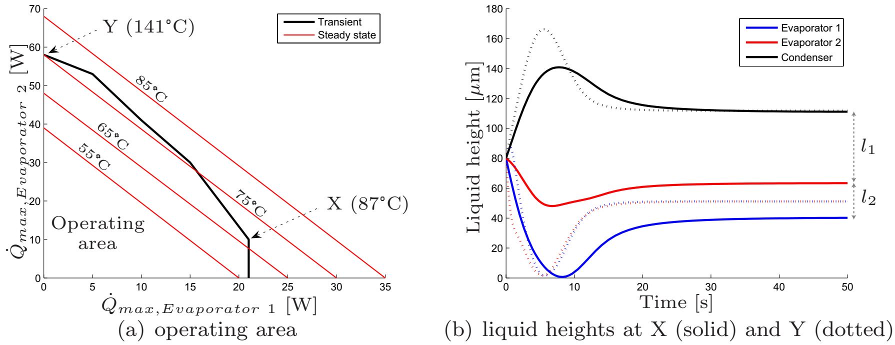

(a) operating area

(b) liquid heights at X (solid) and Y (dotted)

Figure 4.14: *Multiple evaporator analysis.*

tor 1 almost dries out, before reaching a steady state. There is sufficient liquid at evaporator 2 (halfway) at all times.

With all the heat dissipated at the end of the heat pipe (evaporator 1) and no dissipation halfway, the predicted value should agree with the previous transient model prediction. However, the value of 21 W is larger than the previously predicted value of 15 W. As the model contains two liquid transport sections, the first order linearization in Equation (4.25) expands both sections. Instead of one linear decreasing pressure term across the entire heat pipe, two are placed in series. Upon reaching a steady state, an equal distribution is to be expected. However, as shown in Figure 4.14(b), l_1 and l_2 are not equal. This is due to the temperature-dependent values lacking an integration step. In finite element analysis this is referred to as weak coupling. As the temperature difference is minute across the heat pipe's length, the sensitivity of the vapor pressure difference reaches discretization limits. This explains the discrepancy in heat pipe performance between both simulations. To solve this, a direct (strong) coupling between temperature and temperature-dependent value is required. However, as the differences are not of great importance for this conceptual design, this is not further investigated.

The dotted lines in Figure 4.14(b) represent case Y, where all power is dissipated halfway the heat pipe. In both evaporators 1 and 2 the liquid height decreases to almost zero, indicating local dry-out, before reaching a steady state. At the start of the simulation, the liquid height at evaporator 2 decreases more rapidly than at evaporator 1. Therefore, liquid flows to the middle of the heat pipe from both evaporator 1 and the condenser. When a steady state is reached, there is no difference in liquid height, and thus no flow, between both evaporators. As expected, the last section of the heat pipe does not contribute to any heat transport. Also, as the effective heat pipe length is shorter, steady state is reached faster.

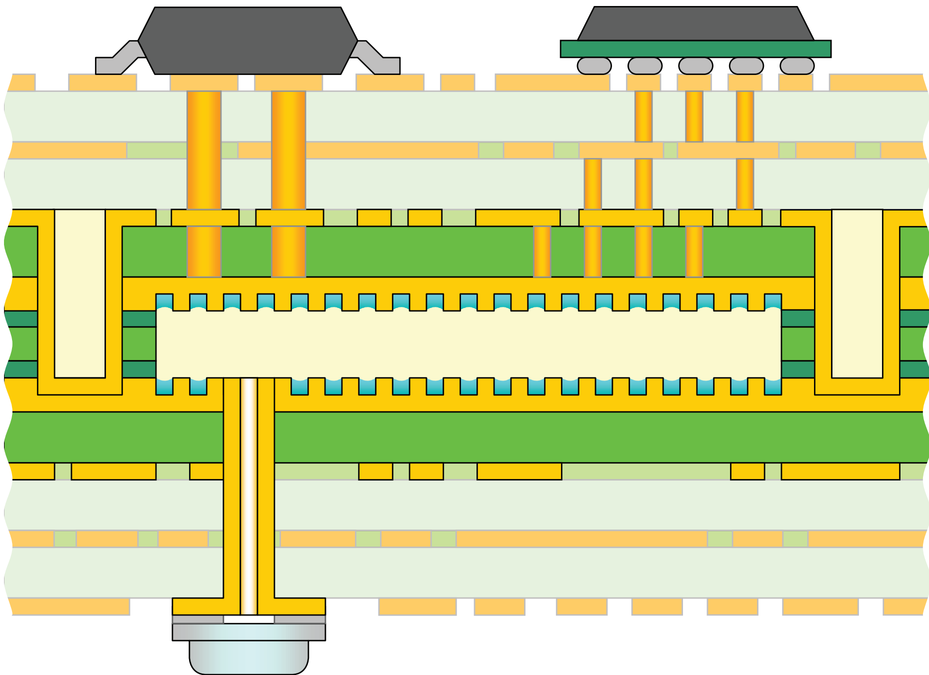

Figure 4.15: *Cross sectional view of a concept design for integrated cooling of multiple components; illustration by Mannak [38].*

4.2.5 Design for High Power Density Cooling

In this concept, the integrated heat pipe is produced using standard PCB production techniques. The heat pipe performance greatly depends on its orientation and geometry. For a small, thin heat pipe, up to 15 W can be transported horizontally over a distance of 170 mm with an extremely low thermal resistance. For shorter distances, larger geometries or gravity assisting orientations this value increases considerably. Hence, depending on the specifications any type of efficient heat transport device, including one for high power density cooling, can be designed. Also, a single heat pipe can be used to cool multiple electronic components simultaneously. A conceptual design of this is illustrated in Figure 4.15.

Here, a relatively complex PCB comprised of seven layers is shown. The two electronic components are cooled via one integrated heat pipe in the middle of the board structure. Also, the diaphragm to charge the heat pipe, is shown on the bottom side. Heat is inserted through thermal vias and transported normal to the presented cross section to the side of the board, where it is extracted again via thermal vias. The layers, responsible for embedding the heat pipe, can also be used for electronic functionality outside the direct heat pipe area.

From a thermal perspective, there is no coupling between the individual com-

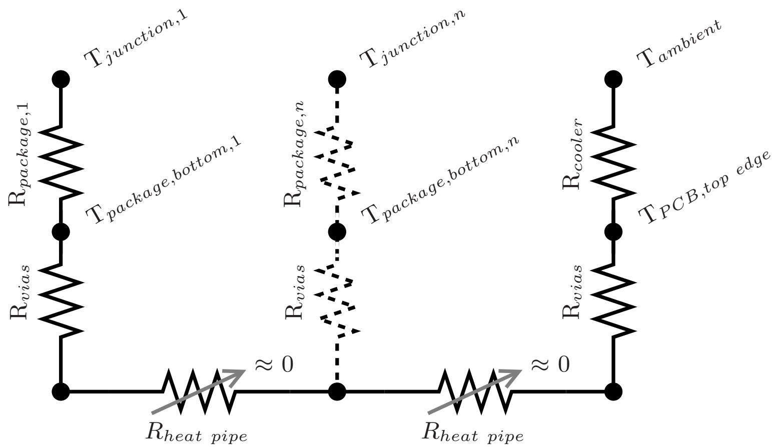

Figure 4.16: *Compact thermal model for the integrated heat pipe.*

ponents, nor to the edge of the board, as the thermal resistance across the heat pipe's length is minute. The thermal properties of the PCB, which normally affected the overall thermal behavior dramatically, is – also in this concept – circumvented by the integrated heat pipe. This is illustrated in the compact thermal model of Figure 4.16.

Thermal properties of each component are affected only by the resistance from the component to the heat pipe and from the heat pipe toward the ambient environment. This is valid for any number of components, as long as they can be connected to the heat pipe and the heat pipe has sufficient heat transport capabilities. Hence, this concept can be used for high power density cooling, as well as high component density cooling; both defined as extreme cases in Chapter 2.

The axial path of the heat pipe is not required to go straight; both vapor and liquid flows can travel through corners. Hence, the heat pipe can be designed to meander through the board, thermally connecting all high power components. Also, parts of the board constrained by, for instance, electronic requirements can be avoided, by positioning the heat pipe around these areas. This makes the integrated heat pipe also very flexible.

4.3 Prototype & Test Set-up

In order to prove the concept of a heat pipe integrated directly into the PCB, a technology demonstrator was developed. Overall geometric board changes should be kept to a minimum; otherwise, the existing rack structures and cabinet set-ups must be changed as well. In general, PCBs are thin; 1.6 mm being a common value. The vapor height of the heat pipe not only influences board thickness, but

also the performance, especially for thin heat pipe. As a compromise, a cavity height of 2 mm is chosen. Although the overall board thickness increases, this is compensated by the dismissal of, for instance, a heat sink or coldplate in the final set-up. According to Figure 4.9, a heat pipe performance of at least 20 W should still be feasible for a vapor width of 20 mm in a horizontal orientation. If a higher performance is required, a wider heat pipe can be considered. Also according to Figure 4.9, the optimal groove width at this vapor height is approximately 100 μm.

One of the manufactured prototypes used for the experimental verification is shown in Figure 4.17. The heat pipe embedded into the PCB is illustrated by the dotted yellow box; its dimensions are 170x20 mm, as shown in the figure. The internal vapor height is 2 mm; the overall board thickness is 4 mm. Detail A shows an X-ray image of the evaporator region. Here, the microgrooves and also the thermal vias in the top layer are visible. Cross section B–B shows an X-ray image of the side-view of the condenser region. The thermal vias in the top and bottom layers are clearly visible. The wick structure of the heat pipe is composed of 114 grooves of 100 μm width and 80 μm height produced on both the top and bottom layers.

Figure 4.18 shows the heat pipe prototype with its mounted components. The diaphragm and pressure gauge are mounted onto two machined openings. The heat pipe was charged through the diaphragm, whereas the pressure gauge was used to measure the internal vapor pressure. Onto the evaporator region a power resistor, acting as a heat source, is assembled. All components are assembled as standardized SMD components. Also visible are seven areas equally distributed along the heat pipe length, where the thermocouples were attached. These were used to measure the internal heat pipe temperature; therefore, underneath these areas also thermal vias were manufactured. Finally the condenser area is shown; here, an external cooler was clamped onto the top side to dispose the heat dissipated by the power resistor.

Charging of the heat pipe proved to be quite cumbersome. The airtight elastomeric barrier inside the diaphragm did not always prevent air from entering the heat pipe. Subsequently the high quality vacuum required was also not always reached. Reliability during the filling process proved to be very important. As the pressure gauge could only detect relative pressure changes and not determine the absolute pressure, the vacuum quality inside the heat pipe could not be monitored consistently during the filling process. A small leakage or contamination would not be detected by the pressure gauge. However during operation, when the measured temperature and pressure values change, these faults became visible.

The heat pipe was tested in both the horizontal and vertical orientations with the previously mentioned power resistor, increasing heat dissipation until evaporator dry-out occurred. In the vertical orientation, gravity assisted the liquid flow. Voltage and current were recorded to determine the amount of power dissipated. Sufficient time was allowed to reach a steady state after changing the power input. During the experiments, heat pipe performance was measured through the

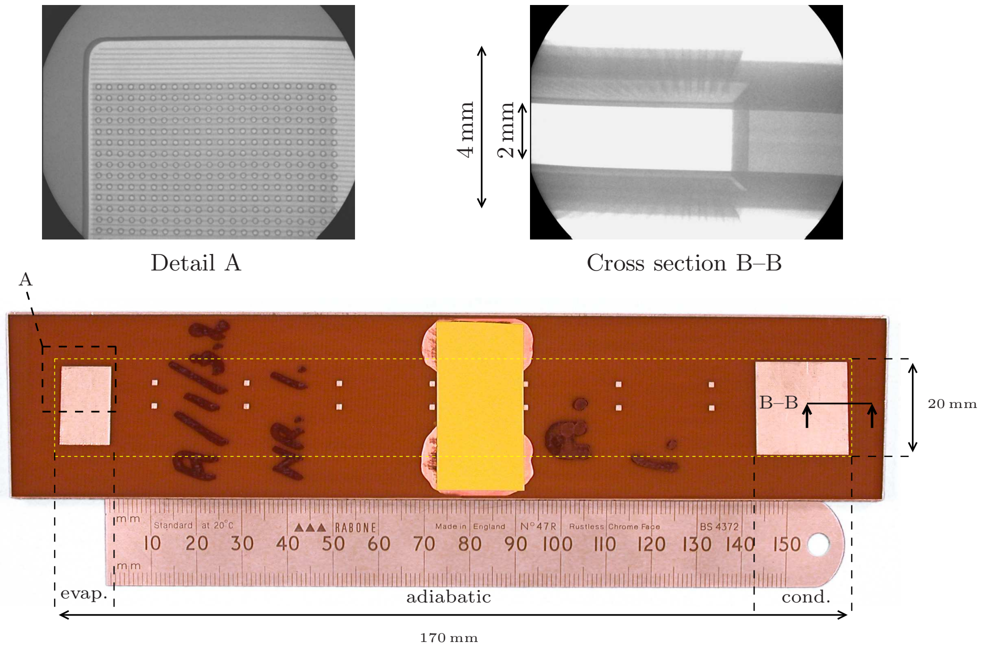

Figure 4.17: *Manufactured prototype with X-ray details.*

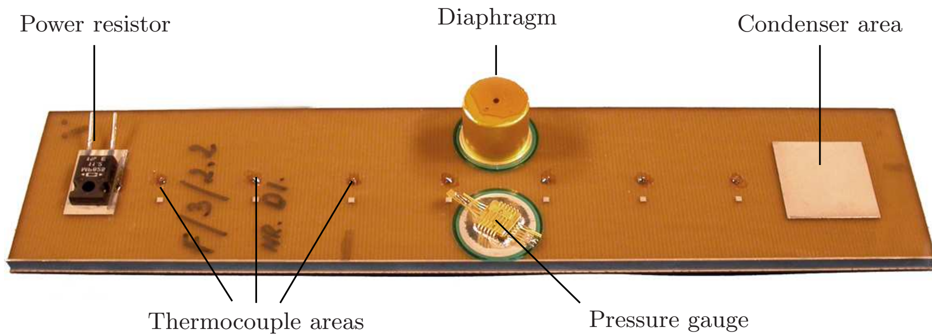

Figure 4.18: *Prototype with mounted components.*

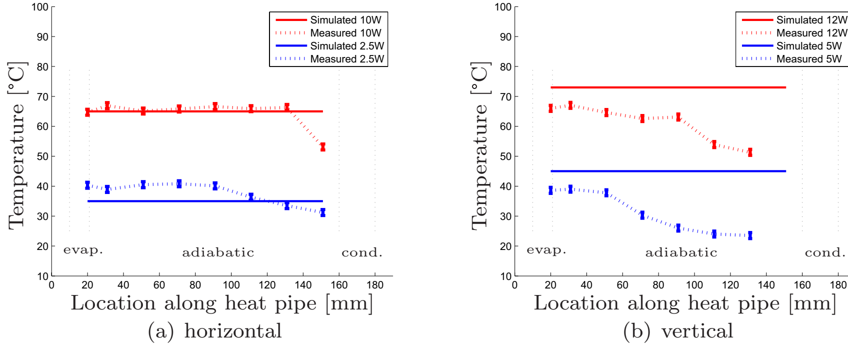

Figure 4.19: *Temperature distribution along the heat pipe's length.*

thermocouples attached to the thermal vias across the heat pipe's length. Also, the pressure gauge was used to measure internal vapor pressure changes. Both steady state and transient responses were monitored. The measurement set-up is discussed in detail in Appendix C.

4.4 Measurement Results

Figure 4.19 illustrates the temperature distribution along the heat pipe's length when subjected to a thermal dissipation of 2.5 and 10 W horizontally, and 5 and 12 W vertically. In all cases, the solid lines represent the simulation predictions of the control volume model, as discussed in Section 4.2.3, whereas the dotted lines indicate the measurement results. In the vertical case, the last thermocouple did not function.

Especially in the horizontal mode, the heat pipe is able to transport the heat with a low temperature gradient along its length; vertically this behavior was recorded less. For both cases, at higher dissipated values the evaporator temperature would rise unacceptably, indicating local dry-out.

In the simulation a value of $R_{c\rightarrow ambient}$ of $4\,{}^{\mathrm{K}}/_{\mathrm{W}}$ was used, as an external cooler was attached only to the top side, instead of being clamped onto the top and bottom sides of the condenser. At the time of the measurements the ambient coolant temperature was approximately 25°C. The heat pipe operating temperature is mainly determined by the amount of dissipated power and the value of $R_{c\rightarrow ambient}$ at the condenser side, where the heat is extracted from the heat pipe. As the heat pipe operates with a low thermal gradient across its length, the equivalent thermal conductivity is extremely high.

The simulation model assumes that condensation occurs in the condenser region. In practice, this is temperature- and thus power-dependent. Horizontally, at 2.5 W of heat dissipation, condensation occurs just over the halfway point along

the heat pipe, as indicated by the temperature drop of the dotted blue line in the adiabatic section of Figure 4.19(a). For the 10 W case, the temperature drop and the area of condensation shift to the end of the heat pipe. The same occurs in the vertical case, only earlier: at 5 W condensation starts already between the 3rd and 4th thermocouple. Also, for a higher power input (12 W) the point of condensation shifts to the right, between the 5th and 6th thermocouple.

The temperature drop in the condenser region is an indication of the presence of NCGs. During the filling process, either the vacuum quality was insufficient or leakage occurred when the working fluid (water) was inserted. As discussed in Section 4.3 and demonstrated here, charging must be done in a reliable manner. Power losses through the insulation also cause premature condensation. This explains the difference between the vertical and horizontal case, as vertically heat is dissipated better by natural convection. Also, the build-up of NCGs in the top of the heat pipe – in the vertical case this is the condenser region – might attribute to the premature condensation.

The pressure gauge, also mounted on the PCB, is useful for the detection of any leakage or permeation of air through the heat pipe's enclosure when the heat pipe is in operation. When the cavity is hermetically sealed and the vapor is in saturated state, temperature and pressure should be correlated proportionally assuming the vapor acts as an ideal gas. This is verified for the previously presented vertical measurement. In Figure 4.20, the red line represents the time evolution of the first thermocouple from the evaporator side; the blue line indicates the pressure profile (right-axis). The figure illustrates the heat pipe reaching a steady state under thermal loads of 5 and 12 W, successively. After approximately 14 minutes the input power was switched off and the heat pipe gradually cools down.

Both quantities (temperature and pressure) follow a linear trend, as can be expected when assuming an ideal gas. In the case of a leakage this linear trend will be disturbed. At 5 W dissipation, the condensation point still lays before the pressure gauge. Hence, the linear trend is less visible here. As mentioned, the presence of any NCGs is not detectable by the pressure gauge; this could only be deduced from the temperature profile across the heat pipe's length.

Also shown in the figure by the dotted red lines is the time evolution of the heat pipe's simulated temperature profile. Both simulations (5 and 12 W) start at an ambient temperature of 25°C. The predicted final temperatures are similar to the simulated temperatures in Figure 4.19(b). Both are approximately 7-8°C too high. For a temperature prediction however, this is still rather accurate.

The simulation model responds more quickly to a change of input than the actual heat pipe. This may be explained by the absence of heat capacitance of the enclosure in the simulation model. As no material needs to be heated up, steady state is reached more quickly. Also, the heat-up time of the power resistor is not taken into account in the simulation. As discussed in Section 4.2.4, additional (thermal) mass dampens the system and diminishes dynamic effects. As a consequence heat pipe performance actually increases.

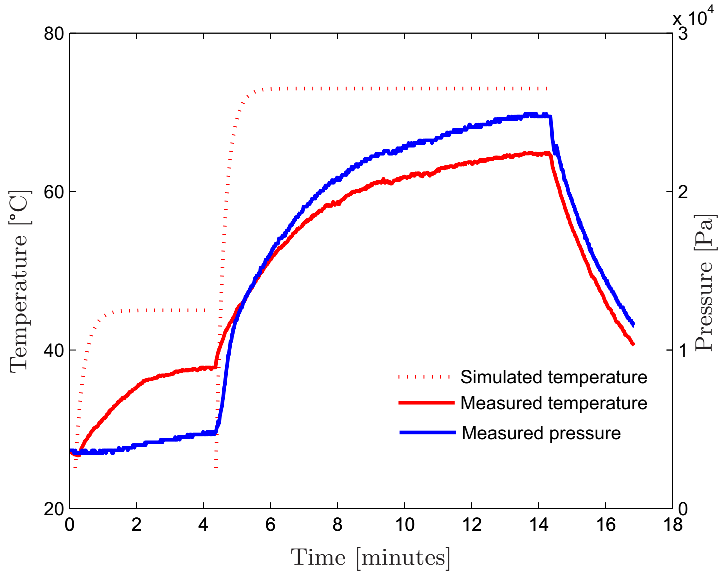

Figure 4.20: *Temperature and pressure profile for 5 and 12 W (vertically).*

Thermal Design Values

Of particular interest from a design point-of-view are the equivalent thermal conductivity and resistance coefficients from the evaporator region to the condenser region, calculated according to Equation (2.3), respectively:

$$k_{eq} = \frac{\dot{Q}_{in} \cdot L_{eff}}{\Delta T_{e \to c} \cdot A} \tag{4.27}$$

$$R_{eq} = \frac{\Delta T_{e \to c}}{\dot{Q}_{in}} \tag{4.28}$$

The thermal properties of both measurements, as well as those of solid copper, are presented in Table 4.2. In the case of 10 W dissipation horizontally, the equivalent thermal conductivity reaches eight times the conductivity of solid copper. This is a good illustration of the high efficiency heat pipes have for heat transport purposes.

Theoretically, every Watt dissipated by an electronic component soldered onto the PCB, may cause as little as 1.2 K temperature increase from the component to the condenser region. In practice this rule is limited, as the heat pipe may eventually dry out in the evaporator region. It must also be noted that in this approximation, heat transfer from the condenser to the ambient environment is assumed to be unrestricted.

Table 4.2: *Equivalent thermal properties.*

	$\dot{Q}_{in}$ [W]	$\Delta T_{e \to c}$ [K]	k_{eq} [W/mK]	R_{eq} [K/W]
Heat pipe (horizontal)	2.5	9.1	1061	3.6
	10	11.6	3330	1.2
Heat pipe (vertical)	5	15.1	1279	3.0
	12	14.7	3153	1.2
Solid copper	-	-	400	9.7

Compared to the theoretical values presented in Section 4.2, the heat pipe transports less power than calculated. Horizontally the heat pipe should have been able to transport 15-20 W, depending on the type of simulation (transient* vs. steady state). This discrepancy may be attributed to several factors:

- The contribution of the bottom layer to the total heat pipe performance. In the current design, heat is not conducted very efficiently to the bottom side, causing the top layer to facilitate most heat transfer. Also, in the condenser region heat exchange with the environment was supplied to only one side.
- The temperature drop at the condenser region in Figure 4.19 indicates the presence of NCGs. They are a consequence of an imperfect filling method. In operation, they block the condensation sites in the condenser, causing undesirable temperature gradients and decreased heat pipe performance.
- The hypothesis of an optimal wetted wick structure. In practice, this assumption may be adversely influenced by small amounts of contamination on the board layers or in the working fluid, also caused by an imperfect filling method.

4.5 Concept Evaluation

The concept of a heat pipe integrated directly into the laminated structure of a PCB has been presented. Analogous to the concept of directly injected cooling, thermal engineering and production aspects are incorporated at an early stage in the design process for this concept as well. Hence, a more integrated solution is realized. Promising results from this novel method have been presented. By machining a cavity in an intermediate layer of the PCB and plating a wick structure on the top and bottom layers of this cavity, an integrated heat pipe was designed. As such, the integrated heat pipe is produced using established, mainstream PCB manufacturing and SMD assembly techniques. In the future, this would allow engineers to design electronic products featuring full integration of thermal management and electronic circuitry. This pushes the boundary further toward more

* With a $R_{c \to ambient}$ of 4 the capillary limit increases to 17 W.

functionality in a smaller form factor and lighter products, as add-on heat sinks or coldplates are no longer required.

As a proof-of-principle, experimental investigation has shown increased heat transfer values can be realized. Components can be cooled with extremely low thermal gradients, within limited power dissipation values. The measured thermal values show a relatively good agreement with model predictions. However, the amount of transportable power is slightly overestimated by the models. As discussed, this may be due to an unoptimized prototype design or an imperfect filling procedure. The dynamic behavior of the measurement is dominated by the heat capacity of the heat pipe enclosure and power resistor. Therefore, accuracy for the time evolution analyses may be further improved by refining the simulation model. However, for fast steady state analyses this is not required.

Most importantly, the filling technique of the heat pipe has to be further perfected, in order to clean, fill and seal the heat pipe reliable and reduce the amount of NCGs inside the heat pipe cavity. To facilitate true mass production, the filling process must be automated. It should be the final step in the production line, after all electronic components are mounted. Also, long-term reliability of the heat pipe needs to be verified. Experiments with an integrated heat pipe in a fully populated PCB with multiple distributed dissipating components is an underexposed area in the present study. This should give more detailed information on the heat transport capabilities inside more complex boards. The issues mentioned must be further investigated, before an industrial application can be considered.

The low thermal resistance values confirm this cooling concept as an excellent candidate for the thermal management of electronic products. As the resistance value between components is low, they can also be considered thermally decoupled. As such, similar to the concept of directly injected cooling, here again the integrated design is less constrained. The increased design freedom facilitates a less restrictive multifunctional product design. Eventually, this would result in a more compact, lighter electronic product, produced at a lower cost.

Also for this concept, Chapter 5 will describe a detailed comparison of production techniques and cost between a state-of-the-art electronic product with a conventional cooling system and a similar product with an integrated heat pipe cooling system. In addition, a comparison is made to another study of embedded heat pipes in PCBs.

Chapter 5

Evaluation of Presented Concepts

In this chapter, both concepts that were developed are evaluated. Both concepts are compared to other state-of-the-art electronic products and conventional cooling systems for these products. The comparison is based on both production techniques and cost efficiency. At the end of this chapter, the conclusions that can be drawn from this evaluation are presented.

5.1 Introduction

The previous chapters of this thesis described the development of two innovative cooling concepts for electronic products. Both concepts developed are characterized by a thermal management system integrated directly into the product structure. Also, both implementations showed promising results during the experimental investigation. In an attempt to realize more cost efficiency, both concepts rely on established manufacturing methods for their production.

This chapter describes a detailed comparison of production techniques and cost efficiency between a state-of-the-art electronic product with a conventional cooling system and an equivalent (redesigned) product with an integrated cooling system. Comparable products were selected either based on recent publications or because the products had just reached a commercial production stage. In the case of the directly injected cooling concept, the comparison is made with a synthetic jet cooling system and cooling of a modular system. The integrated heat pipe concept is compared to a high performance rack cooling system and a heat pipe embedded in a similar manner.

Of particular interest from a commercial point-of-view is the cost relationship between the state of the art and the redesigned product. PCB production and

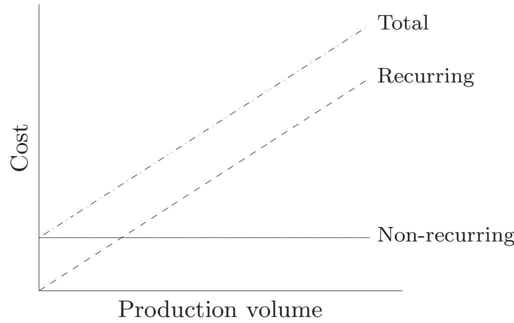

Figure 5.1: *Influence of cost categories on the total cost.*

SMD assembly technologies are mainly based on batch processes. Hence, there are two major cost categories directly related to each electronic product:

- Non-recurring or constant cost, such as PCB design, component layout design, set-up cost.
- Recurring or variable cost, such as material, machine time, assembly cost.

In some studies also a distinction is made for cost applicable to each batch, for instance tooling set-up cost. Here, however these costs are considered non-recurring cost as well. For electronics, in broad terms, non-recurring cost can be considered engineering cost, whereas production and assemblage deal with recurring cost.

The goal of this research was to realize a cost reduction by adhering to mass-market production techniques. Therefore, all costs belonging to the latter category are crucial, as they recur in every single product. This is illustrated in Figure 5.1. As the production volume increases, recurring costs have more influence on the total cost per product.

The next two sections will illustrate that for both developed concepts the redesigned product with an integrated cooling system, recurring cost shift to non-recurring. Hence, for increasing production volume (i.e. mass-market applications) a significant cost reduction can be achieved.

5.2 Directly Injected Cooling Concept

5.2.1 Synthetic Jet Cooling

A synthetic jet can be created by pulsating a flexible membrane inside a partially closed environment. As the membrane oscillates, air is either sucked into the synthetic jet chamber or ejected through the orifice, thus creating a jet. The operation of the flexible membrane can be compared to an acoustic speaker, where

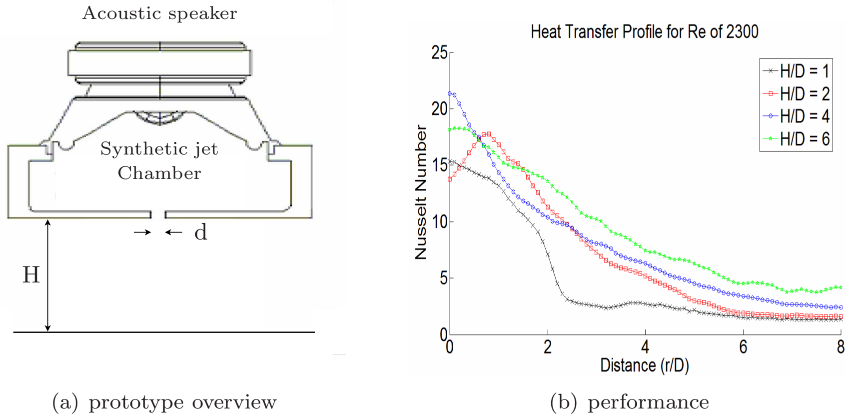

(a) prototype overview (b) performance

Figure 5.2: *The synthetic jet presented by McGuinn et al., 2008 [40].*

the pulsating effect of the air jet is controlled by the operating frequency of the speaker. McGuinn et al. [40] in 2008 reported heat transfer values of such a jet with a constant stroke length. Their prototype is shown in Figure 5.2(a).

The thermal performances for several jet-to-target and jet diameter ratios for a Reynolds number of 2,300 reported by McGuinn are shown in Figure 5.2(b). The heat transfer profile for the synthetic jet differs from the jet data presented in Chapter 3. For the synthetic jet, a larger $\frac{H}{d}$ ratio results in an increased average heat transfer value. Overall however, much lower Nusselt numbers are reached. According to Kercher et al. [30] in 2003, the performance of a synthetic microjet is comparable to COTS available cooling fans for electronics.

The advantage of a synthetic jet cooler compared to other jet set-ups is that it operates autonomously; neither an external pumping system, nor a pressurized air transport system is required. Also, compared to a conventional fan, the pulsating membrane is more reliable. Currently designed electronics that rely on heat sink & fan cooling, can be adapted by mounting a synthetic jet with relative ease, as the PCB and product designs are not required to change.

Cost Comparison

In Table 5.1 both methods, synthetic jet cooling and directly injected cooling, are compared based on the required production steps, components, assembly steps and other significant features. Cost estimates are an approximate value from COTS vendors.

Suppose the thermal performance of a directly injected cooling concept requires drilling 5 to 10 through holes per component. In comparison to procuring one synthetic jet, these additional drilling costs can be neglected. Hence, on a

Table 5.1: *Cost comparison of synthetic jet cooling vs. directly injected cooling.*

	Synthetic jet cooling	Directly injected cooling
Production steps		Drilling through holes – $0.01 each [18]
Components	Synthetic jet – $20 each [44]	Pump – $100 each [17]
Assembly steps	One jet per component	One pump per assembly
Other features		Pressure chamber as part of structure

component cost level, break-even would be around 5 components per assembly, as this equals the cost of one pump.

In addition to the component cost, also cost (time) of assembling should be compared. The exact assembly times are hard to estimate; however, it is clear that for many components, assembling just one pump will be more cost effective than assembling a synthetic jet device onto each component. As the pressure chamber is considered part of the rack structure, no additional cost is introduced here.

Total Evaluation

Compared to synthetic jet cooling, with the directly injected cooling concept an identical jet layout can be realized on the bottom side of the electronic component. Through the external pump system higher Reynolds numbers and thus improved jet performances can be obtained.

The use of synthetic jet devices will not result in a more compact electronic product, as the overall product design barely changes. Also, the synthetic jet relies on cool air to be sucked in, as a jet of hot air would not give high cooling performance. Both are constraining for the design of compact (closed) electronic products. In the case of the directly injected cooling concept, the external pump system can continuously inject cool air with limited usage of space.

For dense boards with many components, the injected cooling system is preferable from both cost and performance perspectives.

5.2.2 Modular System

A modular system is often used to minimize design and production costs. A module in this case refers to a complete functional part of an electronic system. Depending on customer demands the entire system is constructed from modular components. This is illustrated in Figure 5.3(a). If functional and support systems

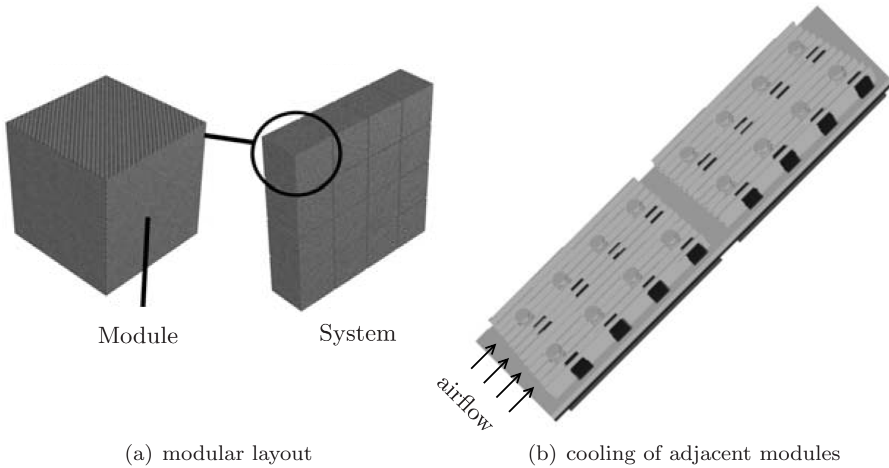

(a) modular layout (b) cooling of adjacent modules

Figure 5.3: *Modular systems.*

of one modular part are independently managed, a system of any size can be constructed using these parts.

Each module can be individually optimized for performance, as well as cost. This does not imply that system performance will also be optimal; a trade-off is made due to overall cost efficiency. Each module must operate independently, however for thermal management this is often not the case. This is shown in Figure 5.3(b), where two modules, comprising multiple electronic components, are placed adjacent of each other, cooled by one airflow from the bottom to the top. This type of cooling does not allow the system to be built-up from any number of modules. The total number of modules across an airflow depends on the power dissipated and subsequent heating of the coolant air as it passes each heat sink. As such, a thermal engineering contribution is required for each produced system.

Redesign

By redesigning the modules to incorporate an individual and independent cooling support, any number of modules can be used to construct the entire system. As discussed in Chapter 3, directly injected cooling excels in this area. The modules have to be designed as BGA packages, and the construction that holds the individual modules has to be adapted to encompass the required pressure chamber. In this case, instead of cooling all electronic components successively, they are cooled in parallel and heating of the coolant air is no longer an issue. Also, the heat sinks attached to each module can be omitted, as the components are cooled from the bottom side.

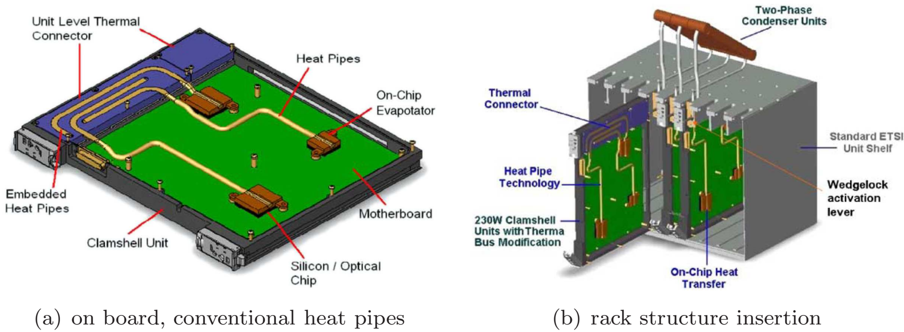

(a) on board, conventional heat pipes (b) rack structure insertion

Figure 5.4: *Prototype presented by McGlen et al. [39].*

The directly injected cooling system, as all other functional requirements, can be optimized for each module. Optimization may also include a standardized pump system, however this also dictates independent piping across the backplane. As modules are interconnected during final assembly, the pressure chambers can be connected as well. In this case the auxiliary equipment, such as the pump system, will have to be scaled as the system grows.

The modules are individually optimized – including thermal effects – for performance and cost, therefore the resulting system arrangement can be produced at a lower cost. As thermal management is analyzed for the modular structure, repetitive thermal system analyses are no longer required for each arrangement. Also, in this particular case the mounted heat sinks can be omitted, cutting down even further on recurring cost. Depending on the size of each system to be constructed and the number of different systems to be produced, a substantial cost reduction can be achieved. Recurring thermal engineering cost no longer exist, as thermal engineering is done once to optimize the module as non-recurring cost.

5.3 Integrated Heat Pipe Concept

5.3.1 Rack Cooling System

McGlen et al. [39] in 2004 presented an integrated thermal management technique for high power electronic devices. They focused on combining two-phase heat transfer and heat pipe technology with forced air convection and liquid condenser systems. Similar to this study, their aim was to increase heat transfer from high power components on an electronic board to the ambient environment. Also, they wanted to save cost by preserving the current standardized rack structure. Their prototype is shown in Figure 5.4

As shown in Figure 5.4(a), conventional heat pipes are mounted on top of the heat dissipating components via a heat sink. The heat is transported to the edge

Table 5.2: *Cost comparison of conventional vs. integrated heat pipes.*

	Conventional heat pipes	Integrated heat pipes
Production steps		Machining cavity and thermal vias
Components	Heat sink and heat pipe module – $50 each [57]	Diaphragm
Assembly steps	One heat sink and heat pipe per component	One diaphragm per heat pipe
Other features	Thermal connector	

of the board, where the heat pipes are embedded in a thermal connector. This resembles the concept of a coldplate attached to an electronic board to conduct the heat toward the edge, as illustrated in Figure 2.6(b). The advantage of using heat pipes in this case, is that they are able to transport more heat with increased efficiency. The assembled electronic board is inserted into the rack structure, as shown in Figure 5.4(b). In this specific case heat is further dissipated through a two-phase condenser unit, however liquid rack cooling can also be considered.

Cost Comparison

For the integrated heat pipe concept, the comparison is also based on the required production steps, components, assembly steps and other significant features. This is presented in Table 5.2. The cost estimate of the heat sink and heat pipe combination is based on a COTS thermal module for laptop assemblies.

In the current design of the integrated heat pipe, there are almost 4,000 thermal vias inserted into the top and bottom layers. This dominates production cost compared to machining the cavity in the intermediate layer. Assuming the cost of a thermal via is dictated by the drilling process, this would amount to 4,000 times $0.01, equaling $40 for each integrated heat pipe. These are rather high recurring costs. By filling the via with a thermally enhanced epoxy (e.g. CB100 [13]), instead of standard board epoxy, the conductance of the thermal via can be improved. As such, both the via diameter can be increased and the number of vias can be lowered, resulting in less recurring cost.

The heat sink and heat pipe modules must be assembled last, because the heat pipes have to interface with the thermal connector as well. This is not very cost efficient. The assemblage of the diaphragm however, can be done during the normal electronic production process. As the diaphragm is designed as SMD component, this can be automated as well. Also in this case, assembly times are hard to estimate; however, it is clear that for many components, the automated assembly of a diaphragm per heat pipe will be more cost effective than the assem-

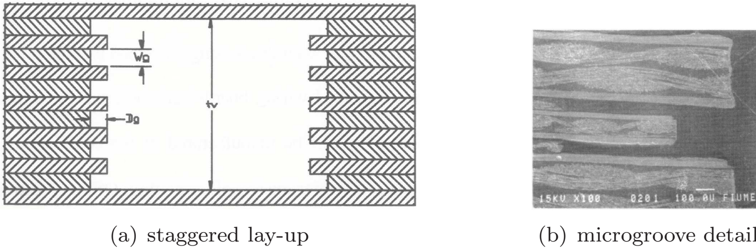

(a) staggered lay-up (b) microgroove detail

Figure 5.5: *Prototype presented by Jones et al., 2002 [28].*

bly of a heat sink and heat pipe module for each component at the very end of the production process. Finally, the thermal connector for each electronic board is no longer required.

Total Evaluation

In the redesigned case, the transport length of the heat pipes remains approximately equal; hence performance is mainly determined by the cross sectional area of the heat pipes. For the integrated heat pipes to have an equal cross section, they can be made wide-and-thin or small-and-high, depending on the electronic circuit density around the component locally. As the external heat sinks, heat pipes and thermal connector are no longer required, to accommodate the integrated heat pipes the thickness of the board structure can be increased. Due to this design freedom, overall a more compact product can be realized.

Assuming the performance of the external heat pipes is equivalent to the integrated heat pipes, in both cases heat is transported with an equal internal efficiency to the edge of the board. However, as the integrated heat pipes are flat, heat is inserted into the heat pipe directly and more efficiently, instead of via a mounted heat sink. In fact, in practice attached heat pipes are often flattened for this purpose.

5.3.2 Other Embedded Heat Pipes

In 2002 Jones et al. [28] reported embedding micro heat pipes in laminate substrates to enhance thermal management. In this section their presented prototype is compared to the manufactured integrated heat pipe of this study. The design, production method and heat pipe performance are compared.

The microgroove wick structure of Jones' prototype was realized by stacking the polymeric layers of the PCB in a staggered lay-up, as shown in Figure 5.5(a). This concept requires the use of multiple intermediate layers, which has the advantage of reaching extreme high aspect ratios. This is shown by the magnified image in Figure 5.5(b). Their working fluid was also water.

To optimize heat pipe performance, they also considered reducing the contact angle of the working fluid. With their cleaning method, based on rinsing with deionized water, they could reduce the contact angle from 104 degrees to 56 degrees. In their case, heat pipe failure occurred around 10 W due to delamination of the PCB.

Comparison

As both heat pipes are integrated into the electronic product and manufactured using PCB technology, this comparison is not so much based on cost, but focuses more on design and production constraints, and performance. The prototype of Jones et al. differs to the presented integrated heat pipe on several points:

- The wick structure is realized on the sides of the heat pipe, instead of on the top and bottom layers. The former allows higher aspect ratios; however, in the latter case heat is transported much more efficient to the evaporation sites, especially with the use of thermal vias. This reduces the temperature gradient from the electronic component to the heat pipe vapor, particularly since the polymeric layers are poor thermal conductors.
- The staggered lay-up introduces an additional constraint on the board design. Heat pipe performance is a function of the number of board layers. For instance, from an electronic perspective three layers suffice; however, to make the embedded heat pipe work, additional, electronically non-functional layers must be introduced.
- The contact angle reduction by applying a surface finish, instead of a cleaning method, is much more significant. For the integrated heat pipe concept the contact angle dropped to almost zero, instead of 56 degrees. This increases the maximum capillary pressure by 75%.
- The presented integrated heat pipe concept did not fail at 10 W. Moreover, even when heat transport failed and the temperature rose unacceptably, delamination did not occur, indicating a stronger hermetic structure.

5.4 Conclusions

As discussed, by focusing on thermal aspects during the conceptual design phase more integrated cooling solutions can be developed. From a production perspective, this leads to a cost reduction for electronic products, especially for mass-market and high volume production. This is applicable to both high component density cooling and high power density cooling, and also for various cooling technologies, such as air cooling and phase change principles.

In the case of directly injected cooling less material is required, hence lighter products are feasible. This is also true in the case of integrated heat pipes, as

no external heat transfer devices need to be attached to the PCB. Both concepts also resulted in an overall more compact electronic product.

In both cases, the electronic product is equipped with an integrated cooling system. Therefore, iterative redesigning without reaching a thermal solution during the embodiment and detail design phase, as illustrated in Figure 1.6, is no longer required. Compared to other state-of-the-art cooling technologies for electronic products, the presented concepts demonstrate improved thermal performances.

Altogether, the substantial cost reduction aimed for seems certainly feasible, especially for mass-market applications. For instance, a modular system densely packed with electronic components cooled via the concept of directly injected cooling with just one pump and no other thermal devices is feasible; also feasible is a cabinet filled with plug-in electronic boards cooled via the concept of integrated heat pipe cooling with no other mounted thermal devices.

Chapter 6

Conclusions & Recommendations

This chapter presents the conclusions that can be drawn from this research. After discussing the chosen design approach and formulated research goals, a wrap-up is given for both the developed cooling concepts. Also, several recommendations are given that would aid the further (industrial) development of the presented concepts.

6.1 Conclusions

By incorporating thermal aspects at an early stage in the design process of electronic products, more integrated solutions can be realized. Two innovative and promising techniques have been identified in this thesis: the concept of *directly injected cooling* and the concept of *integrated heat pipe cooling*. For both concepts a patent was granted [5, 64].

Both cooling strategies developed take into account currently available mass-production techniques. Standardized, mainstream electronic manufacturing processes are utilized to produce both cooling concepts. Due to the multidisciplinary design approach, the cooling systems are totally integrated into the electronic product. Add-on cooling devices are no longer required. In the future, this allows engineers to design electronic products featuring full integration of thermal management systems and electronic circuitry. Thus pushing the boundary further toward more functionality in a smaller form factor.

The integrated design leads to a lighter and more compact electronic product. As thermal management systems are produced integrally, a significant cost reduction is reached. This is especially true for high volume production, where electronic manufacturing technologies, such as PCB production and SMD assembly, are appreciated for their low recurring cost.

For both developed cooling concepts, the electronic components are cooled independently, which renders them thermally decoupled. As such, both cooling strategies pose less thermal constraints on the total design, thereby increasing the flexibility. Also, compared to other state-of-the-art cooling technologies for electronic products, the presented concepts demonstrate improved thermal performances.

By combining the advancements reached in this research, the substantial cost reduction of the complete electronic product aimed for seems certainly feasible for both integrated cooling concepts.

Conclusions to be drawn from both concepts individually, are discussed in the next two sections.

6.1.1 Directly Injected Cooling

The concept of directly injected cooling has been described in detail. By manufacturing a jet inlet port in the PCB underneath an electronic component, this component can be cooled directly from the bottom side. Coolant (air) is supplied by mounting the PCB on a pressure chamber. A heat sink on top of the component is no longer required, as the Ball Grid Array (BGA) that supports the electronic package also acts as an integrated heat transfer device. Components are cooled both simultaneously and independently, with low interaction to the adjacent components.

Theoretical analyses have led to a thermally optimal performing configuration for a single confined impinging air jet. By using this performance value as a design rule, the total number of jets can be determined from the thermal criteria of the electronic component in question.

The jet performance depends on several factors: the ratio of the component's standoff distance and the jet diameter, the number of jets and the Reynolds number of the jet. With a standoff distance of 0.9 mm, best results were recorded for multiple jets of ⌀2 mm. For this arrangement the recirculation zones of the impinging jets have a positive effect on the heat transfer value. For larger jets layouts (3x2, 5x2), increased heat transfer values already occur at lower Reynolds numbers. As such, lower pressures are required, which are favorable for the structural integrity of the board and pump selection.

From a thermal design perspective electronic components can be cooled with thermal resistance values from junction to jet air of approximately 4-5 $^{K}/_{W}$. More importantly, there is no coupling between other components on the board. Hence, all components can be cooled with this resistance value simultaneously, assuming sufficient air pressure can be maintained. As such, a cooling strategy is realized for electronic products featuring a high density of electronic components.

From a production perspective, especially for high volume production, a significant cost reduction is reached. Add-on cooling equipment as heat sinks and fans are no longer required, cutting down on recurring cost. The directly injected cooling system is produced using established, mainstream electronic manufactur-

ing techniques. The cooling system, also for multiple components, is realized by drilling jet inlet ports at the appropriate locations during one of the standardized production processes.

6.1.2 Integrated Heat Pipe Cooling

The concept of integrated heat pipe cooling, where a phase change heat transfer device is manufacturing inside the PCB, has been described in detail. By machining a cavity in an intermediate layer and plating a wick structure on the top and bottom layers, the integrated heat pipe is constructed directly inside the laminated board structure. Heat, dissipated by electronic components on the board, is absorbed by the vaporizing working fluid. Extraction of the (latent) heat out of the heat pipe occurs at the condenser end. In practice this area is often located at the edge of the board, where heat can be further disposed, for instance, through a rack structure.

Theoretical analyses have led to several design graphs that aid to design the integrated heat pipe. Performance is displayed as a function of several key features: internal heat pipe dimensions, groove dimensions, orientation and temperature. With these graphs integrated heat pipes can be optimized for instance for high performances or thin structures.

Heat pipes are able to transfer heat at a very high efficiency in a compact set-up, due to the phase change principles. Experimental investigation proved that heat dissipated by an electronic component could be transported with extremely low thermal gradients. The measurement results showed an equivalent thermal conductivity eight times higher than the conductivity of solid copper.

From a thermal design perspective electronic components can be placed anywhere on the board. The board structure with its integrated heat pipe is able to transport the generated heat to other locations with thermal resistance values as low as $1.2\,{}^{K}/_{W}$. This concept also allows heat dissipated by multiple components to be transported through the board structure.

Also in this case, from a production perspective a significant cost reduction is reached, especially for high volume production. The integrated heat pipe is produced using established, mainstream PCB manufacturing and SMD assembly techniques. The heat pipe can be designed to meander through the board structure, cooling high power components and going around areas constrained by other criteria. This makes the electronic product design more flexible. Also in this case, no add-on cooling equipment is required. As the heat pipe is designed during the PCB layout phase and constructed integrally with the electronic board, recurring cost decrease considerably.

6.2 Recommendations

Both cooling strategies are still in the conceptual phase. More research is required before an industrial application can be considered. Recommendations are discussed for both concepts individually.

Directly Injected Cooling

The focus of this study was to first demonstrate the merits of directly injected cooling, and then find an optimal geometry and jet layout for the cooling of a single component. Therefore cooling of multiple electronic components simultaneously, each having an optimal jet configuration, is an underexposed area. Air flow fully interacting with adjacent, activated components must be further investigated.

Measuring performance with all components activated will give more detailed data on the jet performance for individual components. Because all components are activated, heat cannot spread to adjacent components and must be transported by the cooling air jet.

Integrated Heat Pipe Cooling

Also here the focus was to first demonstrate the merits of integrated heat pipe cooling, and then find optimal geometric features. Therefore cooling of a fully populated PCB with multiple distributed dissipating components is still an underexposed area. This should give more detailed information on the cooling capacity of heat pipes integrated into more complex boards.

The filling accuracy and sealing consistency were initially underestimated. The charging procedure of the heat pipe has to be further perfected, in order to clean, fill and seal the heat pipe reliable and reduce the amount of Non-Condensible Gases (NCGs) inside. A suitable technique, commonly applied in the vacuum industry, is known as pinch-off tubing. By pinching-off a tube after filling, a cold-weld directly seals the tube in a reliable manner. Best results are obtained with relatively soft metals, such as copper. By designing an SMD device with such a copper tube, an improved charging method can be realized, which is still suitable for automated assembly. With a reliable procedure also long-term reliability of the integrated heat pipe can be determined.

As the hermetic seal around the heat pipe is on the outside, part of the bonding layer remains in contact with the heat pipe cavity. Over time working fluid may migrate into this area, thus losing working fluid in circulation. Also, gases may diffuse from the bonding areas introducing additional NCGs in the heat pipe. A sealing technique that seals the cavity from the inside would circumvent this.

For further optimization the use of mixtures might be considered. Thermodynamically, water is the best candidate as a working fluid in this temperature range. This however assumes a perfectly wetted wick structure. Therefore in

practice, for heat pipes integrated into PCBs using a mixture, such as alcohol and water, might improve heat pipe performance.

List of References

[1] Avram Bar-Cohen. Thermal management of microelectronics in the 21st century. In *Proceedings of the Electronic packaging technology conference*. IEEE/CPMT, 1997.

[2] E. Baydar and Y. Ozmen. An experimental and numerical investigation on a confined impinging air jet at high reynolds numbers. *Journal of Applied Thermal Engineering*, 25:409–421, 2005.

[3] Adrian Bejan. *Heat transfer*. John Wiley & Sons, Inc., New York, 1993.

[4] Kenneth G. Brill. The invisible crisis in the data center: the economic meltdown of moore's law. White paper by the Uptime Institute, 2007.

[5] Gerard J.H.M. Brok, Wessel W. Wits, Jan H. Mannak, and Rob Legtenberg. Directly injected forced convection cooling for semiconductor components. Patent number NL-BN 1034420, Thales Nederland B.V., 2007.

[6] Johannes F. Burger. *Cryogenic microcooling: A micromachined cold stage operating with a sorption compressor in a vapor compression cycle*. PhD thesis, Univerisity of Twente, Enschede, The Netherlands, 2001.

[7] Yiding Cao, Amir Faghri, and E. Thomas Mahefkey. Micro/miniature heat pipes and operating limitations. In *Proceedings of the American Society of Mechanical Engineers, Heat Transfer Division*, volume 236, pages 55–62, Atlanta, GA, USA, 1993.

[8] Yiding Cao, M. Gao, J.E. Beam, and B. Donovan. Experiments and analyses of flat miniature heat pipes. In *Proceedings of the IEEE Energy Conversion Engineering Conference (IECEC)*, volume 2, pages 1402–1409, Washington DC, USA, 1996.

[9] S.W. Chi. *Heat pipe theory and practice: A sourcebook.* Series in thermal and fluids engineering. Hemisphere Pub. Corp., Washington, 1976.

[10] D.W. Colucci and Raymond Viskanta. Effect of nozzle geometry on local convective heat transfer to a confined impinging air jet. *Journal of Experimental Thermal and Fluid Science*, 13:71–80, 1996.

[11] Conrad. Heatpipes (Wärmeleitrohre): Datasheet QG-SHP-D6-250G. Technical report, 2008.

[12] T.P. Cotter. Theory of heat pipes. Technical Report No. LA-3246-MS, Los Alamos Scientific Laboratory, 1965.

[13] DuPont Microcircuit Materials. CB100 Conductive ViaPlug. Technical report, 2002.

[14] EIA/JEDEC. Methodology for the thermal measurement of component packages (single semiconductor device), 1995.

[15] Michael J. Ellsworth and Robert E. Simons. High powered chip cooling - Air and beyond. *ElectronicsCooling*, 11(3):14–22, 2005.

[16] Norbert Engelberts. Personal communication, 2008.

[17] Every air compressor. Campbell Hausfeld FP2048, Visited on September 9th, 2008. http://www.everyaircompressor.com/Campbell-Hausfeld-FP2048-CHP1106.html.

[18] Express PCB. Specs 4 Layer Production, Visited on September 9th, 2008. http://www.expresspcb.com/ExpressPCBHtm/Specs4LayerProduction.htm.

[19] Amir Faghri. *Heat pipe science and technology.* Taylor & Francis, Washington, DC, 1995.

[20] Richard S. Gaugler. Heat transfer device. Patent number 2,350,348, General Motors Corporation, 1944.

[21] Colin Glynn, Tadhg S. O'Donovan, and Darina B. Murray. Jet impingement cooling. In *Proceeding of the 9th UK National Heat Transfer Conference*, Manchester, UK, 2005.

[22] George M. Grover. Evaporation-condensation heat transfer device. Patent number 3,229,759, Los Alamos, 1966.

[23] HP. Energy-efficient computing in the next generation data center. Electronic Article, 2006.

[24] Aaron M. Huber and Raymond Viskanta. Effect of jet-jet spacing on convective heat transfer to confined, impinging arrays of axisymmetric air jets. *International Journal of Heat and Mass Transfer*, 37(18):2859–2869, 1994.

[25] Intel. 60 Years of the transistor: 1947-2007. Electronic Article, 2007.

[26] Intersema. MS761: Pressure sensor die (0-1 bar). Technical report, 1999.

[27] K. Jambunathan, E. Lai, M. A. Moss, and B. L. Button. A review of heat transfer data for single circular jet impingement. *International Journal of Heat and Fluid Flow*, 13(2):106–115, 1992.

[28] K. Jones, Y. Cao, and M. Cao. Development of micro heat pipes embedded in laminate substrates for enhanced thermal management for printed wiring boards. Technical Report Number AFRL-PR-WP-TR-2003-2011, Florida International University, Miami, USA, 2002.

[29] Shung-Wen Kang and Derlin Huang. Fabrication of star grooves and rhombus grooves micro heat pipe. *Journal of Micromechanics and Microengineering*, 12:525–531, 2002.

[30] Dan S. Kercher, Jeong-Bong Lee, Oliver Brand, Mark G. Allen, and Ari Glezer. Microjet cooling devices for thermal management of electronics. *IEEE Transactions on Components and Packaging Technologies*, 26(2):359–366, 2003.

[31] D. Khrustalev and Amir Faghri. Estimation of the maximum heat flux in the inverted meniscus type evaporator of a flat miniature heat pipe. *International Journal of Heat and Mass Transfer*, 39(9):1899–1909, 1996.

[32] Clemens J.M. Lasance and Robert E. Simons. Advances in high-performance cooling for electronics. *ElectronicsCooling*, 11(4):22–39, 2005.

[33] Seri Lee. Calculating spreading resistance in heat sinks. *ElectronicsCooling*, 4(1), 1998.

[34] Eric Lutters. *Manufacturing integration based on information management.* PhD thesis, University of Twente, Enschede, The Netherlands, 2001.

[35] Ravi Mahajan, Raj Nair, Vijay Wakharkar, Johanna Swan, John Tang, and Gilroy Vandentop. Emerging directions for packaging technologies. *Intel Technology Journal*, 6(2):62–75, 2002.

[36] Raghav Mahalingam, Samuel Heffington, Lee Jones, and Markus Schwickert. Newisys server processor cooling augmentation using synthetic jet ejectors. *Thermal and Thermomechanical Phenomena in Electronics Systems*, pages 705–709, 2006.

[37] Debendra Mallik, Kaladhar Radhakrishnan, Jiangqi He, Chia-Pin Chiu, Telesphor Kamgaing, Damion Searls, and James D. Jackson. Advanced package technologies for high-performance systems. *Intel Technology Journal*, 9(4):259–272, 2005.

[38] Jan H. Mannak. Senior Development Engineer. Thales Netherlands, 2008.

[39] Ryan J. McGlen, Roshan Jachuck, and Song Lin. Integrated thermal management techniques for high power electronic devices. *Journal of Applied Thermal Engineering*, 24:1143–1156, 2004.

[40] Alan McGuinn, Tim Persoons, Pierre Valiorgue, Tadhg S. O'Donovan, and Darina B. Murray. Heat transfer measurements of an impinging synthetic air jet with constant stroke length. In *Proceedings of the 5th European Thermal-Sciences Conference*, 2008.

[41] T.H. van der Meer. Personal communication, 2008.

[42] Gordon E. Moore. Cramming more components onto integrated circuits. *Electronics*, 38(8), 1965.

[43] Pieter G. Nieboer. Solving technical challanges for integration of heat pipe technology into printed circuit boards. Master's thesis, OPM-869, University of Twente, Enschede, The Netherlands, 2008.

[44] Nuventix. Solid State IC cooler unit, Website visited on September 9th, 2008. http://emwcs.avnet.com/webapp/wcs/stores/servlet/Home_-1_500201_500201_home.

[45] N.T. Obot, W.J.M. Douglas, and A.S. Mujumdar. Effect of semi-confinement on impingement heat transfer. In *Proceedings of the 7th International Heat Transfer Conference*, volume 3, pages 395–400, Munich, Germany, 1982.

[46] Gerald Pahl and Wolfgang Beitz. *Engineering design: A systematic approach*. Springer, London; New York, 1996.

[47] G. P. Peterson. *An introduction to heat pipes: Modeling, testing, and applications*. Wiley series in thermal management of microelectronic & electronic systems. Wiley, New York, 1994.

[48] P. E. Phelan, J. Swanson, F. Chiriac, and V. Chiriac. Designing a mesoscale vapor-compression refrigerator for cooling high-power microelectronics. In *Proceedings of the 9th Intersociety Conference on Thermal and Thermomechanical Phenomena in Electronic Systems*, pages 218–223 Vol.1, 2004.

[49] Martijn Pijpers. Modelling and design of an integrated heat pipe using printed circuit board technology. Master's thesis, OPM-831, University of Twente, Enschede, The Netherlands, 2007.

[50] Stuart Pugh. *Total design: Integrated methods for successful product engineering*. Addison-Wesley Pub. Co., Wokingham, England; Reading, Mass., 1991.

[51] Ioan Sauciuc. Piezo actuators for electronics cooling. *ElectronicsCooling*, 13(1):12–17, 2007.

[52] G.E. Schneider and R. DeVos. Nondimensional analysis for the heat transport capability of axially-grooved heat pipes including liquid/vapor interaction. In *Proceedings of the 18th AIAA Aerospace Sciences Meeting*, Pasadena, California, 1980.

[53] Malcolm E. Schrader and George I. Loeb. *Modern approaches to wettability: Theory and applications*. Plenum Press, New York, 1992.

[54] Jörg Schütze, Herman Ilgen, and R. Fahrner Wolfgang. An integrated micro cooling system for electronic circuits. *IEEE Transactions on Industrial Electronics*, 48(2):281–285, 2001.

[55] R.K. Shah and M.S. Bhatti. Laminar convective heat transfer in ducts. In *Handbook of single-phase convective heat transfer*. John Wiley & Sons, New York, 1987.

[56] Stratedge. 24 Lead glass flatpack: G2626M-1. Technical report, 1998.

[57] The find. Thermal module, Website visited on September 10th, 2008. http://www.thefind.com/computers/info-thermal-module.

[58] Thorrn Micro Technologies, Website visited on September 9th, 2008. http://www.thorrn.com.

[59] L.L. Vasiliev. Micro and miniature heat pipes: Electronic component coolers. *Journal of Applied Thermal Engineering*, 28(4):266–273, 2008.

[60] Arman Vassighi and Manoj Sachdev. *Thermal and Power Management of Integrated Circuits*. Series on Integrated Circuits and Systems. Springer, 2006.

[61] Charles C. J. Vincent and Jim B. W. Kok. Investigation of the overall transient performance of the industrial two-phase closed loop thermosyphon. *International Journal of Heat and Mass Transfer*, 35(6):1419–1426, 1992.

[62] John Walko. IBM looks to liquid jet-impingement for chip cooling. *EE Times*, 2006.

[63] Jinliang Wang and Ivan Catton. Biporous heat pipes for high power electronic device cooling. In *Proceedings of the 17th IEEE SEMI-THERM Symposium*, pages 211–218, 2001.

[64] Wessel W. Wits, Jan H. Mannak, and Rob Legtenberg. Planar heat pipe for cooling. Patent number WO2007EP51533 20070216, Thales Nederland B.V., 2007.

[65] L. T. Yeh. Review of heat transfer technologies in electronic equipment. *Journal of electronic packaging*, 117(4):333–339, 1995.

[66] T. M. Ying and K. C. Toh. A heat spreading resistance model for anisotropic thermal conductivity materials in electronic packaging. In *Proceedings of the 7th Intersociety Conference on Thermal and Thermomechanical Phenomena in Electronic Systems*, volume 1, pages 314–321, 2000.

[67] Davis Media Ziff. Power consumption and cooling in the data center: A survey. Electronic Article, 2005.

Appendices

Appendix A

Electronic Manufacturing Processes

This chapter describes the electronic manufacturing processes considered well-established and mainstream throughout this thesis. PCB production technology is described first, after which SMD assembly is discussed.

A.1 Introduction

Standardized electronic production technology is appreciated for its low recurring cost and is therefore well suited for high volume production. Within the project consortium these production facilities were available on site, giving ample opportunity to design and construct potentially interesting cooling concepts.

A.2 Printed Circuit Board Production

The PCB is the successor of the breadboard, where electronic components were connected by wires. During the manufacturing process of (breadboard) electronic products, these wires were soldered to the components. This was a time-consuming and unreliable procedure. The metallic pattern present on a PCB layer replaces the use of wires, thereby increasing production efficiency and reliability, especially for mass-produced products.

The metallic pattern is commonly realized by a subtractive method that selectively removes copper from a laminate. The untreated laminate consists of a polymeric material* on which a copper cladding is applied. Currently, there are

* FR-4 is currently the base material most commonly used to produce multilayer boards.

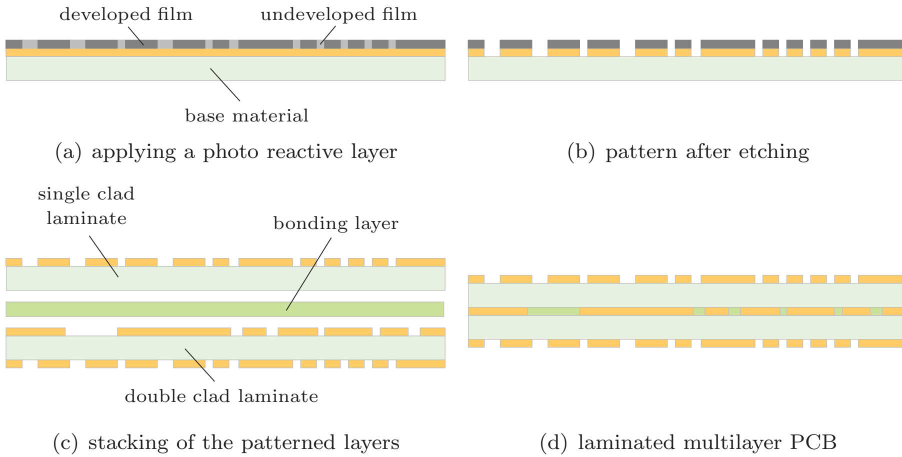

(a) applying a photo reactive layer

(b) pattern after etching

(c) stacking of the patterned layers

(d) laminated multilayer PCB

Figure A.1: *Schematic production steps of a multilayer printed circuit board.*

three common methods to remove the copper from the laminates: (1) by printing an etch-resistant (screen), after which the undesired copper is etched away chemically; (2) by developing a photo reactive layer (resist) to protect the copper locally and etching away the undesired copper; (3) by directly milling away the undesired copper. For high volume, cost effective production, method 2 is preferred due to its low manufacturing time and thus cost. In fact, this method is not only applied in PCB production, but, for instance, also for the production of ICs.

For many electronic products, a PCB of just one layer does not suffice. Hence, multiple layers are laminated together, thus forming a multilayer PCB. Firstly, the individual PCB layers are patterned as described previously. Secondly, the layers are stacked with bonding layers (prepreg) in between. Finally, the stack is laminated in a press at an elevated temperature. To increase cost efficiency, often multiple PCBs are manufactured side by side in one stack of laminated layers and machined apart afterward.

These production steps are also illustrated schematically in Figure A.1. Firstly, the photo reactive layer is developed selectively. Secondly, the undeveloped and underlaying copper is etched away, after which the developed film is also removed from the laminate (this is not depicted). Thirdly, the patterned layers are stacked with bonding layers in between. Fourth and finally, the multilayer PCB is laminated.

A.2.1 Via Production

Vias are used to connect layers to each other electronically within a multilayer board. The vias are manufactured by drilling a hole, depositing (plating) copper

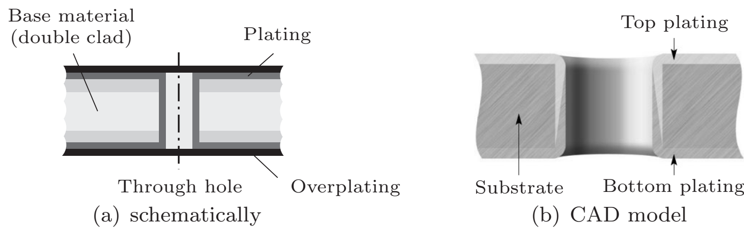

(a) schematically (b) CAD model

Figure A.2: *Through hole via.*

on the edges of this hole. Therefore, they are also referred to as plated through holes. The remainder of the hole can be filled with board material (epoxy), in order to overplate the complete via. This is illustrated schematically in Figure A.2(a).

There are three basic types of vias:

1. *Through hole vias.* Vias that go all the way through the assembled board.
2. *Blind vias.* Vias that do not go through the complete assembly, but partially. They connect the outer surface to an inner layer.
3. *Buried vias.* Vias that are in between other layers and do not extent to the top or bottom surface.

The latter two types of vias must be produced prior to the PCB's lamination process. Therefore, they are considered a cost driver for PCB production. The number of vias in a PCB should be minimized, especially the number of blind and buried vias.

Thermal Vias

As shown in Figure A.2, an electronic signal can be transmitted from one layer to another layer. Because copper is a good conductor, vias can also be used to transport heat from one layer to another, or from the top surface to the bottom surface. The amount of copper present in one via dominates the area's overall thermal conductivity. Suppose a plating of thickness t is applied on through holes of $\varnothing d$ and the spacing between the vias is twice the hole diameter, as shown in Figure A.3.

According to Figure A.3, the percentage of copper present in one via region can be computed as:

$$\varepsilon_{copper} = \frac{\frac{1}{4}\pi d^2 - \frac{1}{4}\pi(d-2t)^2}{(2d)^2} = \frac{\pi t(d-t)}{4d^2} \tag{A.1}$$

Assuming a hole diameter of 250μm and a plating thickness of 25μm, a copper percentage of approximately 7% can be achieved. This results in an equivalent

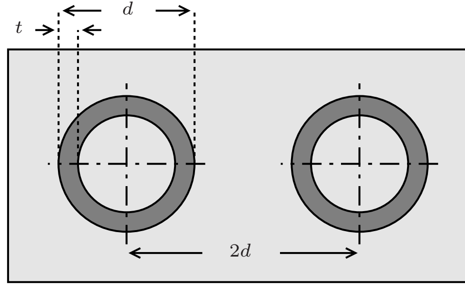

Figure A.3: *Thermal via density*

thermal conductivity of:

$$k_{eq} = \varepsilon_{copper} \cdot k_{copper} + (1 - \varepsilon_{copper}) \cdot k_{FR-4} \approx 29 \frac{W}{mK} \quad \text{(A.2)}$$

Here, k_{copper} and k_{FR-4} are assumed to be 400 and 0.3 W/mK, respectively.

The increase in conductivity from plain FR-4 board material to the equivalent value is substantial. According to Equation (A.1), to further increase the conductivity either the plating thickness should be increased or the hole diameter should be decreased. The latter will also increase the via density.

To further improve the via's conductivity, instead of filling the hole with board material a thermally enhanced epoxy (e.g. CB100 [13]) can also be used. The thermal conductivity of this epoxy is approximately ten times higher, 3.5 W/mK.

A.3 Surface Mounted Device Assembly

Surface Mounted Devices (SMDs) are devices that are directly mountable onto the surface of the PCB. Analogous to the PCB replacing the breadboard, SMDs replace through hole technology because of their increased production efficiency and reliability. The shape of an SMD is designed in such a way that assembling it onto the PCB is optimized. SMDs are placed on the top (or bottom) layer of a PCB. Here, instead of drilling through holes to connect the component, local metalization connects and hold the component by means of a layer of solder. Figure A.4 shows some examples of SMD components.

To increase production efficiency for SMDs, the assembly process can be automated. Firstly, a layer of solder is deposited locally onto the PCB, for instance by screen printing. Subsequently, a pick and place process positions the SMD components onto the surface. Finally, by elevating the temperature, the solder liquefies and bonds the devices onto the surface without overheating and damaging the electronic components. This process is referred to as reflow soldering.

SMD components may interface with the board through various standardized packaging types. At present, the Ball Grid Array (BGA) is one of the com-

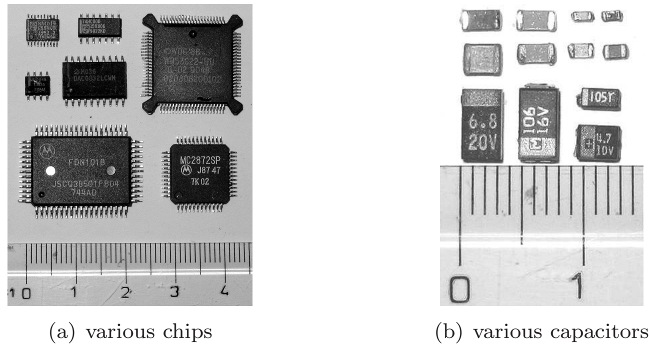

(a) various chips (b) various capacitors

Figure A.4: *Examples of surface mounted devices.*

mon packaging types used by the industry. Solder balls are placed between the board and the component to facilitate the mechanical and electronic connections. Figure A.5 shows an example of such a BGA component. Other standardized packaging types such as Land Grid Arrays (LGA), Pin Grid Arrays (PGA), stud bump arrays and Quad Flat-No leads (QFN) are also often seen.

The advantage of BGA connections compared to other packaging types is the thermal path the solder balls provide. This path conducts heat much better than for instance is the case for pin arrays or package types that use leads. Hence, for the assembly of (high power) components onto an electronic board where cooling through the bottom side of the component is required, the use of a BGA connection is a good option.

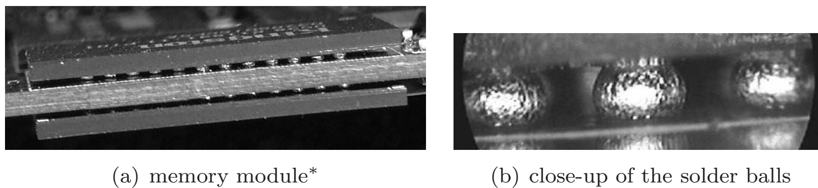

(a) memory module* (b) close-up of the solder balls

Figure A.5: *Ball Grid Array (BGA) example.*

* Image taken by Smial from Wikimedia Commons.

Appendix B

Test Set-up Directly Injected Cooling

In this chapter, the measurement set-up to validate the directly injected cooling concept is discussed. Also, some of the datasets that were recorded are presented as an illustration.

B.1 Measurement Set-up

The measurement set-up to validate the directly injected cooling concept experimentally is shown in Figure B.1. The test board, described in Section 3.3, is clamped onto a pressure chamber. The flow and pressure of the cooling air were monitored by the flow meter and pressure gauge, respectively. The power source was adjusted to dissipate increasing amounts of power during the measurements. The data logger recorded the voltage drop across the diodes. It also recorded the air temperature inside the pressure chamber, as well as the ambient temperature.

A schematic cross section of the assembly of the pressure chamber (5) and the test board (4) is shown in Figure B.2. The pressurized air enters the pressure chamber through the air inlet port (6). Air flow is already measured upstream. The pressure gauge is connected to the pressure gauge port (7). The cooling air is injected into the BGA through the jet opening (9), where it cools the rigid laminate (2) from the bottom side. Heat is dissipated inside the diode (1) and conducted through the rigid laminate. The standoff distance of the laminate is determined by the solder balls (3) of the BGA.

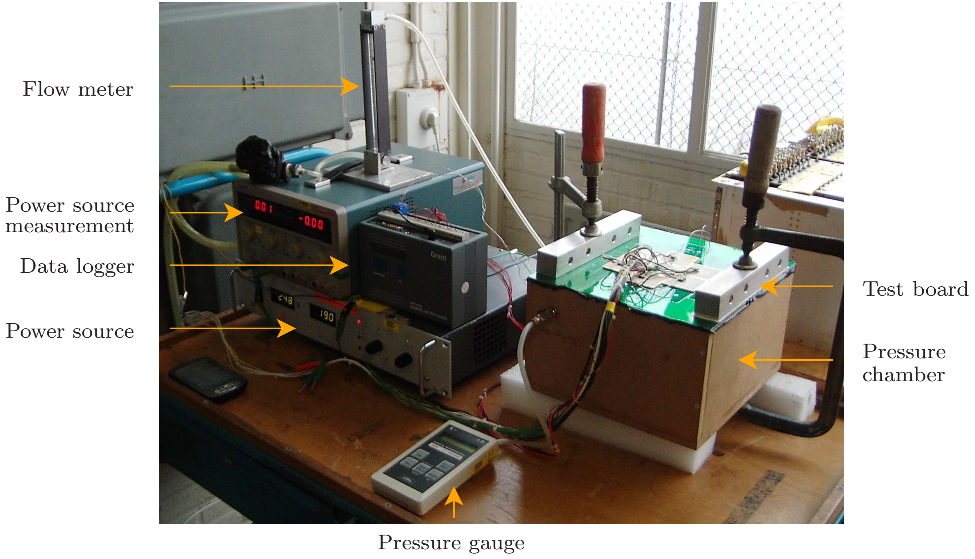

Figure B.1: *Measurement set-up for the directly injected cooling concept.*

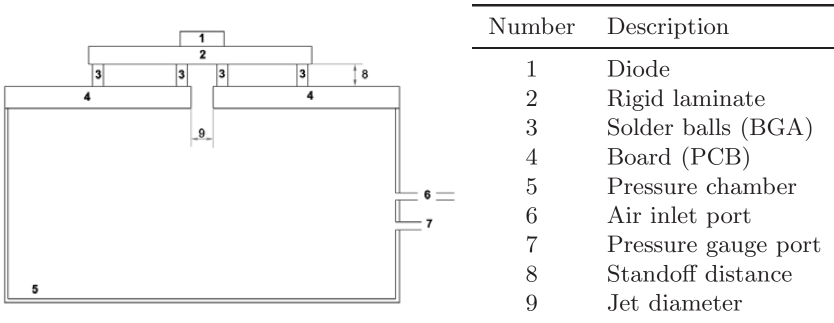

Number	Description
1	Diode
2	Rigid laminate
3	Solder balls (BGA)
4	Board (PCB)
5	Pressure chamber
6	Air inlet port
7	Pressure gauge port
8	Standoff distance
9	Jet diameter

Figure B.2: *Cross section of the pressure chamber and the test board.*

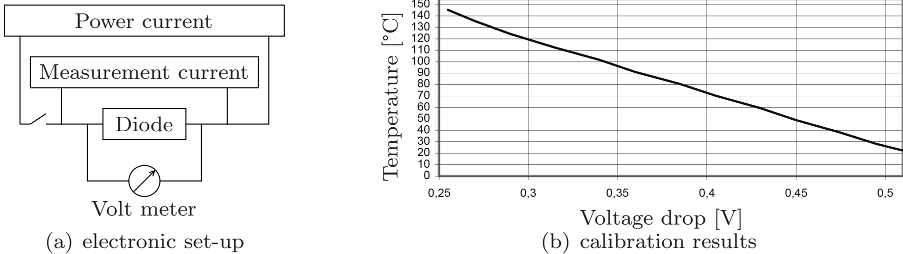

(a) electronic set-up (b) calibration results

Figure B.3: *Diode calibration.*

B.1.1 Diode Calibration

A diode was used to dissipate power (heat) through the package and the rigid laminate. As the electrical resistance of a diode varies proportionally with its temperature, it can also be used to determine the junction temperature. By alternating the power current and measuring current, as shown in Figure B.3(a), the diode was used to measure the junction temperature of the package as well.

After the diodes were mounted onto the test board, they were calibrated. This was done by placing the board in an oven and recording the voltage drop across the diodes for a varying temperature range. For one of the diodes used, the recorded temperature variation is shown in Figure B.3(b). As was expected, the measured variation proved to be very linear. To improve the accuracy, this linear trend was determined for each of the diodes individually before running the actual temperature measurements for the directly injected cooling concept.

It must be noted that due to the time lapse of typically one second between switching to the measurement current and the first actual voltage drop measurement, the junction temperature already decreases. Therefore, junction temperatures are not considered precise; they will always be recorded slightly lower.

B.1.2 Jet Layouts

The jet layouts that were considered during the experimental verification are shown in Figure B.4. The single hole layout was used for three different jet arrangements with increasing diameter. The other four layouts are also presented in the figure. Hence, in total seven different arrangements were tested. Unfortunately, at the time of production the thermally affected area was not considered $4d$, but smaller ($\approx 2d$).

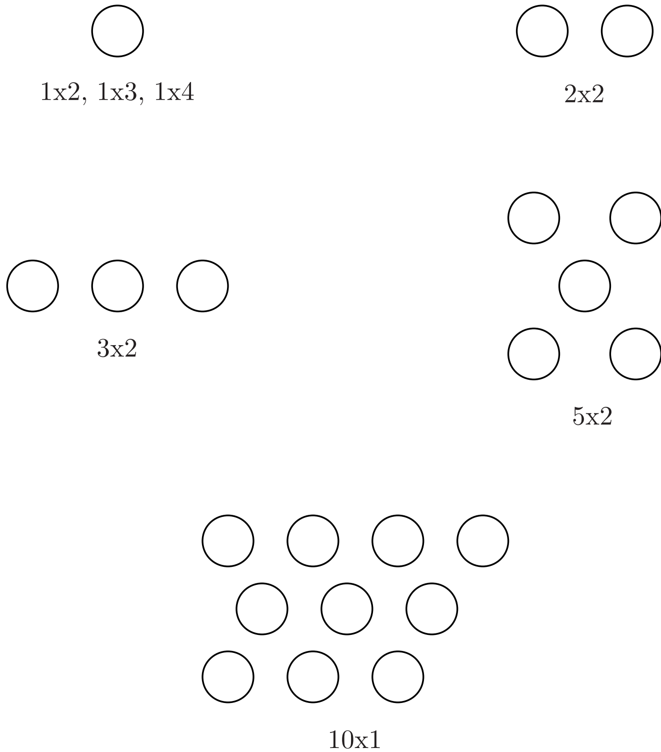

Figure B.4: *Jet layouts (number of holes x hole diameter in mm).*

B.2 Jet Measurement Datasets

Henceforth, two datasets are presented. Table B.1 presents the measured values for the small BGA package with a ⌀2 mm jet inlet hole, whereas Table B.2 presents the measured values for the large BGA package with a similar jet layout.

From the pressure and air flow values, the air velocity and Reynolds number were computed according to the jet geometry and Equation (3.2). The thermal resistance (R) is computed according to:

$$R = \frac{T_{junction} - T_{ambient}}{\dot{Q}_{dissipated}} \tag{B.1}$$

where the ambient temperature equals the inlet's jet air temperature (21°C).

Finally, for each pressure and flow arrangement, the average thermal resistance (R_{avg}) is also determined.

The other datasets are not presented in this thesis; however, the values presented in Figures 3.9 and 3.12 were computed in a similar manner.

Table B.1: *Small BGA package with ⌀2 mm hole.*

P [Pa]	φ_v [l/h]	U [m/s]	Re	$\dot{Q}_{diss}$ [W]	T_{junc} [°C]	R	R_{avg}
0	0	0	0	0	30.5		
				1.4	40.0	13.98	
				4.0	68.6	11.84	
				7.6	121.0	13.23	
				8.5	137.7	13.66	13.18
50	71.3	6.3	839	1.4	42.4	15.85	
				5.3	80.5	11.19	
				9.8	132.9	11.37	
				10.6	163.9	13.45	12.97
100	107.6	9.5	1,266	1.1	40.0	17.29	
				5.3	80.5	11.19	
				9.9	130.5	11.04	
				10.9	144.8	11.37	12.72
500	272.2	24.1	3,204	1.4	40.0	13.98	
				5.4	73.4	9.63	
				10.3	113.9	9.00	
				12.0	135.3	9.55	10.54
1,000	414.7	36.7	4,882	1.4	37.6	12.23	
				6.8	68.6	7.00	
				12.8	121.0	7.81	
				13.3	135.3	8.57	8.90
2,000	557.3	49.3	6,561	1.4	30.5	6.83	
				7.0	61.5	5.82	
				13.2	111.5	6.85	
				14.3	140.1	8.33	6.96
3,000	729.6	64.5	8,590	1.4	30.5	6.83	
				7.0	61.5	5.78	
				13.4	109.1	6.57	
				14.5	125.8	7.22	
				15.2	128.1	7.06	
				15.7	132.9	7.12	6.76
5,000	972.0	85.9	11,443	1.4	30.5	6.83	
				7.1	51.9	4.39	
				13.6	101.9	5.95	
				14.7	99.6	5.33	
				16.0	111.5	5.67	5.63
8,500	1,296.0	114.6	15,258	1.4	30.5	6.83	
				7.1	51.9	4.36	
				13.8	80.5	4.31	
				16.3	121.0	6.13	5.41

Table B.2: *Large BGA package with ⌀2 mm hole.*

P [Pa]	φ_v [l/h]	U [m/s]	Re	$\dot{Q}_{diss}$ [W]	T_{junc} [°C]	R	R_{avg}
0	0	0	0	0.0	21.8		
				1.6	33.5	7.73	
				5.3	60.0	7.38	
				9.2	86.4	7.11	
				13.5	127.6	7.89	7.53
50	90.7	8.0	1,068	1.6	33.5	7.73	
				7.2	62.9	5.79	
				13.5	112.9	6.80	
				14.7	127.6	7.25	
				15.8	148.2	8.03	7.12
100	123.1	10.9	1,449	1.6	33.5	7.73	
				7.2	68.8	6.60	
				13.6	130.6	8.07	
				14.6	127.6	7.29	7.42
500	379.7	33.6	4,471	1.6	33.5	7.78	
				7.3	60.0	5.36	
				13.6	112.9	6.77	
				14.7	133.5	7.65	6.89
1,000	629.9	55.7	7,415	1.6	33.5	7.73	
				7.3	62.9	5.73	
				13.7	95.3	5.41	
				14.9	110.0	5.99	6.22
2,000	1,075.7	95.1	12,664	1.6	33.5	7.73	
				7.3	57.0	4.92	
				13.8	98.2	5.60	
				14.9	110.0	5.96	
				16.1	110.0	5.53	5.95
2,500	1,321.9	116.9	15,563	1.6	30.6	5.91	
				7.4	57.0	4.90	
				13.8	95.3	5.39	
				14.9	98.2	5.17	
				16.2	112.9	5.69	5.41

Appendix C

Test Set-up Integrated Heat Pipe Cooling

In this chapter, the measurement set-up to validate the integrated heat pipe cooling concept is discussed. Also, one of the datasets that were recorded are presented as an illustration.

C.1 Measurement Set-up

The measurement set-up to validate the integrated heat pipe cooling concept experimentally is shown in Figure C.1. The prototype heat pipe, shown in Figure 4.18, was insulated to prevent cooling to the ambient air across its length. The condenser area of the heat pipe was clamped at the hinge element side. The hinge element allows the heat pipe to rotate from -90 to +90 degrees. As such, the evaporator side could be positioned above as well as below the condenser region in order to determine the influence of gravity on the liquid flow. Also, horizontal operation was possible.

The external cooler pumps coolant (water) through a heat exchanger that was clamped against the condenser region of the heat pipe. The absorbed heat was dissipated to the ambient air through a heat sink & fan. The amount of dissipated power at the evaporator side was determined by the power source and measured by the multimeters. The data logger continuously recorded the temperature of the thermocouples that were connected along the heat pipe's length.

During the measurements, the recorded values of the data logger could also be displayed on the monitor. As such, evaporator dry-out and subsequent heat pipe failure could be detected almost instantly. After such a detection, the measurement was stopped to prevent damage to the power resistor mounted onto the evaporator region of the heat pipe.

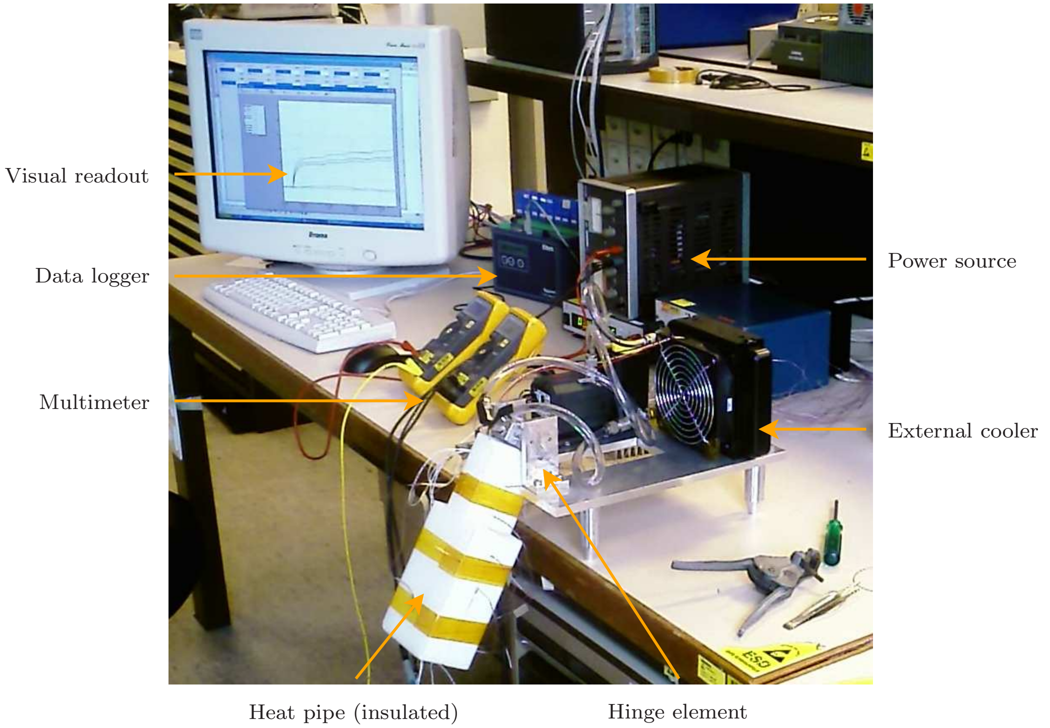

Figure C.1: *Measurement set-up for the integrated heat pipe cooling concept.*

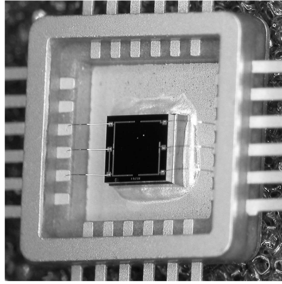

(a) bare die inside package

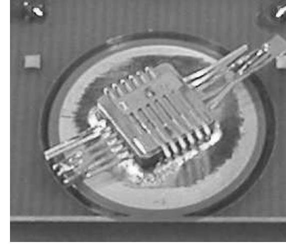

(b) mounted upside down

Figure C.2: *Pressure gauge.*

Pressure Gauge

To measure the pressure of the saturated vapor inside the heat pipe a pressure gauge was used. A bare silicon die sensor [26] was packaged into a lead glass flatpack package [56], as shown in Figure C.2(a). The sensor consists of a micro-machined membrane with a Pyrex glass mounted under vacuum. The implanted resistors make use of the piezo-resistive effect. As it carries a sealed vacuum reference cavity underneath the membrane, it is regarded as an absolute pressure sensor.

The sensor was connected to the package leads through bondwires. These are also visible in Figure C.2(a). To measure the pressure inside the heat pipe, a hole was drilled and metalized into the top layer of the heat pipe. The pressure gauge package was assembled upside down, as shown in Figure C.2(b), directly above this hole. As such, the pressure gauge could measure the pressure inside the heat pipe, without breaking the hermetic seal of the enclosure.

C.2 Heat Pipe Measurements

Figure C.3 shows a measurement of one of the produced heat pipes in a horizontal set-up. First, the heat pipe was exposed to 2.5 W of dissipated heat, after which the dissipation was increased to 10 W. The different lines correspond to the thermocouples attached along the heat pipe's length. The top line recorded the temperature at the evaporator side, whereas the bottom line recorded the temperature at the condenser end. From the temperature differences between the top and bottom lines, the thermal design values could be computed, as discussed in Section 4.4.

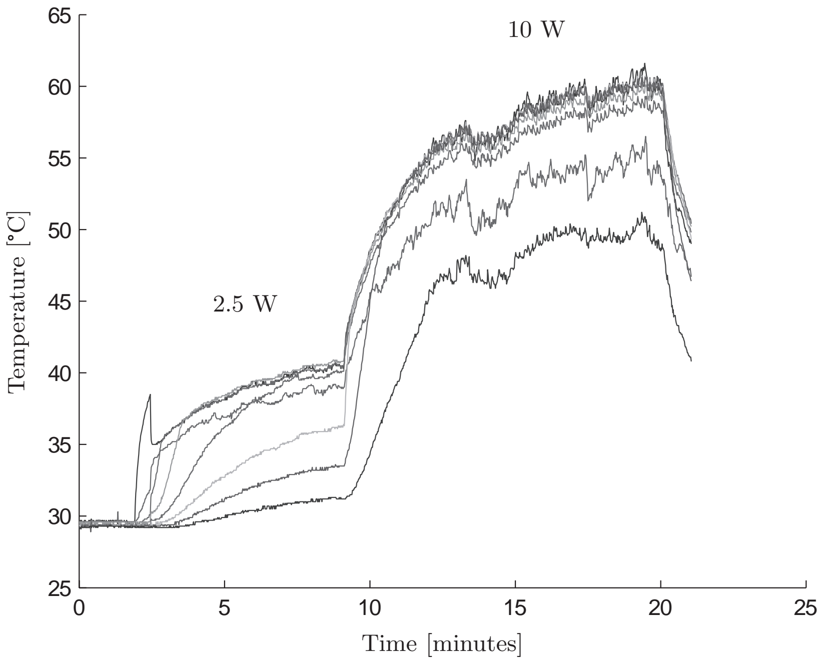

Figure C.3: *Transient measurement for a horizontal set-up.*

Appendix D

Thermal Resistance Values

The thermal resistance values that are assumed during the conceptual design phase are presented in this chapter. Values for the electronic package, BGA, PCB and rack structure are discussed, successively.

D.1 Electronic Package

The thermal resistance of an electronic package is estimated by analyzing the thermal path the heat travels through. For the BGA package of Chapter 2, the heat travels through the IC, die attach and rigid laminate before reaching the bottom side of the package. As the heat enters a larger region (i.e. the laminate) from a finite source (i.e. the IC), thermal spreading resistance also occurs. The heat is assumed to be generated at the junctions at the top of the IC.

The thermal conductivity of the IC is determined by the base material of the chip. For silicon (Si) based ICs this equals 149 W/mK; however, for gallium arsenide (GaAs) based ICs the conductivity is much lower, 56 W/mK. The former material costs less; however, the latter is more commonly used in microwave (RF) devices, due to its superior electronic properties. ICs based on GaAs can be found in, for instance, mobile phones and radar systems.

Suppose the IC has dimensions of 2.5x3.5x0.35 mm (lxbxh) and it is based on GaAs. According to Equation (2.3), the thermal resistance across the IC equals:

$$R_{IC} = \frac{L}{k \cdot A} = \frac{0.35e^{-3}}{56 \cdot 2.5e^{-3} \cdot 3.5e^{-3}} \approx 0.71\frac{K}{W} \tag{D.1}$$

A gold-tin alloy (AuSn) is typically used to attach the IC to a rigid laminate. It has a thickness of approximately 0.025 mm and a thermal conductivity of 59 W/mK. Hence, its thermal resistance equals:

$$R_{Die\ attach} = \frac{L}{k \cdot A} = \frac{0.025e^{-3}}{59 \cdot 2.5e^{-3} \cdot 3.5e^{-3}} \approx 0.05\frac{K}{W} \tag{D.2}$$

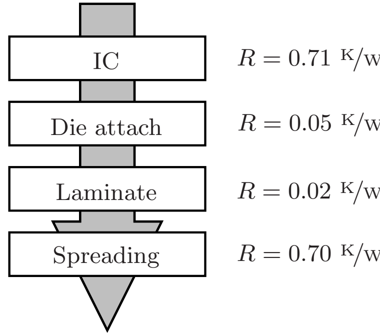

Figure D.1: *Package elements with thermal resistance values.*

The rigid laminate used in this study was comprised of copper and a Liquid Crystal Polymer (LCP). It had an average thermal conductivity of 200 W/mK and dimensions of 15x15x1 mm (lxbxh). Therefore, the thermal resistance across the laminate equals:

$$R_{Laminate} = \frac{L}{k \cdot A} = \frac{1e^{-3}}{200 \cdot (15e^{-3})^2} \approx 0.02 \frac{K}{W} \tag{D.3}$$

Finally, the heat spreading resistance from the small IC to the larger rigid laminate can be estimated according to Lee [33] in 1998, as:

$$R_{Spreading} = \frac{\sqrt{A_p} - \sqrt{A_s}}{k\sqrt{\pi A_p A_s}} \cdot \frac{\lambda k A_p R_0 + tanh(\lambda t)}{1 + \lambda k A_p R_0 tanh(\lambda t)} \tag{D.4}$$

where:

$$\lambda = \frac{\pi^{\frac{3}{2}}}{\sqrt{A_p}} + \frac{1}{\sqrt{A_s}} \tag{D.5}$$

Here, A_s and A_p represent the heat source (IC) area and package (rigid laminate) area, respectively; t denotes the thickness of the laminate; k and R_0 represent the thermal conductivity and average thermal resistance of the laminate, respectively.

In this case, the average thermal resistance R_0 is equal to the value of $R_{Laminate}$ from Equation (D.3). According to Equations (D.4) and (D.5), the thermal resistance of the heat spreading from the IC across the rigid laminate amounts to 0.70 K/W.

Figure D.1 illustrates the thermal resistances of the package elements discussed. The total thermal resistance from the junction to the bottom of the package is determined by the sum of the element resistances. Heat transfer losses between the elements are assumed negligible. In this case, this amounts to a total package thermal resistance of approximately 1.5 K/W.

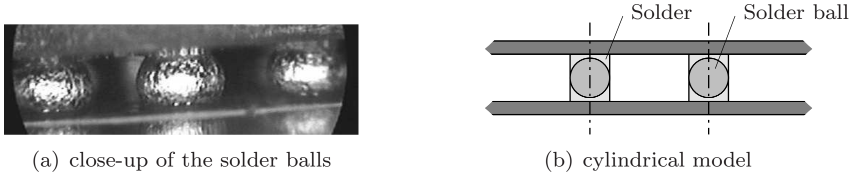

(a) close-up of the solder balls (b) cylindrical model

Figure D.2: *Solder balls in a ball grid array.*

D.2 Ball Grid Array

The solder balls in the BGA are assumed to have a cylindrical shape after soldering, as shown in Figure D.2. Hence, the thermal resistance of the complete array can be estimated using Equation (2.3). A typical solder ball size is ⌀0.65 mm and usually a lead-tin (PbSn) alloy solder is used ($k = 25$ W/mK). The height of the soldered cylinder is approximately 0.75 mm, the standoff distance. Assuming the BGA consists of 25 connections, its thermal resistance amounts to:

$$R_{BGA} = \frac{L}{k \cdot A} = \frac{0.75e^{-3}}{25 \cdot 25 \cdot \frac{1}{4}\pi(0.65e^{-3})^2} \approx 3.6\frac{K}{W} \tag{D.6}$$

D.3 Printed Circuit Board

As the PCB consists of layers pressed together, the thermal conductivity is not uniform in all directions. The polymeric layers are poor conductors; the metallic pattern on the layers however conducts very well. The overall thermal conductivity depends on the amount of layers and percentage of metalization that remains on each layer after producing the electronic circuits. In general, thermal conductivity of a PCB is specified in parallel (in-plane) and perpendicular directions. According to Ying and Toh [66] in 2000, the anisotropic conductivities $k_{\parallel}$ and $k_{\perp}$ of an average PCB are 27.5 W/mK and 0.41 W/mK, respectively.

For a PCB with a thickness of 1.6 mm, the thermal resistance from a BGA package perpendicular through the board would amount to:

$$R_{PCB,\perp} = \frac{L}{k \cdot A} = \frac{1.6e^{-3}}{0.41 \cdot (15e^{-3})^2} \approx 17.3\frac{K}{W} \tag{D.7}$$

When the heat has to travel from the center of the board to the edge, instead of perpendicular through the board, the thermal resistance becomes:

$$R_{PCB,\parallel} = \frac{L}{k \cdot A} = \frac{100e^{-3}}{27.5 \cdot 1.6e^{-3} \cdot 200e^{-3}} \approx 11.4\frac{K}{W} \tag{D.8}$$

In practice, when cooling on the edge of the board is assumed, both values need to be taken into account, as the heat must flow into the board first before it can

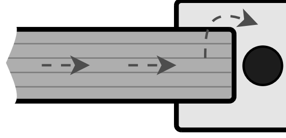

Figure D.3: *Cooling path through the clamped interface.*

spread to the edge. However, for an initial estimation either value can be used, depending on the component layout and cooling set-up.

D.4 Rack Cooling

Rack structures can be used to retain and cool the PCB simultaneously. The board is slid into a U-profile and clamped. Heat conducted through the board is transfered to the rack via the pressurized clamp interface, as shown in Figure D.3. Through the rack structure, the heat may be further dissipated to, for instance, a liquid coolant indicated by the black circle.

The heat transfer value for a properly designed clamp construction typically is in the order of 4,000 $^{W}/_{m^2K}$ [16]. Hence, for a clamp interface width of 20 mm, the thermal resistance equals, according to Equation (2.4):

$$R_{Clamp} = \frac{1}{h \cdot A} = \frac{1}{4000 \cdot 20e^{-3} \cdot 15e^{-3}} = 0.8 \frac{K}{W} \tag{D.9}$$

Here, the length of the cooling area is assumed identical to the width of the electronic package that is discussed in Appendix D.1.

Suppose the rack structure is made of aluminum ($k = 180\,^{W}/_{mK}$) with cooling water running through it. The thermal resistance from the clamp interface to the water amounts to:

$$R_{Aluminum} = \frac{L}{k \cdot A} = \frac{10e^{-3}}{180 \cdot 20e^{-3} \cdot 15e^{-3}} = 0.2 \frac{K}{W} \tag{D.10}$$

Here, the length of the conducting path is assumed to be 10 mm. Also, an equal heat exchange area is assumed.

Finally, the heat is convected to the cooling water. Here, typically heat transfer values of 2,000 $^{W}/_{m^2K}$ [16] can be achieved. Hence, the thermal resistance equals:

$$R_{Water} = \frac{1}{h \cdot A} = \frac{1}{2000 \cdot 20e^{-3} \cdot 15e^{-3}} = 1.7 \frac{K}{W} \tag{D.11}$$

Analogous to the case of the package thermal resistance, the total thermal resistance for the rack cooling set-up is also determined by the sum of the element resistances. In this case, this amounts to a total rack structure thermal resistance of approximately 2.7 $^{K}/_{W}$.

Appendix E

Transient Energy Balance

In this chapter, the fully expanded energy conservation balances are presented. Also, the application of an additional evaporator or an additional condenser is discussed.

E.1 Expanded Energy Balances

In this section, the energy conservation balances are further expanded for the single evaporator heat pipe model. This model is shown in Figure 4.10. According to Equations (4.20) and (4.21), the energy balances for the evaporator and condenser regions are, respectively:

$$\frac{d}{dt}\left[m_e c_{p,e} T_e\right] + \dot{m}_{i,e} H_{fg} = \dot{Q}_{in} + \sum_{in} \dot{m} c_p \Delta T - \sum_{out} \dot{m} c_p \Delta T \tag{E.1}$$

$$\frac{d}{dt}\left[m_c c_{p,c} T_c\right] - \dot{m}_{i,c} H_{fg} = -\dot{Q}_{out} + \sum_{in} \dot{m} c_p \Delta T - \sum_{out} \dot{m} c_p \Delta T \tag{E.2}$$

The amount of mass present in either an evaporator or condenser region is determined by the sum of both the vapor and liquid particles. Although previously neglected, here the influence of the vapor phase is demonstrated. The vapor mass is determined by the geometry (volume) and the temperature. The liquid mass however, is also a function of the local liquid height (h_l), which can be derived from the mass balance equations.

In the following equations, the mass terms are expanded for the evaporator

and condenser regions, respectively:

$$\frac{d}{dt}\Big[(A_{le}\rho_{le}c_{p,le}h_{le} + V_{ve}\rho_{ve}c_{p,ve})(T_e - T_r)\Big] = \dot{Q}_{in} - A_{le}\rho_{ve}U_{ve,i}H_{fg} + A_l\rho_{lc}U_lc_{p,lc}(T_c - T_r) - A_v\rho_{ve}U_vc_{p,ve}(T_e - T_r) \quad \text{(E.3)}$$

$$\frac{d}{dt}\Big[(A_{lc}\rho_{lc}c_{p,lc}h_{lc} + V_{vc}\rho_{vc}c_{p,vc})(T_c - T_r)\Big] = -\dot{Q}_{out} + A_{lc}\rho_{vc}U_{vc,i}H_{fg} - A_l\rho_{lc}U_lc_{p,lc}(T_c - T_r) + A_v\rho_{ve}U_vc_{p,ve}(T_e - T_r) \quad \text{(E.4)}$$

Here, V_v denotes the vapor space volume of the specific region and $U_{v,i}$ represents the velocity of vapor that crosses the liquid-vapor interface (i.e. vapor that either evaporates or condenses). The subscripts e and c refer to the evaporator and condenser regions, respectively. Also, a reference or system temperature is defined, which is equal to the mean temperature of the evaporator and condenser regions:

$$T_r = \frac{1}{2}(T_e + T_c) \quad \text{(E.5)}$$

By comparing the two expanded mass terms on the left hand side in Equations E.3 and E.4, it can be deduced that the vapor contribution is negligible compared to the liquid contribution, due to the large difference between the vapor and liquid densities.

E.2 Additional Elements

In the case of a heat pipe with an addition evaporator or condenser element, also an additional conservation equation must be formulated. Control volume elements that are not on the end of the heat pipe will have two additional terms on the right hand side compared to, for instance, Equations E.3 and E.4. This is also illustrated in Figure 4.13, where evaporator 2 has two inflow and two outflow terms.

The additional terms are: an inflowing vapor term and an outflowing liquid term for an additional evaporator; for an additional condenser an outflowing vapor term and an inflowing liquid term must be added. This applies to both the mass and energy balances. In this case, the reference temperature is defined by the mean temperature of the control volume elements on the ends of the heat pipe model.

Also, in this case, two additional momentum balances must be formulated. The correct pressure terms at both ends of the transport section must be utilized. For the vapor momentum, this depends on the temperature difference across the transport section. For the liquid momentum balance, this depends on both the temperature and local liquid height across the transport section, according to Equation (4.25).

Appendix F

Fluid Flow Assumptions

The assumptions that were made in order to analyze the fluid flow inside the heat pipe are presented in this chapter. The hydraulic diameter is discussed. It is proven that laminar and incompressible flows may be assumed. Also, the vapor and liquid frictional effects are discussed.

F.1 Hydraulic Diameter

For non-circular flow passages the hydraulic diameter is often used in flow calculations. It is defined as:

$$d_h = 4 \cdot \frac{\text{cross sectional area}}{\text{wetted perimeter}} \tag{F.1}$$

For the vapor flowing through the rectangular cross section, the hydraulic diameter can be written as:

$$d_{h,v} = 4 \cdot \frac{HW}{2H + 2W} = \frac{2HW}{H + W} \tag{F.2}$$

For the liquid flowing through the capillary microgrooves, the hydraulic diameter can be written as:

$$d_{h,l} = 4 \cdot \frac{hw}{2h + w} \tag{F.3}$$

The microgrooves are open on one side; therefore, the liquid inside the microgrooves does not wet the entire perimeter. Hence, both hydraulic diameters differ slightly.

F.2 Proof Laminar Flow

The transition from laminar to turbulent flow is characterized by the Reynolds number. In general, for Reynolds numbers below approximately 2,300, the flow is considered to be laminar.

In a steady state, the mass flow rate of both the vapor flow and the liquid flow is determined by Equation (4.8):

$$\dot{m}_v = \frac{\dot{Q}_{in}}{H_{fg}} \tag{F.4}$$

Hence, according to the geometry of the heat pipe, Equation (4.7), the velocity of the vapor flow and the liquid flow can be determined by, respectively:

$$U_v = \frac{\dot{Q}_{in}}{HW\rho_v H_{fg}} \tag{F.5}$$

$$U_l = \frac{\dot{Q}_{in}}{hwN\rho_l H_{fg}} \tag{F.6}$$

Finally, the Reynolds number of both flows is determined by its definition. They are, respectively:

$$Re_{h,v} = \frac{\mu_v d_{h,v} U_v}{\rho_v} \tag{F.7}$$

$$Re_{h,l} = \frac{\mu_l d_{h,l} U_l}{\rho_l} \tag{F.8}$$

For a heat pipe according to the initial dimensions presented in Figure 4.8, charged with water as a working fluid, the Reynolds numbers for the vapor and liquid flows are 373 and 6, respectively. In this calculation, a heat dissipation of 100 W and an internal heat pipe temperature of 55°C are assumed. Hence, even at a dissipated value well above the values predicted in Chapter 4, both flows can be regarded as laminar.

F.3 Proof Incompressible Vapor Flow

The vapor flow from the evaporator region to the condenser region is assumed to be incompressible. This assumption is valid if the Mach number is well below unity. The Mach number is defined as the ratio of an object's velocity in a medium and the speed of sound in the same medium. In the case of the integrated heat pipe, the Mach number can be determined by:

$$Ma = \frac{U_v}{U_{sound}} \tag{F.9}$$

where U_{sound} is the speed of sound in the saturated vapor present inside the heat pipe. For the heat pipe assumed in Chapter 3, the Mach number equals approximately 0.03. As this value is well below unity, an incompressible vapor can be assumed.

F.4 Vapor Friction Factor

In 1987, Shah and Bhatti [55] presented a vapor friction factor ($fRe_{h,v}$), which depends only the aspect ratio of the vapor flow cross section. This relationship is shown in the following equation:

$$fRe_{h,v} = 24(1 - 1.3553\alpha + 1.9467\alpha^2 - 1.7012\alpha^3 + 0.9564\alpha^4 - 0.2537\alpha^5) \quad \text{(F.10)}$$

Here, α represents the aspect ratio of the vapor flow cross section:

$$\alpha = \frac{H}{W} \qquad \textit{for } W > H \quad \text{(F.11)}$$

$$\alpha = \frac{W}{H} \qquad \textit{for } H > W \quad \text{(F.12)}$$

In this analysis, all boundaries of the vapor flow cross section are considered stationary. In a heat pipe, this can be assumed as the counterflowing liquid velocity is far less than the vapor velocity, due to the large difference in density.

F.5 Liquid Friction Factor

In 1980, Schneider and DeVos [52] considered the effect of a planar free liquid surface in their liquid friction factor ($fRe_{h,l}$) for various liquid cross sections. This relationship is shown in the following equation:

$$fRe_{h,l} = (fRe_{h,l})_0 \left(1 + \frac{Nw^3}{6\pi d_{h,v}^3}(fRe_{h,v})\frac{\nu_v}{\nu_l}\left[1 - 1.971e^{\frac{-\pi h}{w}}\right]\right) \quad \text{(F.13)}$$

where:

$$(fRe_{h,l})_0 = 8h^2\left[\left(h + \frac{w}{2}\right)^2\left(\frac{1}{3} - \frac{32w}{\pi^5 h}\tanh\frac{\pi h}{w}\right)\right]^{-1} \quad \text{(F.14)}$$

In this analysis, the frictional effects of the liquid flow are not only dependent on the cross sectional geometry, but also on the counterflowing vapor. As Equation (F.13) suggests, the liquid friction factor will increase for smaller vapor cross sections, wider capillary microgrooves and increasing vapor friction factors.

Appendix G

Thermodynamic Properties

This chapter presents the thermodynamic properties of air and water that were used throughout this thesis.

G.1 Properties of Dry Air

The thermodynamic properties of air, as assumed in this thesis, are presented in Table G.1.

Table G.1: *Dry air properties at 20°C, atmospheric pressure.*

Property	Symbol	Value	Unit
Density	ρ	1.205	$^{kg}/_{m^3}$
Viscosity	μ	$1.81e^{-5}$	$^{Ns}/_{m^2}$
Conductivity	k	0.025	$^{W}/_{mK}$

G.2 Properties of Water

The thermodynamic properties of saturated water, as assumed in this thesis, are evaluated as a function of temperature. The following relations, according to Faghri [19], were used for density (ρ), viscosity (μ), conductivity (k), specific heat (c_p), vapor pressure (P_{sat}), specific latent heat of vaporization (H_{fg}) and liquid surface tension (σ), respectively:

$$\rho_v = exp^{-5.3225+6.8366e^{-2}T-2.7243e^{-4}T^2+8.4522e^{-7}T^3-1.6558e^{-9}T^4+1.5514e^{-12}T^5} \tag{G.1}$$

$$\rho_l = exp^{6.9094-2.0146e^{-5}T-5.9868e^{-6}T^2+2.5921e^{-8}T^3-9.3244e^{-11}T^4+1.2103e^{-13}T^5} \tag{G.2}$$

$$\mu_v = exp^{4.3995+3.8789e^{-3}T+2.1181e^{-5}T^2-3.4406e^{-7}T^3+1.6730e^{-9}T^4-2.8030e^{-12}T^5} \cdot 1e^{-7} \tag{G.3}$$

$$\mu_l = exp^{9.7620-3.1154e^{-2}T+2.0029e^{-4}T^2-9.5815e^{-7}T^3+2.7772e^{-9}T^4-3.5075e^{-12}T^5} \cdot 1e^{-7} \tag{G.4}$$

$$k_v = exp^{-4.0406+3.2288e^{-3}T+5.3383e^{-6}T^2-6.7139e^{-8}T^3+4.0967e^{-10}T^4-6.9579e^{-13}T^5} \tag{G.5}$$

$$k_l = exp^{-5.6528e^{-1}+3.1743e^{-3}T-1.4392e^{-5}T^2-1.3224e^{-8}T^3+2.5534e^{-10}T^4-6.4454e^{-13}T^5} \tag{G.6}$$

$$c_{p,v} = exp^{6.2084e^{-1}+3.1420e^{-4}T+1.6110e^{-6}T^2+4.0156e^{-8}T^3+3.4841e^{-11}T^4-2.0709e^{-13}T^5} \cdot 1e^{3} \tag{G.7}$$

$$c_{p,l} = exp^{1.4338-2.2638e^{-4}T+4.2819e^{-6}T^2-2.7411e^{-8}T^3+1.4669e^{-10}T^4-2.2589e^{-13}T^5} \cdot 1e^{3} \tag{G.8}$$

$$P_{sat} = exp^{-5.0945+7.2280e^{-2}T-2.8625e^{-4}T^2+9.2341e^{-7}T^3-2.0295e-9T^4+2.1645e-12T^5} \cdot 1e^{5} \tag{G.9}$$

$$H_{fg} = exp^{7.8201-5.8906e^{-4}T-9.1355e^{-6}T^2+8.4738e^{-8}T^3-3.9635e^{-10}T^4+5.9150e^{-13}T^5} \cdot 1e^{3} \tag{G.10}$$

$$\sigma = exp^{4.3438-3.0664e^{-3}T+2.0743e^{-5}T^2-2.5499e^{-7}T^3+1.0377e^{-9}T^4-1.7156e^{-12}T^5} \cdot 1e^{-3} \tag{G.11}$$

Here, T denotes the temperature in degrees Celsius. These relations are valid in the temperature range of 20-200°C.

The thermodynamics properties of saturated water at 55°C, according to the previous equations, are presented in Table G.2.

Table G.2: *Saturated water properties at 55°C.*

Property	Symbol	Value	Unit
Vapor density	ρ_v	0.104	kg/m^3
Liquid density	ρ_l	986.0	kg/m^3
Vapor viscosity	μ_v	$1.029e^{-5}$	Ns/m^2
Liquid viscosity	μ_l	$5.007e^{-4}$	Ns/m^2
Vapor conductivity	k_v	0.021	W/mK
Liquid conductivity	k_l	0.648	W/mK
Vapor specific heat	$c_{p,v}$	1915	J/kgK
Liquid specific heat	$c_{p,l}$	4183	J/kgK
Saturated vapor pressure	P_{sat}	$1.574e^{4}$	Pa
Specific latent heat of vaporization	H_{fg}	$2.371e^{6}$	J/kg
Liquid surface tension	σ	0.067	N/m

About the Author

Wessel Willems Wits was born on November 5th, 1977 in Amsterdam. He attended primary school and secondary school (Atheneum) in his hometown Mijdrecht. During secondary school, he already developed an interest for technical and science oriented topics. Mathematics and Physics were his favorite subjects.

One year before finishing secondary school, he became an exchange student and lived in the United States for one year. Here, he attended Waitsburg High School where he graduated Class of 1996. During this year, he enjoyed the American way of life and played many sports for his high school.

Back in the Netherlands and after finishing his last year of Atheneum, he started his study Mechanical Engineering at the University of Twente. In 2004, he finished this study at the Laboratory of Mechanical Automation with a Master's thesis on the development of a design tool for drive optimization of mechatronic systems.

His interest in and joy for academic research persuaded him to continue studying and pursue his doctoral degree as a Ph.D. student. He stayed within the Department of Mechanical Engineering, but switched to the Laboratory of Design, Production and Management. The thesis presented here, is a result of this work.

Next to his academic accomplishments, he was also very active in playing sports. Basketball was and still is his favorite sport. He turned out to be a late bloomer, as in the spring of 2007, he possibly reached his athletic climax by winning the Dutch National Championship for Amateur Basketball.

List of Publications

Journal Papers

- Wessel W. Wits, Tom H.J. Vaneker, Jan H. Mannak and Rob Legtenberg, “Novel cooling strategy for electronic packages: Directly injected cooling”, *CIRP Journal of Manufacturing Science and Technology*, Article in press, November 2008.

Patents

- Wessel W. Wits, Jan H. Mannak and Rob Legtenberg, “Planar heat pipe for cooling”, WIPO Patent Application WO/2007/096313, Thales Nederland B.V., 2007.
- Gerard J.H.M. Brok, Wessel W. Wits, Jan H. Mannak and Rob Legtenberg, “Directly Injected Forced Convection Cooling for Semiconductor Components”, Patent number NL-BN 1034420, Thales Nederland B.V., 2007.

Conference Papers

- Juan M. Jauregui-Becker, Wessel W. Wits and Fred J.A.M. van Houten, “Reducing design complexity of multidisciplinary domain integrated products: A case study”, *Proceedings of the 41st CIRP Conference on Manufacturing Systems:* CIRP MS 2008, pp. 149-154, Tokyo, Japan, 26-28 May 2008. (This paper was awarded best paper.)
- Wessel W. Wits and Jim B.W. Kok, “Modelling the transient analysis of flat miniature heat pipes in printed circuit boards using a control volume approach”, *Proceedings of the 5th European Thermal-Sciences Conference:* Eurotherm 2008, Eindhoven, The Netherlands, 18-22 May 2008.
- Wessel W. Wits, Jan H. Mannak and Rob Legtenberg, “Selecting capillary structures for heat pipes in multilayer printed circuit boards”, *Proceedings of the 5th European Thermal-Sciences Conference:* Eurotherm 2008, Eindhoven, The Netherlands, 18-22 May 2008.
- Wessel W. Wits, Gerard J.H.M. Brok, Jan H. Mannak and Rob Legtenberg, “Novel cooling strategy for electronic packages: Directly injected cooling”, *Proceedings of the CIRP Design Conference 2008:* Design Synthesis, Enschede, The Netherlands, 7-9 April 2008.
- Wessel W. Wits, Tom H.J. Vaneker, Jan H. Mannak and Fred J.A.M. van Houten, “Domain integration and cost reduction in electronic product design: A case study”, *Proceedings of the 40th CIRP Conference on Manufacturing Systems:* CIRP MS 2007, Liverpool, United Kingdom, 30 May-1 June 2007.

- Wessel W. Wits, Jim B.W. Kok, Rob Legtenberg, Jan H. Mannak and Bas van Zalk, “Manufacturing and modelling of flat miniature heat pipes in multilayer printed circuit board technology”, *Proceedings of the 14th International Heat Pipe Conference:* 14th IHPC, pp. 169-175, Florianópolis, Brazil, 22-27 April 2007.

- Wessel W. Wits, Rob Legtenberg, Jan H. Mannak and Bas van Zalk, “Thermal management through in-board heat pipes manufactured using printed circuit board multilayer technology”, *Proceedings of the 31st International Conference on Electronic Manufacturing and Technology:* IEMT 2006, Putrajaya, Malaysia, 8-10 November 2006.

Student Assignments

Several student assignments have been conducted as a part of the research described in this thesis. These were:

- Pieter G. Nieboer, “Solving technical challenges for integration of heat pipe technology into printed circuit boards”, M.Sc. Thesis, OPM-869, University of Twente, Enschede, The Netherlands, 2008.

- Bob Rots, “Modeling & testing of heat pipes”, Internship Report, Saxion University, Enschede, The Netherlands, 2008.

- Martijn Pijpers, “Modelling and design of an integrated heat pipe using printed circuit board technology”, M.Sc. Thesis, OPM-831, University of Twente, Enschede, The Netherlands, 2007.

- Gerard J.H.M. Brok, “Development and application of a thermal modeling tool for electronics cooling”, M.Sc. Thesis, OPM-822, University of Twente, Enschede, The Netherlands, 2007.

- Mark de Gier, “Printed circuit board koelen d.m.v. heatpipes” (in Dutch), B.Sc. Thesis, Saxion University, Enschede, The Netherlands, 2006.